UNIVERSITY OF CALIFORNIA SAN DIEGO

Translation of an Injectable Decellularized Extracellular Matrix Hydrogel for Promoting Skeletal Muscle Regeneration

A dissertation submitted in partial satisfaction of the
requirements for the degree Doctor of Philosophy

in

Bioengineering

by

Melissa Jenee Hernandez

Committee in Charge:

Professor Karen L. Christman, Chair
Professor Adam J. Engler
Professor Ehtisham Mahmud
Professor Sameer B. Shah
Professor Samuel R. Ward

2019

The Dissertation of Melissa Jenee Hernandez is approved, and it is acceptable in quality and form for publication on microfilm and electronically:

_____

_____

_____

_____

_____

Chair

University of California San Diego

2019

DEDICATION

To my unwavering supporters – Dad, Mom, Jessica, Michaela, Eric, Maya, and last but not least Michael

TABLE OF CONTENTS

LIST OF ABBREVIATIONS

ABC = Ammonium Bicarbonate

ANOVA = Analysis of Variance Test

bFGF = Basic Fibroblast Growth Factor

CLI = Critical Limb Ischemia

CSA = Cross-Sectional Area

CVD = Cardiovascular Disease

DI = Deionized

DMMB = 1,9-Dimethylmethylene Blue

DMSO = Dimethyl Sulfoxide

ECM = Extracellular Matrix

EV = Extracellular Vesicle

FGF = Fibroblast Growth Factor

GLP = Good Laboratory Practice

H&E = Hematoxylin and Eosin

HGF = Hepatocyte Growth Factor

GuHCl = Guanidine Hydrochloride

LASCA = Laser Speckle Contrast Analysis

LC = Liquid Chromatography

MiRNA = MicroRNA

MS = Mass Spectrometry

PAA = Peracetic Acid

PAD = Peripheral Artery Disease

PBS = Phosphate Buffered Saline

Quantitative Concatamer = QconCAT

RCT = Rotator Cuff Tear

SDS = Sodium Dodecyl Sulfate

SEM = Scanning Electron Microscopy

sGAG = Sulfated Glycosaminoglycans

SKM = Skeletal Muscle Extracellular Matrix Hydrogel

SRM = Selected Reaction Monitoring

VEGF = Vascular Endothelial Growth Factor

LIST OF FIGURES

LIST OF TABLES

ACKNOWLEDGEMENTS

I would like to begin by thanking Professor Karen Christman for her exceptional mentorship and support during the past 5 years. Her experience in both academia and industry has allowed me to expand my scientific knowledge and acquire invaluable skills for entering industry. She has motivated me to think independently, and our scientific discussions have allowed me to grow as a scientist and engineer. I would also like to acknowledge Professor Sam Ward for his outstanding mentorship. He has trained me to thoroughly critique scientific data and has given me many opportunities and guidance to become a stronger leader. Additionally, Dr. Shami Mahmud has provided instrumental expertise for translating our research to the clinic and understanding our target patient population. I would also like to acknowledge my remaining committee members Professors Adam Engler and Sameer Shah for their suggestions and support with improving my dissertation. Lastly, I am also incredibly grateful for the mentorship of Professors Eva Chi (University of New Mexico) and Laura Segatori (Rice University), both of whom inspired and encouraged me to pursue graduate school.

I would also like to recognize the support from members of the Christman and Ward labs. From the Christman lab, I would like to thank Dr. Jessica Ungerleider, Dr. Roberto Gaetani, Dr. Raymond Wang, Pamela Duran, Emma Zelus, Holly Sullivan, Miranda Diaz, Marty Spang, Hillary Lam, Dr. Gina Policastro, and Rebecca Braden for their friendship and valuable input. In particular, I am incredibly thankful for Jessica Ungerleider who trained me as a PhD student and continuously served as a sounding board and source of encouragement. I am also indebted to all of the undergraduates whose help was essential for me to complete my research projects: Grace Yakutis, Nathan Ng, Audrey Chang, Haley Sherburne, Vivienne Gunadhi, Alana Gonzales, Cori Espelien, Preety Shakya, and Alex Bale. From the Ward lab, I would like to acknowledge Mary Esparza and Shanelle Dorn for their instrumental assistance with animal studies and subsequent analyses and Dr. Michael Gibbons, who was and continues to be a remarkable mentor and who motivated me during the most difficult parts of this journey.

Finally, I am forever grateful for all of my family and friends whose endless encouragement and love propelled me through graduate school. I would like to thank my closest friends Lauren Deveraux, Kim McCabe, Pamela Duran, Hillary Lam, Courtney Green, Lizzy Stasiowski, Kara Johnson, Ray Wang, and Alex Williams who were always available and with whom I have countless memories. Additionally, I would like to thank the entire Hernandi clan – my parents, Mike and Roni Hernandez, my sisters, Jessica Larson and Michaela Hernandez, my brother, Eric Larson, and the newest addition, Maya Larson. My family has and continues to provide me with endless love, motivation, inspiration, and support to accomplish whatever goals I set out to achieve. And lastly, I would again like to recognize Michael Gibbons for always encouraging me to reach my full potential. From initially serving as a scientific mentor and role model, he has since become my biggest support system and continuously challenges me to pursue more ambitious goals. His friendship, guidance, and unconditional love have been and will continue to be essential to my personal and professional development.

Chapter 2, in part, is a reprint of the material as it appears in the Journal of the American College of Cardiology: Basic to Translational Science 2017. Melissa J. Hernandez and Karen L. Christman. The dissertation author was the primary investigator and author of this material.

Chapter 3, in part, is currently being prepared for submission for publication of the material. Melissa J. Hernandez, Emma I. Zelus, Martin T. Spang, Rebecca L. Braden, Karen L. Christman. The dissertation author was the primary investigator and author of this material.

Chapter 4, in part, is currently being prepared for submission for publication of the material. Melissa J. Hernandez, Michael C. Gibbons, Holly L. Sullivan, Emma I. Zelus, Jessica L. Ungerleider, Mary C. Esparza, Shanelle Dorn, Karen L. Christman, Samuel R. Ward. The dissertation author was the primary investigator and author of this material.

Chapter 5, in part, is a reprint of the material as it appears in Advanced Therapeutics 2018. Melissa J. Hernandez, Roberto Gaetani, Vera M. Peiters, Nathan W. Ng, Audrey E. Chang, Taylor R. Martin, Eva van Ingen, Emma A. Mol, Monika Dzieciatkowska, Kirk C.

Hansen, Joost P.G. Sluijter, Karen L. Christman. The dissertation author was the primary investigator and author of this material.

Chapter 6, in part, is a reprint of the material as it appears in Methods 2019. Melissa J. Hernandez, Grace E. Yakutis, Emma I. Zelus, Ryan C. Hill, Monika Dzieciatkowska, Kirk C. Hansen, Karen L. Christman. The dissertation author was the primary investigator and author of this material.

VITA

2014 Bachelor of Science, University of New Mexico

Major Field: Chemical Engineering
Professor Eva Chi

2019 Doctor of Philosophy, Bioengineering, University of California San Diego

Major Field: Bioengineering
Professor Karen Christman

ABSTRACT OF THE DISSERTATION

Translation of an Injectable Decellularized Extracellular Matrix Hydrogel for Promoting Skeletal Muscle Regeneration

by

Melissa J. Hernandez

Doctor of Philosophy in Bioengineering

University of California San Diego, 2019

Professor Karen L. Christman, Chair

Unlike many organs, skeletal muscle possesses the ability to naturally regenerate. However, chronic muscle injuries, including ischemia and chronic unloading, interrupt this regenerative process. We sought to investigate the therapeutic potential of a decellularized skeletal muscle extracellular matrix (ECM) hydrogel in ischemia and chronic unloading muscle injury models with a main focus on translating this material into the clinic. A rat hindlimb ischemia model was utilized for a dose optimization study in which three concentrations (4 mg/mL, 6 mg/mL, and 8 mg/mL) were compared to a saline control and non-tissue specific myocardial ECM hydrogel. The 6 mg/mL concentration produced the largest increase in blood perfusion, and efficacy of the 6 mg/mL skeletal muscle ECM hydrogel was then further confirmed in an aged mouse hindlimb ischemia model to more accurately depict patient pathophysiology. Similar to the dose optimization study, significant increases in blood perfusion

were observed after 4 weeks. Since the hindlimb ischemia model is an acute model, the skeletal muscle ECM hydrogel was also probed in a more chronic model, specifically a rabbit model of chronic rotator cuff tears. The timing for the ECM hydrogel injection was investigated, and a delayed injection encouraged more muscle regeneration, as demonstrated by upregulation of key muscle transcription factors and the presence of larger diameter arterioles. Although ECM hydrogels possess regenerative capabilities, efficacy may be limited, and, therefore, the material was also evaluated as a delivery vehicle for microRNAs and exosomes. Incorporation of these therapeutics into the hydrogels yielded prolonged release profiles, and the released molecules remained bioactive *in vitro*. Lastly, several manufacturing considerations were investigated to ensure efficacy of the final product would be maintained during scale-up. Animal-to-animal variability and a bioburden reducing step did not present issues for manufacturing, but the various harvesting conditions yielded differences with the protein content of the final ECM product. All in all, the skeletal muscle ECM hydrogels demonstrated efficacy in multiple skeletal muscle injury models and as a delivery platform for small therapeutics. In addition, the manufacturing of these materials for clinical translation remains feasible amidst additional processing steps.

Chapter 1. Skeletal Muscle Injuries and Associated Repair Mechanisms

Categories of Skeletal Muscle Injury

Skeletal muscle constitutes approximately 30-38% of body mass and can be affected by a wide range of injuries.[1] Due to the superficial location of many muscles, this tissue is prone to acute injuries, which include contusions, lacerations, burns, and exposure to toxins. Conversely, skeletal muscle can also be subjected to chronic injuries, such as cachexia, neuromuscular disease, ischemia, and unloading.

Cachexia, also known as wasting syndrome, is a condition that arises due to the presence of chronic, systemic inflammation and is associated with high mortality rates.[2-4] This is commonly associated with cancer, chronic renal failure, congestive heart failure, HIV, and chronic obstructive pulmonary disease and is estimated to affect more than 5 million Americans.[5] Patients with cachexia experience extreme and involuntary muscle mass loss, which may or may not be accompanied by fat loss. More specifically, cachexia leads to increased protein degradation in skeletal muscle, alterations in fat metabolism, and a persistent acute inflammatory response.

Neuromuscular disorders encompass diseases such as muscular dystrophy, amyotrophic lateral sclerosis, and multiple sclerosis. These diseases can be hereditary or sporadic, and the morbidity and mortality rates vary between conditions. For instance, Duchenne muscular dystrophy, caused by an inherited mutation in the dystrophin gene, induces wide-scale muscle degeneration and necrosis, and individuals, most commonly men, do not typically survive past 30.[6] Amyotrophic lateral sclerosis, on the other hand, occurs sporadically with patients only surviving between 3 to 5 years due to degeneration of the motor neurons and accompanying muscle atrophy, weakness, and fasciculation.[7]

Ischemia is the inadequate supply of oxygen-rich blood to skeletal muscle, which is secondary to compression injuries, including compartment syndrome or crush syndrome, or caused by atherosclerosis. Focusing on the latter, this describes a condition known as peripheral artery disease (PAD) in which narrowed or occluded arteries fail to deliver sufficient blood flow to the skeletal muscle. Approximately 8.5 million Americans suffer from PAD, and the chronic ischemia can lead to muscle weakness, muscle atrophy, varying degrees of tissue loss, and in severe cases may require amputation.[8]

Chronic muscle unloading can result from prolonged disuse or occurs following a tendon tear or rupture. In the United States, approximately 10% of the population over 60 years old experiences a torn rotator cuff, and these tears necessitate an estimated 75,000 surgical repair procedures each year.[9,10] For chronic rotator cuff tears, the chronic muscle unloading leads to muscle atrophy, fatty infiltration, and muscle degeneration. Although the patients often undergo surgeries to reattach the torn tendons, thereby allowing the muscle to reload, tendon retear rates may approach 94%.[11]

Although the mechanisms for these various muscle injuries contrast significantly and produce different symptoms, skeletal muscle relies on similar repair mechanisms. Acutely injured muscle typically resolves via these normal repair and regeneration processes, but chronic injuries often fail to completely restore healthy skeletal muscle tissue. Therefore, therapeutic strategies are needed to restore or replace the regenerative capacity of skeletal muscle.

Skeletal Muscle Repair Mechanism

Acute and chronic skeletal muscle injuries damage the skeletal muscle to varying extents, but repair and regeneration mechanisms exist to circumvent the damage.[12,13] When skeletal muscle is injured, an acute inflammatory cascade is initiated, and resident populations

of quiescent muscle progenitor cells ($Pax7^+$), known as satellite cells, are activated. Meanwhile, macrophages infiltrate the injured region and remove debris from the damaged muscle fibers. Once the cytoplasmic components of the damaged fibers have been removed, the original basil lamina remains, and the process of regeneration can begin. Activated satellite cells ($Pax7^+/MyoD^+/Myf5^+$) will divide asymmetrically in which some cells will return to a quiescent state and the remaining will undergo further expansion into myoblasts. These myoblasts will proliferate ($MyoD^+/Myf5^+$) and once committed will differentiate into myocytes ($MyoD^+/myogenin^+$), which then fuse together into myotubes ($eMHC^+$). Ultimately, further fusion of the myotubes yields healthy, functioning myofibers.

Resolution for Skeletal Muscle Injuries

In the event of injury to the skeletal muscle, normal repair and regeneration mechanisms are utilized, but healthy muscle is not always restored, particularly with chronic muscle injuries, as shown in Figure 1.1.[14] While myoblasts typically differentiate into myotubes, some of those myoblasts differentiate into myofibroblasts due to the activation of fibroblasts and persistent inflammatory cell infiltration. The accumulation of myofibroblasts then leads to the buildup of fibrotic tissue in the muscle, which can eventually impact overall muscle function. Similarly, a persistent inflammatory response can also induce fatty accumulation. Although the mechanisms leading to fatty infiltration and fibrosis are mostly unknown, it is hypothesized that the regenerative capacity of satellite cells may dwindle, or populations of satellite cells may be depleted in certain disease pathologies or with aging. Moreover, aging, which is a risk factor for many of the previously described muscle injuries, causes sarcopenia, or age-related muscle loss, and ECM remodeling processes can also be altered. All in all, the presence of muscle atrophy, fatty accumulation, fibrosis, and/or muscle degeneration creates heterogeneity in the muscle tissue, which can be detrimental to overall muscle function. Interventions to remove

damaged muscle and induce muscle regeneration are paramount for the abundance of muscle injuries that are associated with significant morbidity and mortality rates. This dissertation will focus on a therapeutic for addressing the skeletal muscle repair in models of peripheral artery disease (PAD) and chronic rotator cuff tears (RCT).

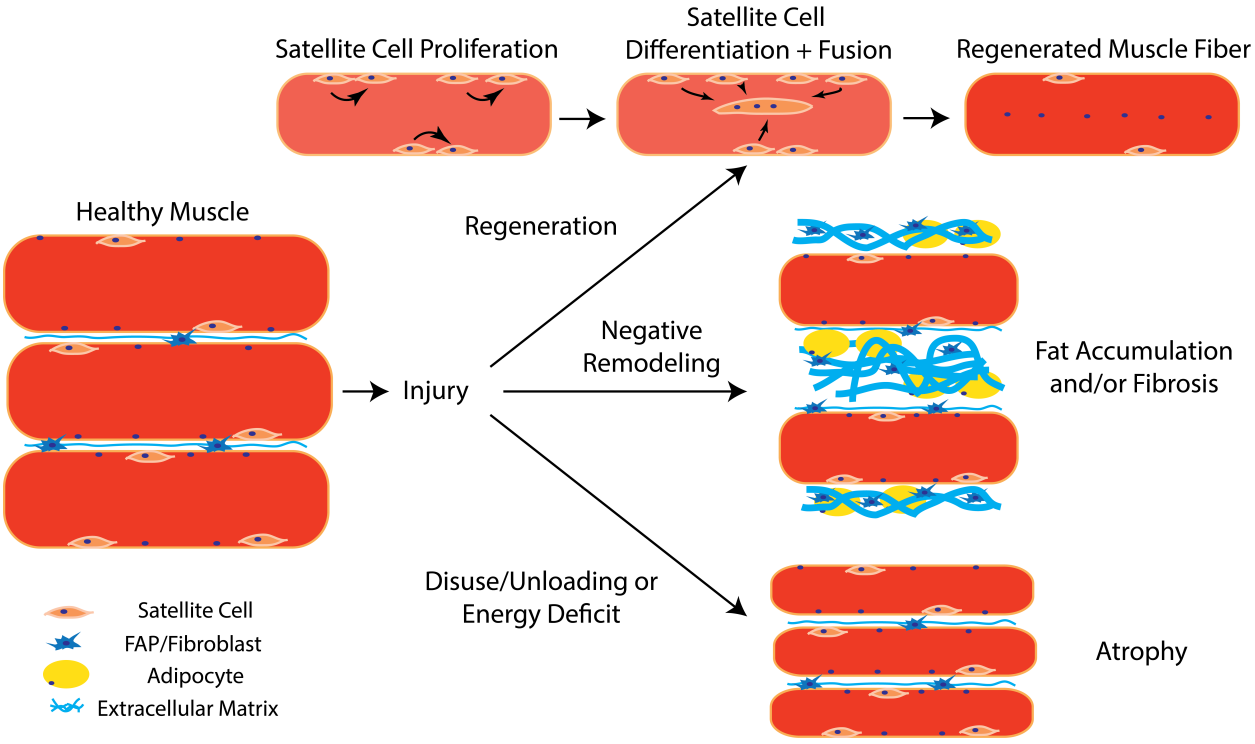

Figure 1.1 Overview of the skeletal muscle's response to injuries. Skeletal muscle possesses the ability to regenerate unlike the majority of other organs in the body. However, the regeneration mechanism is often impaired in the presence of certain injuries, especially chronic injuries. Contractile tissue is replaced with non-contractile tissue such as adipose and fibrosis, or muscle fiber atrophy can also occur.

References

1. Janssen I, Heymsfield SB, Wang ZM, Ross R. Skeletal muscle mass and distribution in 468 men and women aged 18-88 yr. *J Appl Physiol (1985)* **89**, 81-88, doi:10.1152/jappl.2000.89.1.81 (2000).

2. Kotler DP. Cachexia. *Ann Intern Med* **133**, 622-634 (2000).

3. Evans WJ, Morley JE, Argiles J, Bales C, Baracos V, Guttridge D, Jatoi A, Kalantar-Zadeh K, Lochs H, Mantovani G, Marks D, Mitch WE, Muscaritoli M, Najand A,

Ponikowski P, Rossi Fanelli F, Schambelan M, Schols A, Schuster M, Thomas D, Wolfe R, Anker SD. Cachexia: a new definition. *Clin Nutr* **27**, 793-799, doi:10.1016/j.clnu.2008.06.013 (2008).

4. Lainscak M, Filippatos GS, Gheorghiade M, Fonarow GC, Anker SD. Cachexia: common, deadly, with an urgent need for precise definition and new therapies. *Am J Cardiol* **101**, 8E-10E, doi:10.1016/j.amjcard.2008.02.065 (2008).

5. Morley JE, Thomas DR, Wilson MM. Cachexia: pathophysiology and clinical relevance. *Am J Clin Nutr* **83**, 735-743, doi:10.1093/ajcn/83.4.735 (2006).

6. Deconinck N, Dan B. Pathophysiology of duchenne muscular dystrophy: current hypotheses. *Pediatr Neurol* **36**, 1-7, doi:10.1016/j.pediatrneurol.2006.09.016 (2007).

7. Rowland LP, Shneider NA. Amyotrophic lateral sclerosis. *N Engl J Med* **344**, 1688-1700, doi:10.1056/NEJM200105313442207 (2001).

8. Allison MA, Ho E, Denenberg JO, Langer RD, Newman AB, Fabsitz RR, Criqui MH. Ethnic-specific prevalence of peripheral arterial disease in the United States. *Am J Prev Med* **32**, 328-333, doi:10.1016/j.amepre.2006.12.010 (2007).

9. Eljabu W, Klinger HM, von Knoch M. The natural history of rotator cuff tears: a systematic review. *Arch Orthop Trauma Surg* **135**, 1055-1061, doi:10.1007/s00402-015-2239-1 (2015).

10. Vitale MA, Vitale MG, Zivin JG, Braman JP, Bigliani LU, Flatow EL. Rotator cuff repair: an analysis of utility scores and cost-effectiveness. *J Shoulder Elbow Surg* **16**, 181-187, doi:10.1016/j.jse.2006.06.013 (2007).

11. Randelli P, Spennacchio P, Ragone V, Arrigoni P, Casella A, Cabitza P. Complications associated with arthroscopic rotator cuff repair: a literature review. *Musculoskelet Surg* **96**, 9-16, doi:10.1007/s12306-011-0175-y (2012).

12. Carlson BM, Faulkner JA. The regeneration of skeletal muscle fibers following injury: a review. *Med Sci Sports Exerc* **15**, 187-198 (1983).

13. Tedesco FS, Dellavalle A, Diaz-Manera J, Messina G, Cossu G. Repairing skeletal muscle: regenerative potential of skeletal muscle stem cells. *J Clin Invest* **120**, 11-19, doi:10.1172/JCI40373 (2010).

14. Mann CJ, Perdiguero E, Kharraz Y, Aguilar S, Pessina P, Serrano AL, Munoz-Canoves P. Aberrant repair and fibrosis development in skeletal muscle. *Skelet Muscle* **1**, 21, doi:10.1186/2044-5040-1-21 (2011).

Chapter 2. Designing Acellular Injectable Biomaterial Therapeutics for Peripheral Artery Disease

Introduction

Cardiovascular disease (CVD) has long been the leading cause of death worldwide. In 2013, CVD accounted for 31% of all deaths,[1] representing a 41.7% increase since 1990.[2] Of the conditions classified as CVD, peripheral artery disease (PAD) is associated with significant morbidity and mortality. In the United States alone, approximately 8.5 million individuals are afflicted by PAD,[3] and critical limb ischemia (CLI) and potential limb amputation significantly reduce the life expectancy of these individuals. Therefore, treatments for repairing ischemic damage and restoring muscle function for PAD are needed. Although current medical interventions mitigate some symptoms, they remain unavailable for many patients with PAD. Stenting and balloon angioplasty treat severe conditions, but restenosis often occurs. In fact, restenosis rates for stenting and balloon angioplasty with optional stenting were both over 45% 2 years after the initial intervention.[4] The extent of occlusions and resulting ischemic damage also fluctuates greatly among PAD patients, ranging from intermittent claudication to CLI. This variability contributes to difficulties with identifying a widespread treatment, demonstrated by only 40% of individuals being eligible for existing surgical procedures.[5] Ultimately, new medical interventions must be developed to overcome the limitations of current approaches for PAD.

Within the past 15 years, biomaterials have emerged as a therapeutic approach to fill the existing gaps in treatments (Table 2.1). To maximize therapeutic efficacy, biomaterials should be engineered according to specific design criteria, including material selection, mechanical properties, chemical properties, and so on. Design parameters and accompanying modifications are shown in Figure 2.2. This review will highlight design criteria and mechanisms of actions for biomaterial applications in PAD patients and will discuss the progress towards engineering

effective biomaterial-based therapies. These biomaterial applications will include material-alone approaches, as well the use of biomaterials as delivery vehicles for acellular biologics (Figure 2.1).

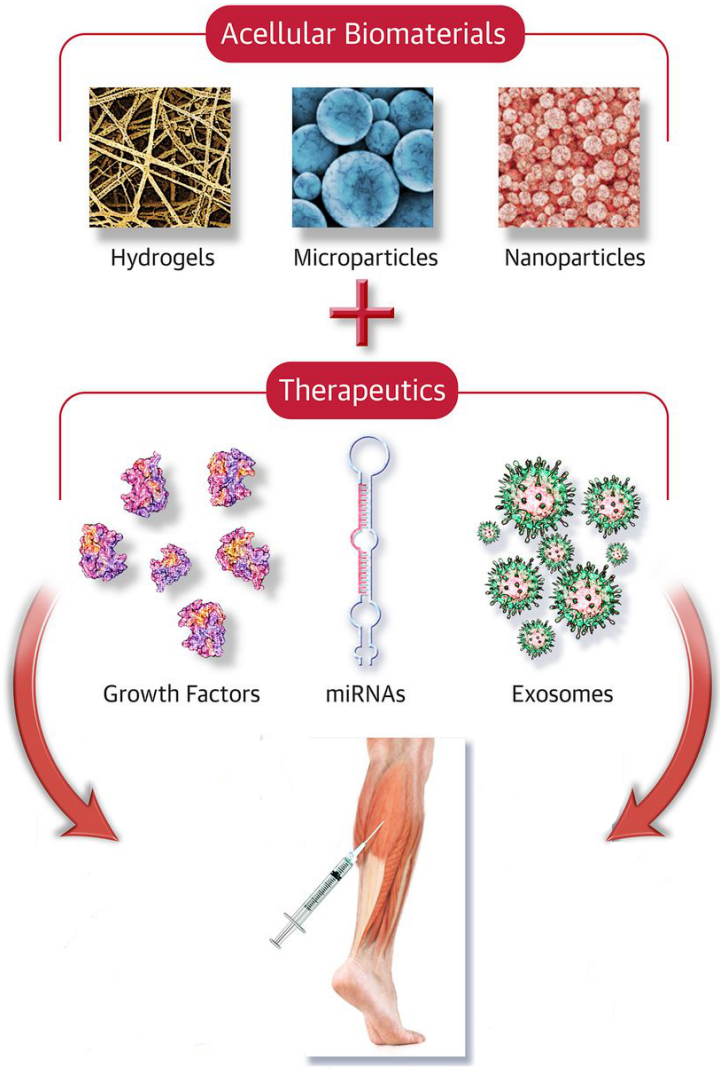

Hernandez, M.J. et al. J Am Coll Cardiol Basic Trans Science. 2017;2(2):212-26.

Figure 2.1 *Central Illustration*. Acellular Biomaterial Therapeutics for Repairing Ischemic Damage from PAD. Preclinical studies have currently been investigating biomaterial-alone therapies or biomaterials loaded with therapeutics as potential treatment options for peripheral artery disease (PAD). Other therapeutics, like microribonucleic acids (miRNAs) or exosomes, also show promise as factors to be delivered with a biomaterial. However, the success of these therapies largely depends on satisfying specific design criteria.

Table 2.1 Acellular injectable biomaterial applications for PAD

Material	Material Form	Biologics Delivered	Modifications	References
Alginate	Hydrogel; microspheres	IGF-1, VEGF; HGF; VEGF-F; SDF-1	Combination with poly(d,l-lactide-*co*-glycolide microspheres; sulfation; combination with collagen hydrogel	[16,28,31,35]
Chitosan	Hydrogel	FGF-2	Combination with lactose moieties and a periodate-oxidized IO_4 heparin solution	[22]
Collagen	Hydrogel; microsponges; microspheres	SDF-1; bFGF; bFGF, HGF	Combination with alginate microspheres	[25,28,33]
Decellularized skeletal muscle ECM	Hydrogel	N/A	N/A	[13,14]
Dextran	Nanoparticles	VEGF	Copolymerization with gelatin	[36]
Fibrin	Hydrogel; particles	FGF-2	Conjugation with heparin	[11,12,37]
Fucoidan	Hydrogel	FGF-2	N/A	[32]
Gelatin	Microspheres; hydrogel	FGF-4; bFGF; FGF-2; G-CSF	Crosslinking with poly-L-glutamic acid, crosslinking with poly-L-lysine	[19,21,23,24,26,27,29,30, 34,38]
PLGA based	Nanoparticles	FGF-2	N/A	[20]

Designing Acellular Injectable Biomaterial Therapies for PAD

Biomaterials Alone

Current experimental treatments for PAD, including stem cells and growth factors, have not been entirely successful, but biomaterials represent a potentially more promising approach in terms of translation and commercialization.[6] Biomaterial hydrogels allow for more precise treatment since the material remains localized upon injection unlike small molecule or protein therapeutics, which rapidly diffuse away from the injection site,[7,8] or cell injections, which also migrate and have poor survival.[9,10] Biomaterials alone also represent a more cost-effective option since incorporation of additional therapeutics can dramatically increase expenses. This approach has shown considerable promise for repairing ischemic muscle by encouraging reperfusion and neovascularization,[11-14] but the success of these biomaterials as a stand-alone

approach for PAD lies in satisfying particular design constraints (Table 2.1, Figure 2.2). Important design properties include material selection, physical properties, and degradation properties, but the design criteria vary for PAD and may fluctuate depending on the disease spectrum of the patient (i.e., intermittent claudication vs. CLI).

Beginning with material selection, which is extremely important for PAD to encourage perfusion restoration and muscle regeneration, biomaterials can be divided into two classes: natural and synthetic biomaterials. For eventual translation into PAD patients, factors like biocompatibility, manufacturing ease, and cost must be considered. For naturally derived biomaterials, two main advantages include the ability to mimic native biochemical cues and potentially more cost-effective manufacturing by avoiding complex chemical synthesis.

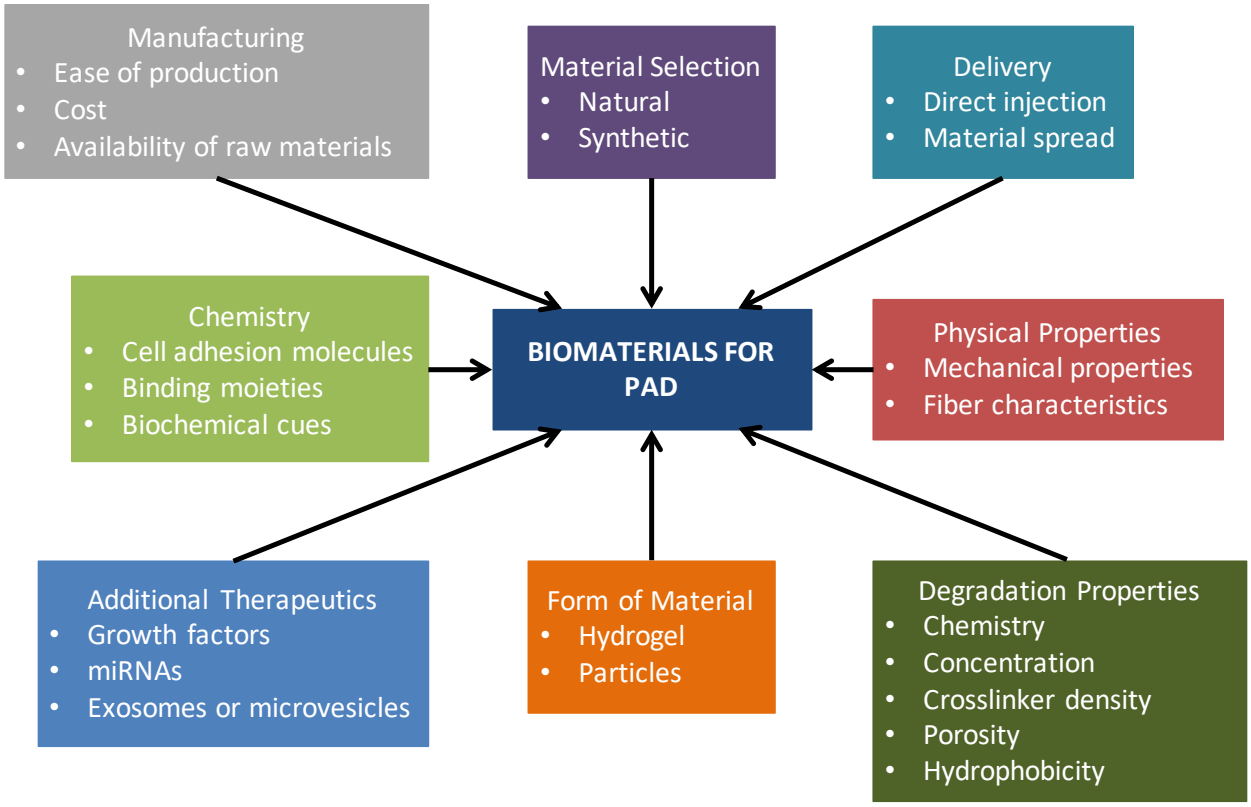

Figure 2.2 Design variables to be considered when developing biomaterial applications for PAD. To successfully translate biomaterials to the clinic, specific design criteria must be considered to ensure that the final product remains biocompatible while maintaining its full therapeutic efficacy. Extensive engineering of a biomaterial can maximize therapeutic benefits, but these benefits must counterbalance accompanied costs and manufacturing difficulties. miRNA = microribonucleic acid; PAD = peripheral artery disease.

However, naturally derived materials can suffer from batch-to-batch variability due to variations in biological sources. With synthetic biomaterials, the material properties can be customized more extensively, and there are fewer issues with limited availability of raw materials. Conversely, disadvantages include potential biocompatibility issues and difficulty replicating the complex native tissue structure. Regardless of these advantages and disadvantages, each biomaterial must be engineered or evaluated to promote cell infiltration and proliferation/differentiation to treat both the ischemia and muscle atrophy associated with PAD.[15] As such, the materials must allow for cell adhesion and have appropriate pore size for cell migration. Figure 2.3 illustrates an example of a cellular response to a biomaterial, specifically an alginate hydrogel.[16] Several preclinical studies have investigated naturally derived biomaterials like fibrin[11,12] and decellularized ECM hydrogels,[13,14] but synthetic biomaterials have yet to be studied in detail. Fibrin is well known to encourage vascularization and has likewise been shown in rabbit hindlimb ischemia models to increase perfusion;[11,12] however, only ECM

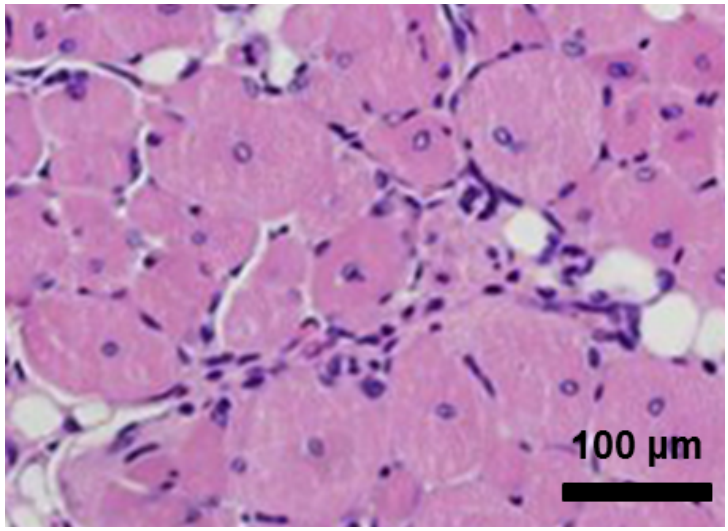

Figure 2.3 Cellular responses to an injected biomaterial. Upon injection of a biomaterial, the resulting cellular responses can largely affect eventual tissue regeneration. A hematoxylin and eosin image is shown for an alginate hydrogel in skeletal muscle (14 days post-injection). Reproduced with permission from Borselli et al.

hydrogels have been evaluated for muscle repair.[14] Chekanov et al.[11] utilized a fibrin sealant and observed significant increases in collateral vessel development and the area occupied by capillaries compared with no treatment or saline alone. Similarly, fibrin particles used by Fan et al.[12] yielded significantly augmented capillary density and perfusion recovery compared with control subjects. DeQuach et al.[13] utilized an injectable porcine-derived skeletal muscle ECM hydrogel in a rat hindlimb ischemia model and showed an increase not only in vascular cells, but also in proliferating muscle cells and muscle progenitor cells. Even after selecting a naturally derived material, however, the source for that material must still be chosen. With decellularized ECM hydrogels, for example, the tissue source can affect therapeutic outcomes. In a study conducted by Ungerleider et al.,[14] two different decellularized ECM hydrogels, a porcine-derived skeletal muscle ECM and human umbilical cord ECM, were assessed in a rat hindlimb ischemia model. Although improvements in perfusion were seen for both hydrogels, the muscles injected with the skeletal muscle ECM hydrogel resembled the healthy morphology more closely than those injected with the human umbilical cord matrix, suggesting that tissue-specific cues may be important for regeneration.

The last two design criteria to be discussed for a biomaterial-alone approach in PAD are degradation properties and delivery. The main factor to be considered for degradation properties is whether the biomaterial will yield sufficient therapeutic improvements before it completely degrades. Because PAD most often affects the lower limbs, the mechanical environment caused by a load-bearing region can cause biomaterials to degrade more quickly. As a result, appropriate animal models must be used to generate results that are representative of the human mechanical environment. For delivery of these therapeutics, direct intramuscular injections should be utilized (ideally #26-gauge for patients); however, the number and timing of these injections must be determined. Due to the large surface area of the lower limbs, multiple injections of the biomaterials will be necessary. Results from small animal studies can provide insight for the appropriate concentration and required volume of injections, but these results

must then be scaled up for larger animals and clinical studies. To date, limited work has been performed on developing a suitable large animal model, although a few recent studies suggest that this may be forthcoming.[17,18] Overall, there is still a great deal of research to be done for biomaterial-alone approaches in PAD; however, it is a promising approach that should be pursued.

Biomaterials and Growth Factors

Although biomaterial-alone approaches have not been extensively investigated for PAD, biomaterials have been utilized to deliver growth factors, as shown in Table 2.1.[16,19-38] To maximize therapeutic efficacy of a biomaterial and growth factor complex, design criteria, including selecting or engineering materials based on physical form, chemistry, and degradation properties, should be applied. Physical form, such as selecting particles as opposed to hydrogels, can alter the delivery method due to the ability to engineer particles for targeting (Figure 2.4). For chemical properties, modifications like binding moieties for growth factors, such as sulfate groups, can be added to encourage longer retention. Lastly, degradation plays an equally important role in controlling retention and release since rapid degradation will lead to a similar release rate for the therapeutic payload.

By incorporating these design principles, researchers have advanced some therapies into pre- clinical studies with rabbits and larger animal models and even one clinical trial. An early study conducted by Kasahara et al.[26] utilized gelatin microparticles to deliver fibroblast growth factor (FGF)-4 in a rabbit hindlimb ischemia model. Under vasodilatory conditions, the perfusion levels and angiographic scores were significantly higher in the gelatin/FGF-4 complex compared with gelatin or FGF-4 alone. In another study by Doi et al.,[21] gelatin hydrogels encapsulated with bFGF were injected intramuscularly in Japanese white rabbits 2 weeks post-hindlimb ischemia surgery. Animals treated with the gelatin and bFGF hydrogel had significantly

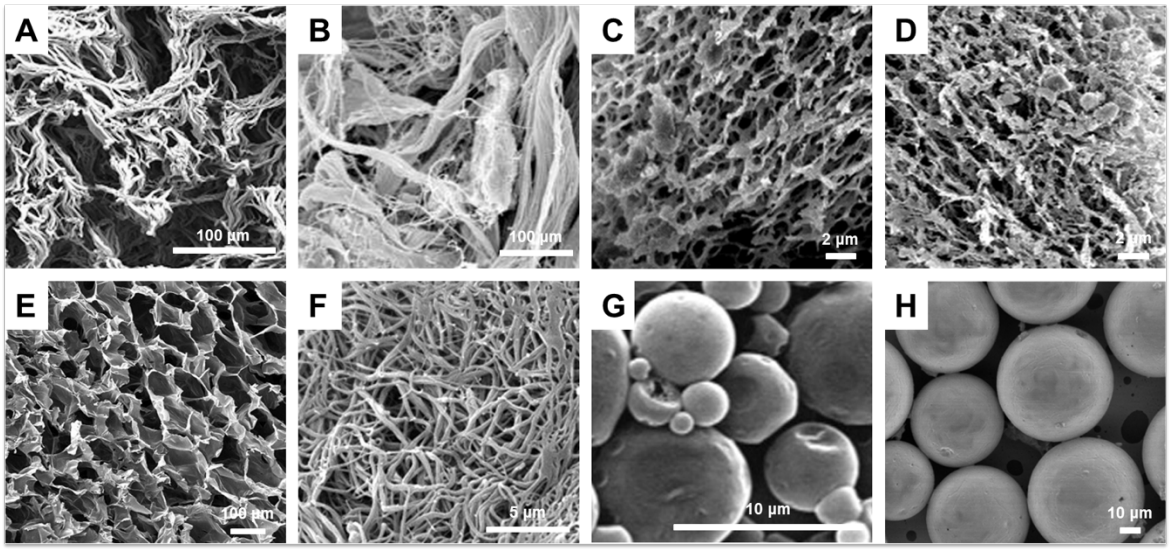

Figure 2.4 Structures of biomaterials for PAD applications.Biomaterial structures dictate important parameters including degradation and controlled release of therapeutics. The architecture, shown by scanning electron micrographs, varies among hydrogels, such as (A) keratin, (B) porcine-derived skeletal muscle extracellular matrix (ECM), (C) porcine-derived pericardial ECM, (D) collagen, (E) alginate, or (F) fibrin. Additionally, hydrogel architecture differs from particles like (G) poly(lactic-co-glycolic acid) microparticles or (H) acetalated dextran microparticles. Reproduced with permission from Shen et al., DeQuach et al., Seif-Naraghi et al., Freeman et al., Losi et al., Formiga et al., and Suarez et al. Abbreviations as in Figure 2.2.

higher perfusion levels and vascular density compared with no treatment or gelatin alone at 4 weeks post-injection. A large animal study performed in mongrel dogs by Zhao et al.[38] studied bFGF encapsulated in gelatin microspheres. Significantly higher capillary densities and numbers of mature vessels were observed with the gelatin microspheres and bFGF-treated group relative to bFGF alone and empty microspheres. The final study to be mentioned includes the findings of a phase I to IIa clinical trial. In a rabbit hindlimb ischemia model, Hirose et al.[23] injected gelatin hydrogel microspheres containing bFGF and saw increased perfusion, capillary density, and collateral vessel development compared with a no treatment control group. This led to an investigation by Marui et al.[34] in which biodegradable gelatin hydrogels loaded with bFGF were administered with a single intramuscular injection in patients with CLI; no controls were used for this study. At 4 and 24 weeks post-treatment, improvements were seen in the perfusion compared with values prior to treatment. By utilizing biomaterials as delivery vehicles, the

growth factor release can be precisely controlled, and biomaterials can prevent degradation of growth factors to fully harness their therapeutic potential.

Designing Biomaterials as Delivery Vehicles for Emerging Therapeutics

Although numerous studies presented in this review demonstrate the efficacy of utilizing biomaterials alone or a combination of growth factors and biomaterials for treating PAD, growth factors are not the only acellular therapeutic that should be considered for biomaterial-based therapies. Emerging therapeutics, such as exosomes or microribonucleic acids (miRNAs), may also enhance the beneficial properties of biomaterials, while avoiding obstacles plaguing cellular-based treatments. Previous studies investigated the efficacy of these therapeutics in PAD preclinical models,[39-44] but limited research has been conducted to optimize delivery. For exosomes, microvesicles, and miRNAs, maximized therapeutic efficiency has been hindered by poor retention upon injection. Because these therapeutics are typically injected alone, they rapidly diffuse from the injection site, similar to growth factors, therefore leading to minimal improvements in the targeted region.

This study emphasizes the importance of local delivery, but utilizing a biomaterial as a delivery vehicle is likely to further improve results. Because miRNAs are quickly degraded after injection due to the large amount of RNases circulating throughout the body, biomaterials can provide a shielded environment to maximize therapeutic effects. Additionally, the controlled release provided by biomaterials can also contribute to improved efficacy. Based on the current advancements in biomaterial-based therapies, many of the design principles discussed earlier could overcome these obstacles.

The physical form and chemistry of a biomaterial can significantly contribute to slower release kinetics in addition to providing a protected environment from degradation. By changing the physical form of the biomaterial, the release can be tuned for the specific payload, and

targeting can also be incorporated with particles. Additionally, altering the biomaterial's concentration often leads to changes in pore size, which can be utilized to change the release profile. The same microscale or nanoscale architecture being modified for desired release kinetics can also be used to protect the payload from degradation. In terms of the chemistry, modifications can be made to allow for better retention of additional therapeutics or release only upon cell infiltration.

Although no biomaterial-based therapies have been published for microvesicle or miRNA delivery in PAD, there are a few studies related to other applications, which validate the use of biomaterials for the delivery of these newer therapeutics. For bone repair, a miR-29a inhibitor, intended to increase ECM deposition, was delivered with gelatin nanofibers.[45] The investigators demonstrated the feasibility of this approach, as well as efficacy in terms of a slow release profile and sustained bioactivity of the miRNA inhibitor once released compared with a scrambled miRNA control. The Burdick lab has also begun investigating a hydrogel system for small interfering ribonucleic acid delivery,[46] but further studies are still ongoing. Therefore, this represents a promising area of research for improving the delivery of the next generation of therapeutics and should be explored for PAD.

Finding the Optimal Therapy for PAD Patients: Balancing Therapeutic Potential and Commercialization Challenges

Extensive research has validated the use of acellular biomaterials, but difficulties must still be overcome before implementation into the clinic. When considering incorporation of additional factors, an acellular approach is optimal for multiple reasons. Including cells dramatically reduces shelf life due to instability and significantly increases manufacturing expenses for a large-scale setting. The addition of growth factors encompasses many of these same issues, including reduced shelf life and high cost, but new manufacturing methods are

being studied to overcome these obstacles. For example, Cochran and colleagues[47] have developed an engineered HGF fragment with increased stability and lower cost of manufacturing, while maintaining its therapeutic effects. With new methods being optimized for growth factor delivery, these lower-cost options could result in more feasible biomaterial-based treatments for PAD patients.

As discussed earlier, biomaterials may also be delivered alone and have produced significant improvements in animal models of PAD. From a manufacturing perspective, a biomaterial-alone approach is the preferred method, as the increased costs and manufacturing time associated with additional therapeutics are negated. However, several studies previously mentioned suggest that a combinatorial approach may be more effective. Although current growth factor therapies may not be ideal for eventual translation to the clinic, due to difficult and expensive manufacturing, less expensive, engineered growth factors, like the one mentioned previously, or other therapeutics may augment the benefits of injectable biomaterials. The studies utilizing microvesicles, exosomes, or miRNAs alone have also demonstrated substantial therapeutic efficacy in PAD animal models, but more research must be done to optimize the delivery of these factors. In conclusion, research must be conducted to investigate the delivery of additional therapeutics with biomaterials, but the added therapeutic efficacy must outweigh the additional costs.

Conclusions

Acellular biomaterial-based therapies may be a solution for many patients experiencing PAD. By harnessing the ability to engineer these biomaterials and employing the minimally invasive nature of many of these therapies, patients may soon receive treatments designed to stimulate tissue regeneration and improved muscle function. Although further research must be conducted to develop optimal biomaterial strategies, and manufacturing expenses must be

carefully considered, the field is rapidly progressing towards identifying new treatments for PAD patients. The following chapters will discuss one potential biomaterial therapeutic for promoting muscle regeneration, its evaluation in two pre-clinical models, further augmentation of the material, and manufacturing considerations for eventual clinical translation.

Acknowledgements

The authors thank Raymond Wang, Jessica Ungerleider, and Vivienne Gunadhi for providing feedback and editing for this review. Funding was provided in part by the National Institutes of Health, National Heart, Lung, and Blood Institute grants R01HL113468 and R01HL117326 (to Dr. Christman). Ms. Hernandez was supported by National Institutes of Health, National Heart, Lung, and Blood Institute funded training grant T32HL105373. Dr. Christman is a cofounder of, consultant for, and board member of Ventrix, Inc.; and holds equity interest in Ventrix, Inc.

This chapter, in part, is a reprint of the material as it appears in the Journal of the American College of Cardiology: Basic to Translational Science 2017. The authors are Melissa J. Hernandez and Karen L. Christman. The dissertation author was the primary investigator of this material.

References

1. Bloom DE CE, Jané-Llopis E, Abrahams-Gessel S, Bloom LR, Fathima S, Feigl AB, Gaziano T, Mowafi M, Pandya A, Prettner K, Rosen- berg L, Seligman B, Stein AZ, Weinstein C. The Global Economic Burden of Non-communicable Diseases. *Geneva: World Economic Forum* (2011).

2. Global, regional, and national age-sex specific all-cause and cause-specific mortality for 240 causes of death, 1990-2013: a systematic analysis for the Global Burden of Disease Study 2013. *The Lancet* **385**, 117-171, doi:10.1016/S0140-6736(14)61682-2 (2015).

3. Allison MA, Ho E, Denenberg JO, Langer RD, Newman AB, Fabsitz RR, Criqui MH. Ethnic-specific prevalence of peripheral arterial disease in the United States. *Am J Prev Med* **32**, 328-333, doi:10.1016/j.amepre.2006.12.010 (2007).

4. Schillinger M, Sabeti S, Dick P, Amighi J, Mlekusch W, Schlager O, Loewe C, Cejna M, Lammer J, Minar E. Sustained benefit at 2 years of primary femoropopliteal stenting compared with balloon angioplasty with optional stenting. *Circulation* **115**, 2745-2749, doi:10.1161/CIRCULATIONAHA.107.688341 (2007).

5. Dormandy J, Heeck L, Vig S. The fate of patients with critical leg ischemia. *Semin Vasc Surg* **12**, 142-147 (1999).

6. Ungerleider JL, Christman KL. Concise review: injectable biomaterials for the treatment of myocardial infarction and peripheral artery disease: translational challenges and progress. *Stem Cells Transl Med* **3**, 1090-1099, doi:10.5966/sctm.2014-0049 (2014).

7. Laham RJ, Post M, Rezaee M, Donnell-Fink L, Wykrzykowska JJ, Lee SU, Baim DS, Sellke FW. Transendocardial and transepicardial intramyocardial fibroblast growth factor-2 administration: myocardial and tissue distribution. *Drug Metab Dispos* **33**, 1101-1107, doi:10.1124/dmd.104.002774 (2005).

8. Anitua E, Sanchez M, Orive G, Andia I. Delivering growth factors for therapeutics. *Trends Pharmacol Sci* **29**, 37-41, doi:10.1016/j.tips.2007.10.010 (2008).

9. Muller-Ehmsen J, Whittaker P, Kloner RA, Dow JS, Sakoda T, Long TI, Laird PW, Kedes L. Survival and development of neonatal rat cardiomyocytes transplanted into adult myocardium. *J Mol Cell Cardiol* **34**, 107-116, doi:10.1006/jmcc.2001.1491 (2002).

10. Zhang M, Methot D, Poppa V, Fujio Y, Walsh K, Murry CE. Cardiomyocyte grafting for cardiac repair: graft cell death and anti-death strategies. *J Mol Cell Cardiol* **33**, 907-921, doi:10.1006/jmcc.2001.1367 (2001).

11. Chekanov VS, Rayel R, Nikolaychik V, Kipshidze N, Baibekov I, Karakozov P, Bajwa T, Akhtar M. Direct fibrin injection to promote new collateral growth in hind limb ischemia in a rabbit model. *J Card Surg* **17**, 502-511; discussion 512 (2002).

12. Fan CL, Gao PJ, Gu YJ, Tang XF, Liu JJ, Wei J, Inoue K, Zhu DL. Therapeutic angiogenesis by intramuscular injection of fibrin particles into ischaemic hindlimbs. *Clin Exp Pharmacol Physiol* **33**, 617-622, doi:10.1111/j.1440-1681.2006.04416.x (2006).

13. DeQuach JA, Lin JE, Cam C, Hu D, Salvatore MA, Sheikh F, Christman KL. Injectable skeletal muscle matrix hydrogel promotes neovascularization and muscle cell infiltration in a hindlimb ischemia model. *Eur Cell Mater* **23**, 400-412; discussion 412 (2012).

14. Ungerleider JL, Johnson TD, Hernandez MJ, Elhag DI, Braden RL, Dzieciatkowska M, Osborn KG, Hansen KC, Mahmud E, Christman KL. Extracellular Matrix Hydrogel Promotes Tissue Remodeling, Arteriogenesis, and Perfusion in a Rat Hindlimb Ischemia Model. *JACC: Basic to Translational Science* **1**, 32-44, doi:10.1016/j.jacbts.2016.01.009 (2016).

15. Regensteiner JG, Wolfel EE, Brass EP, Carry MR, Ringel SP, Hargarten ME, Stamm ER, Hiatt WR. Chronic changes in skeletal muscle histology and function in peripheral arterial disease. *Circulation* **87**, 413-421 (1993).

16. Borselli C, Storrie H, Benesch-Lee F, Shvartsman D, Cezar C, Lichtman JW, Vandenburgh HH, Mooney DJ. Functional muscle regeneration with combined delivery of angiogenesis and myogenesis factors. *Proc Natl Acad Sci U S A* **107**, 3287-3292, doi:10.1073/pnas.0903875106 (2010).

17. Long CA, Sweet M, Chadid T, Koutakis P, Goodchild T, Lefer D, Pipinos I, Casale G, Taylor WR, Brewster L. A Novel Large-Animal Model of Peripheral Arterial Disease. *Journal of Vascular Surgery* **63**, 293-294, doi:10.1016/j.jvs.2015.10.045.

18. Stacy MR, Yu da Y, Maxfield MW, Jaba IM, Jozwik BP, Zhuang ZW, Lin BA, Hawley CL, Caracciolo CM, Pal P, Tirziu D, Sampath S, Sinusas AJ. Multimodality imaging approach for serial assessment of regional changes in lower extremity arteriogenesis and tissue perfusion in a porcine model of peripheral arterial disease. *Circ Cardiovasc Imaging* **7**, 92-99, doi:10.1161/CIRCIMAGING.113.000884 (2014).

19. Arai Y, Fujita M, Marui A, Hirose K, Sakaguchi H, Ikeda T, Tabata Y, Komeda M. Combined treatment with sustained-release basic fibroblast growth factor and heparin enhances neovascularization in hypercholesterolemic mouse hindlimb ischemia. *Circ J* **71**, 412-417 (2007).

20. Chappell JC, Song J, Burke CW, Klibanov AL, Price RJ. Targeted delivery of nanoparticles bearing fibroblast growth factor-2 by ultrasonic microbubble destruction for therapeutic arteriogenesis. *Small* **4**, 1769-1777, doi:10.1002/smll.200800806 (2008).

21. Doi K, Ikeda T, Marui A, Kushibiki T, Arai Y, Hirose K, Soga Y, Iwakura A, Ueyama K, Yamahara K, Itoh H, Nishimura K, Tabata Y, Komeda M. Enhanced angiogenesis by gelatin hydrogels incorporating basic fibroblast growth factor in rabbit model of hind limb ischemia. *Heart Vessels* **22**, 104-108, doi:10.1007/s00380-006-0934-0 (2007).

22. Fujita M, Ishihara M, Shimizu M, Obara K, Nakamura S, Kanatani Y, Morimoto Y, Takase B, Matsui T, Kikuchi M, Maehara T. Therapeutic angiogenesis induced by controlled release of fibroblast growth factor-2 from injectable chitosan/non-anticoagulant heparin hydrogel in a rat hindlimb ischemia model. *Wound Repair Regen* **15**, 58-65, doi:10.1111/j.1524-475X.2006.00185.x (2007).

23. Hirose K, Fujita M, Marui A, Arai Y, Sakaguchi H, Huang Y, Chandra S, Tabata Y, Komeda M. Combined treatment of sustained-release basic fibroblast growth factor and sarpogrelate enhances collateral blood flow effectively in rabbit hindlimb ischemia. *Circ J* **70**, 1190-1194 (2006).

24. Huang Y, Marui A, Sakaguchi H, Esaki J, Arai Y, Hirose K, Bir SC, Horiuchi H, Maruyama T, Ikeda T, Tabata Y, Komeda M. Sustained release of prostaglandin E1 potentiates the impaired therapeutic angiogenesis by basic fibroblast growth factor in diabetic murine hindlimb ischemia. *Circ J* **72**, 1693-1699 (2008).

25. Kanematsu A, Marui A, Yamamoto S, Ozeki M, Hirano Y, Yamamoto M, Ogawa O, Komeda M, Tabata Y. Type I collagen can function as a reservoir of basic fibroblast growth factor. *Journal of Controlled Release* **99**, 281-292, doi:10.1016/j.jconrel.2004.07.008 (2004).

26. Kasahara H, Tanaka E, Fukuyama N, Sato E, Sakamoto H, Tabata Y, Ando K, Iseki H, Shinozaki Y, Kimura K, Kuwabara E, Koide S, Nakazawa H, Mori H. Biodegradable gelatin hydrogel potentiates the angiogenic effect of fibroblast growth factor 4 plasmid in rabbit hindlimb ischemia. *J Am Coll Cardiol* **41**, 1056-1062 (2003).

27. Kawamura I, Takemura G, Tsujimoto A, Watanabe T, Kanamori H, Esaki M, Kobayashi H, Takeyama T, Kawaguchi T, Goto K, Maruyama R, Fujiwara T, Fujiwara H, Tabata Y, Minatoguchi S. Treatment of leg ischemia with biodegradable gelatin hydrogel microspheres incorporating granulocyte colony-stimulating factor. *J Cardiovasc Pharmacol* **57**, 416-423, doi:10.1097/FJC.0b013e31820c9776 (2011).

28. Kuraitis D, Zhang P, Zhang Y, Padavan DT, McEwan K, Sofrenovic T, McKee D, Zhang J, Griffith M, Cao X, Musaro A, Ruel M, Suuronen EJ. A stromal cell-derived factor-1 releasing matrix enhances the progenitor cell response and blood vessel growth in ischaemic skeletal muscle. *Eur Cell Mater* **22**, 109-123 (2011).

29. Layman H, Sacasa M, Murphy AE, Murphy AM, Pham SM, Andreopoulos FM. Co-delivery of FGF-2 and G-CSF from gelatin-based hydrogels as angiogenic therapy in a murine critical limb ischemic model. *Acta Biomaterialia* **5**, 230-239, doi:10.1016/j.actbio.2008.07.024 (2009).

30. Layman H, Spiga M-G, Brooks T, Pham S, Webster KA, Andreopoulos FM. The effect of the controlled release of basic fibroblast growth factor from ionic gelatin-based hydrogels on angiogenesis in a murine critical limb ischemic model. *Biomaterials* **28**, 2646-2654, doi:10.1016/j.biomaterials.2007.01.044 (2007).

31. Lee J, Bhang SH, Park H, Kim BS, Lee KY. Active blood vessel formation in the ischemic hindlimb mouse model using a microsphere/hydrogel combination system. *Pharm Res* **27**, 767-774, doi:10.1007/s11095-010-0067-0 (2010).

32. Luyt CE, Meddahi-Pelle A, Ho-Tin-Noe B, Colliec-Jouault S, Guezennec J, Louedec L, Prats H, Jacob MP, Osborne-Pellegrin M, Letourneur D, Michel JB. Low-molecular-weight fucoidan promotes therapeutic revascularization in a rat model of critical hindlimb ischemia. *J Pharmacol Exp Ther* **305**, 24-30, doi:10.1124/jpet.102.046144 (2003).

33. Marui A, Kanematsu A, Yamahara K, Doi K, Kushibiki T, Yamamoto M, Itoh H, Ikeda T, Tabata Y, Komeda M. Simultaneous application of basic fibroblast growth factor and hepatocyte growth factor to enhance the blood vessels formation. *J Vasc Surg* **41**, 82-90, doi:10.1016/j.jvs.2004.10.029 (2005).

34. Marui A, Tabata Y, Kojima S, Yamamoto M, Tambara K, Nishina T, Saji Y, Inui K, Hashida T, Yokoyama S, Onodera R, Ikeda T, Fukushima M, Komeda M. A novel approach to therapeutic angiogenesis for patients with critical limb ischemia by sustained release of basic fibroblast growth factor using biodegradable gelatin hydrogel: an initial report of the phase I-IIa study. *Circ J* **71**, 1181-1186 (2007).

35. Ruvinov E, Leor J, Cohen S. The effects of controlled HGF delivery from an affinity-binding alginate biomaterial on angiogenesis and blood perfusion in a hindlimb ischemia model. *Biomaterials* **31**, 4573-4582, doi:10.1016/j.biomaterials.2010.02.026 (2010).

36. Xie J, Wang H, Wang Y, Ren F, Yi W, Zhao K, Li Z, Zhao Q, Liu Z, Wu H, Gu C, Yi D. Induction of angiogenesis by controlled delivery of vascular endothelial growth factor using nanoparticles. *Cardiovasc Ther* **31**, e12-18, doi:10.1111/j.1755-5922.2012.00317.x (2013).

37. Yang HS, Bhang SH, Hwang JW, Kim DI, Kim BS. Delivery of basic fibroblast growth factor using heparin-conjugated fibrin for therapeutic angiogenesis. *Tissue Eng Part A* **16**, 2113-2119, doi:10.1089/ten.TEA.2009.0673 (2010).

38. Zhao Y, Liu Z, Pan C, Li Z, Zhou J, Wang J, Yin Z, Wang X. Preparation of gelatin microspheres encapsulated with bFGF for therapeutic angiogenesis in a canine ischemic hind limb. *J Biomater Sci Polym Ed* **22**, 665-682, doi:10.1163/092050610X489880 (2011).

39. Bonauer A, Carmona G, Iwasaki M, Mione M, Koyanagi M, Fischer A, Burchfield J, Fox H, Doebele C, Ohtani K, Chavakis E, Potente M, Tjwa M, Urbich C, Zeiher AM, Dimmeler S. MicroRNA-92a controls angiogenesis and functional recovery of ischemic tissues in mice. *Science* **324**, 1710-1713, doi:10.1126/science.1174381 (2009).

40. Ranghino A, Cantaluppi V, Grange C, Vitillo L, Fop F, Biancone L, Deregibus MC, Tetta C, Segoloni GP, Camussi G. Endothelial progenitor cell-derived microvesicles improve neovascularization in a murine model of hindlimb ischemia. *Int J Immunopathol Pharmacol* **25**, 75-85 (2012).

41. Zhang HC, Liu XB, Huang S, Bi XY, Wang HX, Xie LX, Wang YQ, Cao XF, Lv J, Xiao FJ, Yang Y, Guo ZK. Microvesicles derived from human umbilical cord mesenchymal stem cells stimulated by hypoxia promote angiogenesis both in vitro and in vivo. *Stem Cells Dev* **21**, 3289-3297, doi:10.1089/scd.2012.0095 (2012).

42. Hazarika S, Farber CR, Dokun AO, Pitsillides AN, Wang T, Lye RJ, Annex BH. MicroRNA-93 controls perfusion recovery after hindlimb ischemia by modulating expression of multiple genes in the cell cycle pathway. *Circulation* **127**, 1818-1828, doi:10.1161/CIRCULATIONAHA.112.000860 (2013).

43. Endo-Takahashi Y, Negishi Y, Nakamura A, Ukai S, Ooaku K, Oda Y, Sugimoto K, Moriyasu F, Takagi N, Suzuki R, Maruyama K, Aramaki Y. Systemic delivery of miR-126 by miRNA-loaded Bubble liposomes for the treatment of hindlimb ischemia. *Scientific Reports* **4**, 3883, doi:10.1038/srep03883 (2014).

44. Hu GW, Li Q, Niu X, Hu B, Liu J, Zhou SM, Guo SC, Lang HL, Zhang CQ, Wang Y, Deng ZF. Exosomes secreted by human-induced pluripotent stem cell-derived mesenchymal stem cells attenuate limb ischemia by promoting angiogenesis in mice. *Stem Cell Res Ther* **6**, 10, doi:10.1186/scrt546 (2015).

45. James EN, Delany AM, Nair LS. Post-transcriptional regulation in osteoblasts using localized delivery of miR-29a inhibitor from nanofibers to enhance extracellular matrix deposition. *Acta Biomater* **10**, 3571-3580, doi:10.1016/j.actbio.2014.04.026 (2014).

46. Wang LL, Sloand JN, Gaffey AC, Venkataraman CM, Wang Z, Trubelja A, Hammer DA, Atluri P, Burdick JA. Injectable, Guest-Host Assembled Polyethylenimine Hydrogel for siRNA Delivery. *Biomacromolecules* **18**, 77-86, doi:10.1021/acs.biomac.6b01378 (2017).

47. Liu CJ, Jones DS, 2nd, Tsai PC, Venkataramana A, Cochran JR. An engineered dimeric fragment of hepatocyte growth factor is a potent c-MET agonist. *FEBS Lett* **588**, 4831-4837, doi:10.1016/j.febslet.2014.11.018 (2014).

Chapter 3. Dose Optimization of Decellularized Skeletal Muscle Extracellular Matrix Hydrogels for Improving Perfusion and Subsequent Validation in an Aged Hindlimb Ischemia Model

Introduction

Peripheral artery disease (PAD) can be categorized into two main classifications – intermittent claudication and critical limb ischemia (CLI). For individuals with CLI, the more severe form of PAD, patients experience fatigue while at rest, and the lack of blood flow to the skeletal muscle can result in muscle atrophy, muscle fiber loss and damage, denervation, and may necessitate amputation. In fact, amputations become necessary for 120,000 patients in the United States and 100,000 patients in the European Union.[1] Current treatment strategies for these patients include endovascular procedures, such as atherectomies or balloon angioplasty with or without stenting, or surgical approaches, like bypass grafting. However, due in part to the diffuse nature of the condition, only 40% of patients are eligible for existing procedures,[2] and restenosis rates may exceed 45% following these interventions.[3]

To overcome the challenges associated with treating PAD patients, biomaterials have been investigated as a possible solution, as mentioned in the previous chapter.[4,5] Specifically, biomaterial-alone approaches have utilized a decellularized skeletal muscle extracellular matrix (ECM) hydrogel,[6,7] fibrin,[8] and fucoidan.[9] In particular, decellularized ECM has been studied extensively for regenerative medicine applications due to its ability to mimic the biochemical cues of the native ECM[10,11] and its degradation products, which are angiogenic[12] and promote cell migration and proliferation.[12-18] In one study, a decellularized skeletal muscle ECM hydrogel at a concentration of 6 mg/mL demonstrated efficacy in a rat hindlimb ischemia model of PAD.[7] With a single intramuscular injection of the ECM hydrogel administered one week post-hindlimb

ischemia surgery, an increase in blood perfusion relative to a saline control was observed, which was attributed to increases in arteriogenesis.[7]

Although the efficacy of the skeletal muscle ECM hydrogel has been shown, an optimal concentration has not been investigated. In another study, a higher concentration of the skeletal muscle ECM hydrogel (8 mg/mL) was used to improve cellular retention and survival of myoblasts and fibroblasts in a mouse hindlimb ischemia model, but the higher concentration was not investigated independently of the cells.[19] Altering the material concentration could impact both the density of biochemical cues as well as the physical properties of the material, both of which could impact the biological response. Therefore, determining an optimal concentration of the skeletal muscle ECM hydrogel could be critical for enhancing therapeutic outcomes. In addition to investigating the efficacy of various concentrations of the ECM hydrogel, it is also paramount to evaluate these materials in more relevant animal models. Many regenerative medicine applications, such as cells and growth factors, have been investigated in Phase I clinical trials, but the majority of these studies have failed, likely due in part to the use of poor animal models in pre-clinical studies. For PAD, in particular, pre-clinical studies have mainly utilized young rodents or rabbits, which fail to accurately depict the pathophysiology of PAD patients. Additionally, certain risk factors, including age, diabetes, smoking, hypertension, and hypercholesterolemia, lead to an increased prevalence of PAD. In particular, the prevalence of PAD increases by age group – 1.43% for 40-49 years, 3.41% for 50-59 years, 7.77% for 60-69 years, and 16.62% for 70 years and older.[20] Aging has been shown to impair essential biological processes[21] such as angiogenesis,[22,23] vasculogenesis,[23] innervation,[24,25] and satellite cell activity[26-28] and may also contribute to increased muscle fibrosis.[27,29,30] Therefore, it is necessary to evaluate these hydrogels in an animal model that is more representative of human pathophysiology. Many hindlimb ischemia studies utilize younger animals, but young rodents possess remarkable regenerative capabilities. As a result, these young rodents can regenerate regardless of intervention, which makes it difficult to determine the full potential of a therapeutic.

Here we performed a dose optimization study with three concentrations (4, 6, and 8 mg/mL) of a decellularized skeletal muscle ECM hydrogel. We evaluated the physical properties of these hydrogels with rheological measurements and imaging of the nanofibrous architectures. In addition, the material retention and *in vivo* spread was evaluated prior to performing hindlimb ischemia surgeries in young rats. The optimal concentration was then further examined in an aged mouse hindlimb ischemia model. These results further demonstrate the translational potential of a decellularized skeletal muscle ECM hydrogel for PAD patients.

Material and Methods

All experiments in this study were performed in accordance with the guidelines established by the Institutional Animal Care and Use Committee at the University of California San Diego and the American Association for Accreditation of Laboratory Animal Care.

Material processing

Based on previously published protocols,[31,32] longissimus dorsi muscles, commonly known as pork loin, were obtained from Yorkshire farm pigs (4-7 months old, S&S Farms) from the UC San Diego medical school. Briefly, the muscle was harvested, frozen for a minimum of 24 hours, and then chopped into 0.5 cm^3 pieces. Tissue was decellularized for 4-5 days in a solution of 1% wt/vol sodium dodecyl sulfate (SDS) in 1X phosphate buffered saline (PBS) with 10,000 U penicillin/streptomycin (ThermoFisher Scientific, Waltham, MA), placed in isopropanol for 18-24 hours to remove residual lipids, and then rinsed in water for another 24 hours. The tissue was then removed, frozen at -80°C, lyophilized, and milled using a Wiley Mini-Mill (Thomas Scientific, Swedesboro, NJ) with a #60 filter. The milled powder was then partially digested with pepsin (Sigma-Aldrich, St. Louis, MO) in 0.1 M HCl (1 mg/mL) at a final concentration of 10 mg ECM/1 mL pepsin solution for 48 hours. Following digestion, the ECM

solution was neutralized to pH 7.4 and adjusted to 1X PBS for 4, 6, and 8 mg/mL concentrations. Aliquots were then lyophilized once more for long-term storage at -80°C.

Resuspension of ECM hydrogels

Lyophilized aliquots of the decellularized skeletal muscle ECM hydrogels were resuspended to their respective concentrations with deionized (DI) water (i.e. 300 µL DI water for a 2 mg ECM aliquot for 6 mg/mL concentration). The lyophilized particulates were initially broken up by pipetting up and down gently, and the aliquots were then left on ice for ~10 minutes to allow for the material to solubilize. After 10 minutes, the aliquots were fully resuspended by pipetting the mixture until no large particulates remained. A 25G syringe was then used to shear the material further, which ultimately yielded a homogenous liquid.

Scanning electron microscopy

Prior to performing scanning electron microscopy (SEM), 300 µL of each concentration of the skeletal muscle ECM hydrogels were prepared according to section 2.2. Gels were formed by incubating at 37°C for 24 hours. Each gel was then fixed for 24 hours in an aqueous mixture of EM-grade 4% paraformaldehyde and 4% glutaraldehyde. Following fixation, the gels were then dehydrated with a series of ethanol rinses (30%, 50%, 75%, 90%, and 100%), each one lasting 30 minutes. Once the dehydration was complete, the ethanol was aspirated from the gels, and the gels were suspended in isopropyl alcohol. Fixed and dehydrated hydrogels were then loaded into Teflon sample holders and processed in an AutoSamdri 815A automated critical point drier (Tousimis, Rockville, MD). The protocol included 40 exchange cycles of CO_2 at medium speed and 40% stirring. The fill and heating steps were performed at slow speed, while the venting step was performed at medium speed. Mounted samples were then sputter coated using a Leica EM SCD500 (Leica Microsystems, Wetzlar, Germany) with approximately

7 nm of iridium while being rotated. The samples were then imaged on a FEI Quanta 250 FEG scanning electron microscope (ThermoFisher Scientific, Waltham, MA) at 3 kV using the in-lens SE1 detector.

Rheometry

To perform complex viscosity measurements, 200 µL of resuspended ECM was pipetted onto the stage of a parallel plate ARG2 rheometer (TA Instruments, New Castle, DE). With a fixed plate temperature set to 25°C to maintain a liquid solution and the gap height adjusted to 500 µm, a flow procedure was run with shear rates varying from 0.1 to 100 Hz. To ensure delivery via syringe, the materials were assessed for shear thinning properties.

To determine the storage and loss moduli, 500 µL of the ECM mixtures were pipetted into 4 mL scintillation vials and allowed to gel at 37°C for 24 hours. The hydrogels were then carefully removed and placed on the rheometer stage with a fixed plate temperature of 37°C. The gap height was then adjusted to 1100 µm, and an oscillatory sweep run was performed with the frequency ranging from 0.1 to 100 rad/s. Values for the storage and loss moduli were reported at 1 rad/s.

Animals

For the material retention and dose optimization studies, female Sprague Dawley rats (~10 weeks, Charles River, Wilmington, MA) were used. Male C57BL/6 mice (~32 weeks, Jackson Laboratory, Bar Harbor, ME) were utilized for the aged hindlimb ischemia study. All animals were provided with food and water *ad libitum*.

Material spreading and retention

An Alexa Fluor™ 568 NHS ester (succinimydl ester) dye was prepared by diluting the lyophilized powder to 10 mg/mL in sterile dimethyl sulfoxide (DMSO). Sterile ECM aliquots were then resuspended as described in section 2.2. The dye was mixed with the resuspended ECM according to the following ratios to account for the varying ECM protein concentrations: 6.7 µL/1 mL 4 mg/mL ECM, 10 µL dye/1 mL 6 mg/mL ECM, and 13.3 µL/1 mL 8 mg/mL ECM. Once thoroughly mixed by pipetting, the solutions were left on ice in the dark for 1 hour to allow the dye to conjugate to the primary amines of the proteins. Syringes with a 27G needle were prepared with 150 µL of one of the three concentrations and kept in the dark until use.

Healthy rats (n=2/concentration) were anesthetized with isoflurane (VetOne, Boise, ID), and the anterior sides of both hindlimbs were prepared for injections. While extending the limb with one hand, 150 µL of the ECM hydrogel was injected at a ~30° angle into the middle of the gracilis muscle over approximately 30 seconds. The needle was then held in place for another 15 seconds to prevent the material from leaking out. This injection procedure was repeated for both hindlimbs with the same concentration used on both sides.

At 1 and 2 weeks post-injection, the rats were euthanized with an intraperitoneal injection of 200 mg/kg Fatal-Plus® (Vortech Pharmaceuticals, Dearborn, MI). Both gracilis muscles (n=4/concentration) were harvested and flash frozen in liquid nitrogen-chilled 2-methylbutane. The muscles were then allowed to freeze at -80°C for a minimum of 24 hours before individually embedding the muscles in Tissue-Tek® O.C.T. (Sakura Finetek, Torrance, CA) and once again flash freezing the samples in liquid nitrogen-chilled 2-methylbutane.

Samples were cryosectioned into 10-µm thick sections on a Leica CM3050 S cryostat (Leica Biosystems, Nussloch, Germany). A total of 13 evenly-spaced locations were sampled. One microscope slide from each location was then stained with Hoechst 33342 (1 µL/10 mL DI water, ThermoFisher Scientific, Waltham, MA). Slides were dried overnight before imaging with

an Ariol DM6000 B microscope (Leica Microsystems, Wetzlar, Germany). An overview image was captured for each microscope slide, and ImageJ was then used to manually outline the entire tissue section based on the blue channel. The material in the red channel was then individually thresholded for each image, and the areas of the entire tissue section and labelled material were extracted for analysis. Calculations were performed to quantify the ECM hydrogel at each location and for the entire muscle.

Hindlimb ischemia surgery

Animals were anesthetized with isoflurane and then placed in a supine position on a DSx vented warming table (VetEquip, Livermore, CA). Prior to beginning the surgery, a subcutaneous injection of 0.05 mg/kg buprenorphine (Pfizer, New York, NY) was administered and a 1% lidocaine (Hospira, Lake Forest, IL) line block was injected along the right hindlimb. In addition, 0.5 mL (mouse) or 3 mL (rat) of lactated ringers (B. Braun Medical, Melsungen, Germany) were administered subcutaneously to keep the animals hydrated. The right hindlimb was shaved and disinfected with Betadine (Purdue Pharma L.P., Stamford, CT) and 70% isopropanol. Sterile saline was used throughout the surgery to keep the tissues from drying out. An incision was made through the skin beginning in the inguinal region and extending along the visible femoral vessels to the branch of the saphenous. Fat in the inguinal regions was cauterized to improve visibility, and the nerve was then carefully dissected from the vessels. A 5-0 Solfsilk suture (Covidien, Dublin, Ireland) was used for permanent occlusion of the arteries and veins. Two ligatures were placed proximal to the branch of the saphenous vessels, one ligature each was placed on the popliteal and genicular vessels, and two ligatures were placed around the lateral circumflex femoral vessels distal to the inguinal ligament. The vessels were carefully transected between the occlusion points, and all other vessels were cauterized as needed. The skin was then closed with 5-0 monocryl (Ethicon, Somerville, NJ) for the mice and 9 mm autoclips (MikRon Precision Inc., Gardena, CA) for the rats. Lastly, another 1% lidocaine

line block was injected subcutaneously and triple antibiotic ointment (Activis, Parsipanny-Troy Hills, NJ) was applied. Animals were then immediately transferred for blood perfusion imaging.

Laser speckle contrast analysis imaging

To monitor the blood perfusion levels in the hindlimbs, laser speckle contrast analysis (LASCA) imaging was utilized.[7,33,34] All recordings were performed with a PeriCam PSI System (Perimed, Stockholm, Sweden) using the following settings: ~20 cm working distance, high point density, 19 images/s frame rate, recorded with averaging of 60 images, and effective frame rate of 0.3 images/s. Animals were anesthetized with isoflurane, transferred to a face mask on a heated deck (Hallowell EMC, Pittsfield, MA) and placed in a prone position. Prior to beginning a recording, regions of interest (ROIs) were placed around both paws, with particular attention paid to avoid including extra fur with the rats. Imaging was continued until the blood perfusion values plateaued, which typically occurred around 20 minutes. All animals were imaged immediately pre- and post-hindlimb ischemia surgery to ensure the blood perfusion levels in both paws were similar (<30% difference) prior to surgery and to confirm the hindlimb ischemia surgeries decreased the blood perfusion in the right (ischemic) paw. Rat perfusion levels were recorded on days -2, 7, 21, and 35, and mouse perfusion levels were recorded on days -2, 3, 7, 14, 21, and 28. All perfusion values are reported relative to the left (healthy) paw.

Intramuscular injections

One week post-hindlimb ischemia surgery (Day 0), the skeletal muscle ECM hydrogel (n=7 or 8 for rats; n=6 for mice) or saline (n=8 for rats; n=6 for mice) was injected intramuscularly. Animals were randomized according to day -7 and -2 blood perfusion measurements to ensure no significant differences existed between experimental groups prior to the injection. The ECM hydrogels were resuspended under aseptic conditions as described in section 2.2, and a 27G needle was used for all of the injections. Animals were anesthetized with

5% isoflurane, transferred to a heated deck with a face mask, and then placed in a supine position. For the rats, both hindlimbs were extended to fully expose the gracilis muscles, the paws were taped down, and any remaining staples were removed from the right (ischemic) hindlimb. The needle was inserted at the medial point of the suture line at a ~30° angle, and 150 µL of saline or ECM were injected into the right (ischemic) gracilis muscle. For the mice, the right paw was held with the knee at a 120° angle, and 25 µL of saline or ECM were injected at a ~15° angle into the tibialis anterior muscle. Material injections were performed over ~30 seconds, and the needle was left in place for ~15 seconds after the injection to ensure material would not leak out.

Statistical analysis

Results are reported as mean ± SEM. Prism 8 (GraphPad Software, San Diego, CA) was utilized for all statistical analyses. For the mechanical properties and material retention experiments, a one-way ANOVA with a Tukey's post hoc test was used to assess the three ECM hydrogel concentrations. Blood perfusion improvements (day -2 vs. day 35) from the rat hindlimb ischemia study were analyzed with a one-way ANOVA with a Dunnet's post hoc test, and the aged mouse hindlimb ischemia study utilized an unpaired Student's t-test for the day 28 perfusion measurements. Significance for all statistical tests was accepted at $p < 0.05$.

Results and Discussion

Physical properties

For processing the decellularized skeletal muscle ECM hydrogels, a digestion procedure was used, which was based on an existing protocol for the manufacturing of a decellularized myocardial ECM hydrogel. With this digestion procedure, which is performed at 10 mg/mL, it is difficult to reliably achieve concentrations much higher than 8 mg/mL, and higher concentrations

pose difficulties with injecting through high gauge needles. Subcutaneous injections of the ECM hydrogels at concentrations of 2 mg/mL, 4 mg/mL, 6 mg/mL, and 8 mg/mL (data not shown) demonstrated that the 2 mg/mL hydrogel did not sufficiently gel and instead diffused quickly following the injection. As a result, only skeletal muscle ECM hydrogels with a concentration of 4 mg/mL, 6 mg/mL, or 8 mg/mL were investigated in this study.

Physical properties and biochemical cues, both of which change with differing concentrations, represent possible mechanisms by which biomaterials may promote regeneration. Therefore, identifying an optimal concentration was necessary to confirm whether various concentrations of an ECM hydrogel impacted *in vivo* efficacy. To first investigate the physical properties of the ECM hydrogels, SEM images were collected to examine the nanofibrous architecture of the ECM hydrogels (Figure 3.1). As the concentration of the ECM hydrogels and therefore ECM proteins increased, the proteins became more densely packed together. The fibers in the 4 mg/mL hydrogel were less densely packed, whereas the 8 mg/mL ECM hydrogel was more densely packed, and the nanofibers were more closely aligned. The architecture of the 6 mg/mL ECM hydrogel was more densely packed than the 4 mg/mL ECM hydrogel but less so than the 8 mg/mL ECM hydrogel. Since the samples were dehydrated as part of the preparation process for SEM imaging, the ECM proteins likely collapsed to some degree, and, consequently the images cannot fully recapitulate how these hydrogels appear *in vivo*. Nonetheless, the increased packing density of the ECM proteins in the higher

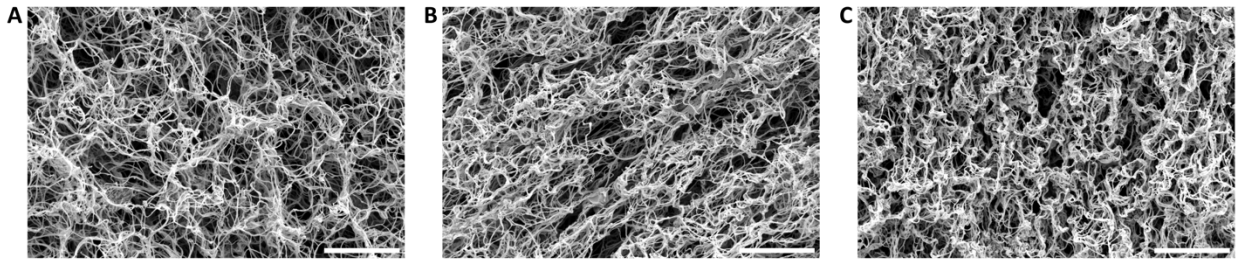

Figure 3.1 Scanning electron microscopy images demonstrated the nanofibrous architecture of (A) 4 mg/mL, (B) 6 mg/mL, and (C) 8 mg/mL decellularized skeletal muscle ECM hydrogels.Scale bar is 5 μm.

concentration ECM hydrogels could affect a cell's ability to infiltrate the material and begin remodelling the environment.

The three concentrations of the skeletal muscle ECM hydrogels were also probed for their mechanical properties. Gels were formed for each of the three concentrations, and rheological measurements were obtained. The higher values for the storage modulus over the loss modulus indicated that all three concentrations were in fact hydrogels (Figure 3.2). At 1 rad/s, the values for the storage and loss moduli increased in conjunction with the higher concentrations of the skeletal muscle ECM hydrogel. Statistical analyses for these values yielded significant differences for all comparisons, excluding the 4 mg/mL and 6 mg/mL ECM hydrogels for the loss modulus. These results were expected based on the increased amount of ECM proteins associated with the higher concentrations, and the higher packing density observed in the SEM images also supports these outcomes.

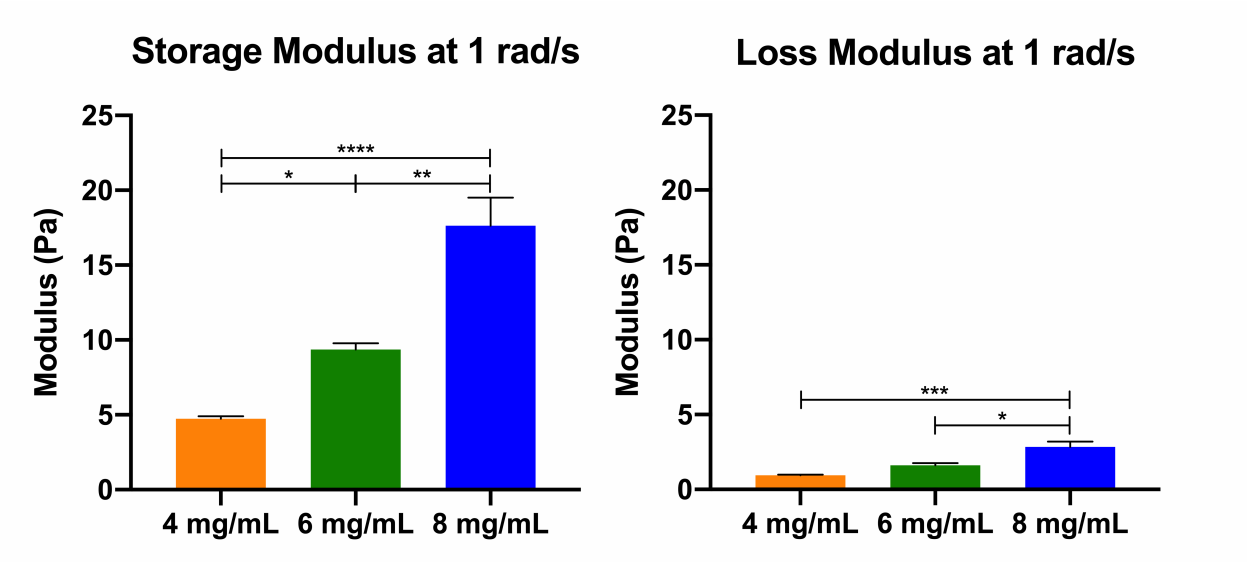

Figure 3.2 Storage and loss moduli values increased with the higher concentrations of the ECM hydrogels.*p < 0.05, **p < 0.01, ***p < 0.001, ****p < 0.0001. Data are mean ± SEM.

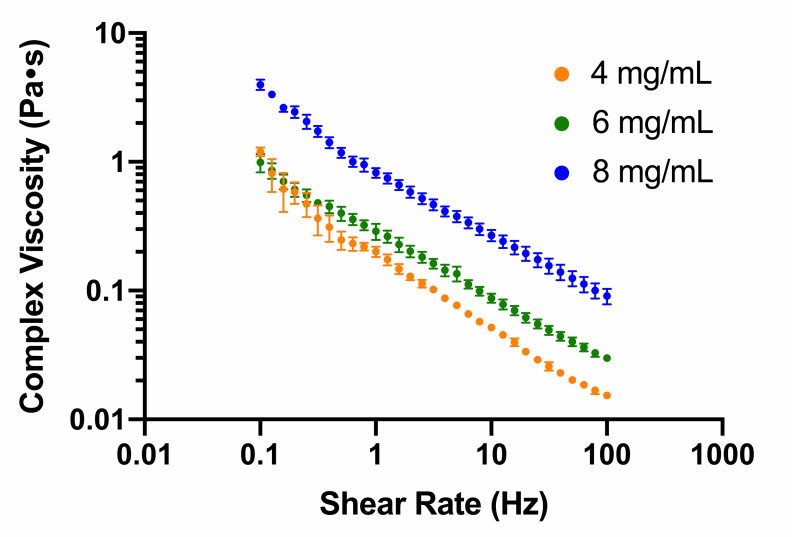

Figure 3.3 Viscosity measurements for all three ECM hydrogels demonstrated shear thinning properties.Data are mean ± SEM.

In addition to the storage and loss moduli measurements, viscosity data was also collected on a rheometer (Figure 3.3). Viscosity measurements were performed with the liquid form of the ECM hydrogels to ensure each concentration would retain its shear thinning properties, and therefore injectability. All three ECM hydrogels were determined to be shear thinning since the viscosity of the materials decreased with increasing shear rate. The viscosities of the 4 and 6 mg/mL ECM hydrogels were similar, particularly in the 0.1 to 1 Hz shear rate range. However, the viscosity measurements for the 8 mg/mL ECM hydrogel were higher than the other two concentrations. Although all three ECM hydrogels were shear thinning, the increasing viscosity with the 8 mg/mL could contribute to some difficulty with injecting these ECM hydrogels through high gauge needles.

Material spreading and retention

Increased concentration and enhanced mechanical properties are expected to increase material retention and delay degradation, but it was necessary to confirm this *in vivo*. When intramuscularly injecting the three skeletal muscle ECM hydrogels, the increasing concentration

affected the ease of injection. All three concentrations were successfully injected, but for the 4 mg/mL hydrogel, the material was more likely to leak out of the tissue following the injection due to the low viscosity. Moreover, the resistance was higher for injecting the 8 mg/mL hydrogel; therefore, the timing of the injection was slightly longer (~45 seconds) compared to the other injections.

Upon harvesting the muscles at 1 and 2 weeks post-injection, some dye-labelled material was immediately visible near or at the surface of the gracilis muscles. However, the distribution and retention of the skeletal muscle ECM hydrogels could only be visualized with fluorescence microscopy (Figure 3.4A). At 1 week post-injection, the ECM hydrogel was distributed throughout all of the sampled regions with all three concentrations having similar amounts of hydrogel present at each location (data not shown). However, the majority of the material for all three concentrations was more localized to the distal region of the muscle. Boluses of the material were seen for all three concentrations, but the spreading from these boluses varied amongst the concentrations. For the 4 and 6 mg/mL ECM hydrogels, the material spread between the muscle fascicles, and in some samples, the material was also found in the interstitial space. However, the 8 mg/mL ECM hydrogel had very little intrafascicular spreading and instead remained localized to the surfaces of the muscles. Since this localization was consistently observed in the 8 mg/mL samples, it likely resulted from the material being forced out of the muscle along the original track of the needle. Therefore, it is hypothesized the 8 mg/mL ECM hydrogel was too viscous to spread into the intrafascicular space.

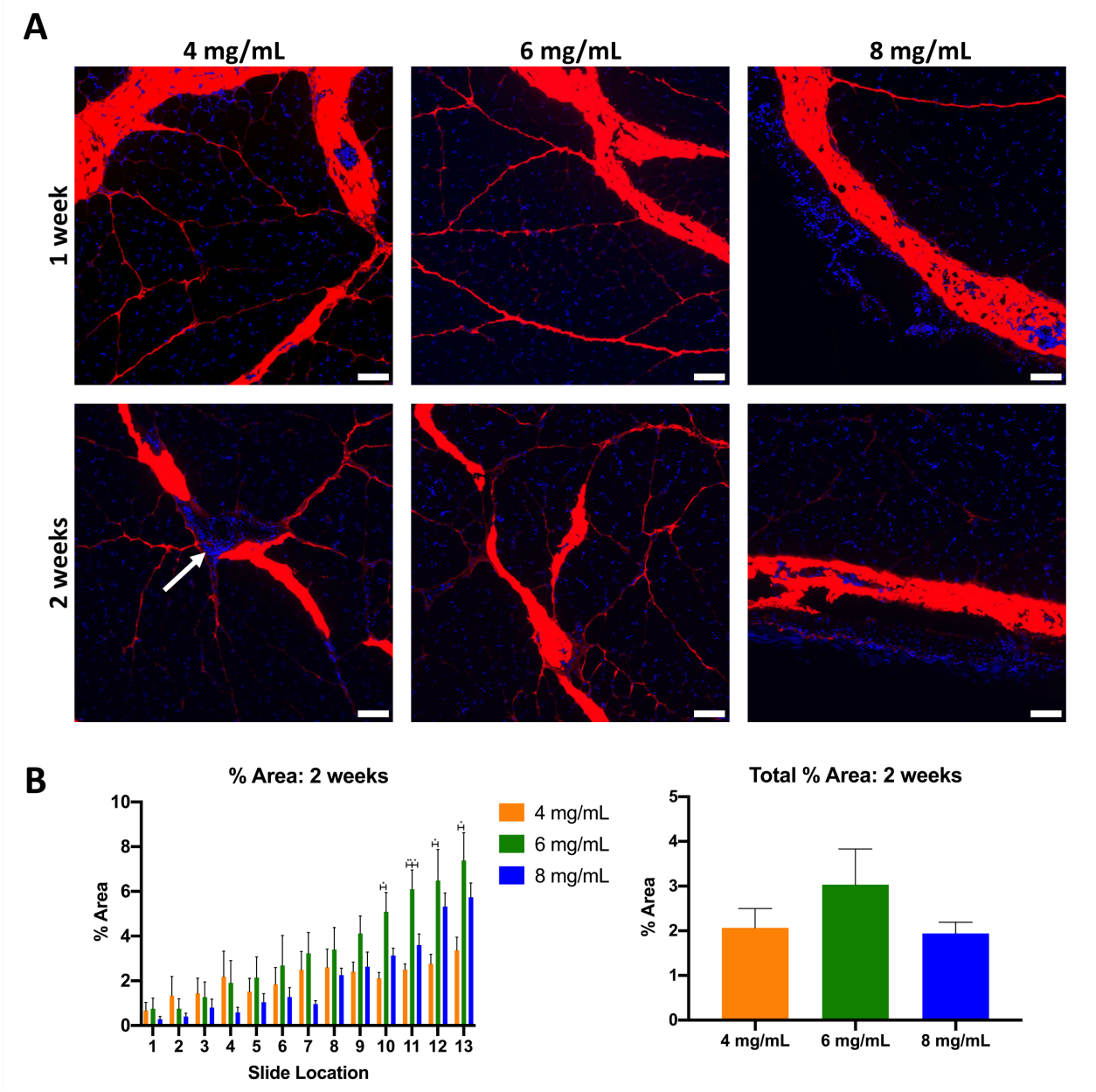

Figure 3.4 (A) Dye-labelled skeletal muscle ECM hydrogels (red) were injected into the gracilis muscles of healthy rats.The material was distributed along the length of the muscle, but the 4 mg/mL and 6 mg/mL hydrogels had the highest degree of spreading with material visualized in the intrafascicular space, whereas the 8 mg/mL ECM hydrogel was mostly localized to the surface of the muscle. By 2 weeks post-injection, the 4 mg/mL and 8 mg/mL ECM hydrogels had lower retention than the 6 mg/mL ECM hydrogel, and the 4 mg/mL ECM hydrogel had regions of hypercellularity (nuclei in blue) present within the material, likely indicative of active degradation. (B) The material distribution and retention were quantified at 2 weeks post-injection (n = 4/concentration) with 1 being the most proximal region and 13 being the most distal region. Scale bar is 100 μm. *$p < 0.05$, **$p < 0.01$. Data are ± SEM.

Although the retention of the three concentrations was similar at 1 week post-injection, differences were seen at 2 weeks post-injection. Based on the fluorescence microscopy images (Figure 3.4A), the 4 and 6 mg/mL ECM hydrogels still maintained some intrafascicular spreading, but the boluses of material were smaller compared to the 1 week post-injection images. Similarly, the boluses of the 8 mg/mL ECM hydrogel had decreased in size, but the intrafascicular spreading was virtually absent. To quantify these observations at 2 weeks post-injection, the area covered by the dye-labelled ECM hydrogels was calculated relative to the total area of the tissue sections at each location (Figure 3.4B). Similar amounts of the 4 mg/mL ECM hydrogel were visible throughout the muscle at each location, but the large boluses of material were not as prevalent in the distal locations. This was likely due to the 4 mg/mL ECM hydrogel being degraded more rapidly since areas of hypercellularity were seen within the material, which overlapped with decreased signal from the dye-labelled material. Compared to the 4 mg/mL ECM hydrogel, the 6 mg/mL hydrogel had similar amounts of material in the proximal locations, but significantly larger amounts of the 6 mg/mL ECM hydrogel were still present in the distal locations at 2 weeks post-injection. The large boluses of 8 mg/mL ECM hydrogel were also conserved at 2 weeks post-injection, but the small amounts of material between muscle fascicles in the proximal regions were diminished, likely due to degradation. For the total percentage of material over the 13 sampled regions, the most material (although not statistically significant) was retained with the 6 mg/mL ECM hydrogel at $3.03 \pm 0.80\%$, while the 4 mg/mL and 8 mg/mL ECM hydrogels had $2.07 \pm 0.43\%$ and $1.94 \pm 0.25\%$ retained, respectively.

Since the material spreading and retention was evaluated in healthy hindlimbs of rats, the inflamed, ischemic environment was not fully recapitulated. However, these results still provided valuable information to determine which concentration may produce enhanced therapeutic outcomes. The 8 mg/mL ECM hydrogel had poor spreading, which may limit its

therapeutics effects. Conversely, the 4 mg/mL ECM hydrogel spread well throughout the muscle, thereby potentially affecting more of the muscle. However, the 4 mg/mL ECM hydrogel leaked out of the muscle to a greater extent than the other concentrations, and the material was more degraded than the 6 mg/mL ECM hydrogel at 2 weeks post-injection. In contrast, the 6 mg/mL ECM hydrogel was injected with relative ease while avoiding leakage, spreading extensively throughout the muscle, and degrading at a slower rate.

Dose optimization

Due to previous success with evaluating these skeletal muscle ECM hydrogels in a young, rat hindlimb ischemia model,[7] the same species and surgical procedure were used for a dose optimization study. The previous study yielded a significant improvement in blood perfusion with a 6 mg/mL skeletal muscle ECM hydrogel compared to saline, but an optimal concentration was not identified.[7] We therefore wanted to screen the three ECM hydrogel

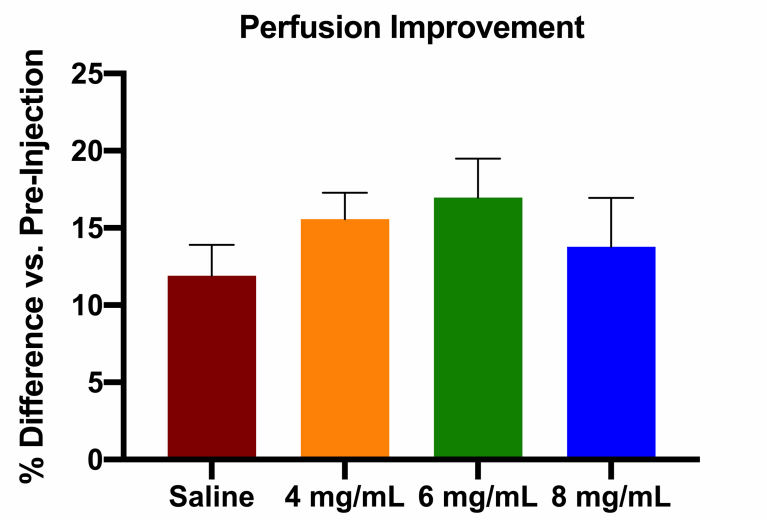

Figure 3.5 Blood perfusion measurements were recorded using LASCA imaging.The 6 mg/mL ECM hydrogel (n=8) yielded the largest improvement in blood perfusion relative to the other two concentrations (n=7) and the saline control (n=8). Improvements in perfusion were calculated using the difference between day 35 post-injection versus pre-injection (day -2). Data are mean ± SEM.

concentrations to evaluate changes in dose. The experiment was not powered due to the high number of animals that would be required to evaluate the expected small changes in perfusion between the multiple groups, and therefore, our goal was to evaluate trends related to increases in perfusion.

Relative to the injections performed in the healthy, non-ischemic rats, the ECM hydrogel injections were similar in the ischemic muscles with comparable leakage occurring, but the surgical incision offered a reliable landmark for guaranteeing similar injection sites across all of the animals. Immediately post-hindlimb ischemia surgery, the blood perfusion values for all experimental groups averaged at 33.80 ± 1.33%, and by day -2 post-injection, the average of the blood perfusion values had already increased to 56.85 ± 1.43%. At the conclusion of the study, the differences between the perfusion values at day 35 and pre-injection (day -2) were calculated (Figure 3.5). The 6 mg/mL ECM hydrogel (n=8) ultimately yielded the highest improvement in blood perfusion at 16.98 ± 2.50% compared to the saline control (n=8) at 11.90 ± 2.01%. The 4 mg/mL (n=7) and 8 mg/mL (n=7) ECM hydrogels also trended higher over the saline control at 15.58 ± 1.71% and 13.79 ± 3.16%, respectively, but to a lesser degree compared to the 6 mg/mL ECM hydrogel. The lack of improvement observed from the 4 and 8 mg/mL concentrations were likely a result of the material spreading patterns and degradation rates as described above. Although the 4 mg/mL ECM hydrogel shared a similar spreading pattern to the 6 mg/mL ECM hydrogel, the increased presence of inflammatory cells due to the hindlimb ischemia surgery could have amplified the degradation rate. In addition, the lower viscosity of the 4 mg/mL ECM hydrogel resulted in more material leaking from the injection site. With a weaker structure and fewer ECM proteins to degrade, the 4 mg/mL ECM hydrogel likely degraded before beneficial processes, such as neovascularization, could be initiated. For the 8 mg/mL ECM hydrogel, the restricted spreading and slower degradation of the material likely

limited an arteriogenic response to a smaller area of the muscle, which resulted in smaller improvements in blood perfusion relative to the 6 mg/mL ECM hydrogel.

Other researches have also demonstrated the importance of material spreading and degradation rates for eventual *in vivo* efficacy.[35-37] The effects of material spreading are not well documented in skeletal muscle applications but for other therapeutic targets, such as the heart, poor material spreading can lead to dangerous outcomes like causing arrhythmias.[37] In the case of skeletal muscle, large boluses of an ECM hydrogel would be more difficult for cells to fully infiltrate and degrade, which could subsequently impede or prevent regeneration. Degradation rates have been more extensively studied both *in vitro* and *in vivo* for several decellularized ECM materials.[38-41] These researchers have demonstrated how highly crosslinked or dense biomaterials attenuate cell migration, and the mechanical properties of these materials dissipate quickly upon degradation. As a result, optimal physical properties and biochemical cues are paramount to ensure cells can infiltrate and subsequently remodel a biomaterial to form native tissue in the injured region.

All of the ECM hydrogels yielded higher improvements in blood perfusion over the saline control when calculating the differences between the perfusion values at day 35 versus pre-injection (day -2). As mentioned above, this study was intended to identify trends amongst the three concentrations; therefore, no significant differences were detected between the experimental groups. Nonetheless, the 6 mg/mL ECM hydrogel yielded the highest improvement in blood perfusion, whereas the 4 mg/mL and 8 mg/mL ECM hydrogels produced marginal improvements over the saline control. These results indicated that 6 mg/mL was the optimal concentration for performing further validation.

Efficacy in aged mice

Many pre-clinical studies for PAD rely on small animal models to evaluate therapies, but the limited success in humans could be attributed to the use of insufficient animal models. Researchers have incorporated the use of aged animals for hindlimb ischemia studies, and those animals have failed to regenerate as readily, which more accurately mimics the PAD patient population.[23,42-44] In addition, when evaluating therapeutics including growth factors, cells, and biomaterials, the interventions did not perform as effectively in aged animals.[45-47] Consequently, after confirming 6 mg/mL was the optimal concentration, we additionally wanted to confirm its efficacy in a more relevant animal model of PAD. For this experiment, aged mice were used to investigate whether age-related impairments would inhibit blood perfusion recovery due to the ECM hydrogel (Figure 3.6).

After performing the hindlimb ischemia surgeries in the mice, some animals developed necrosis in the toes of the ischemic paw, which was not evident in any of the young rats in previous experiments. The hindlimb ischemia surgeries were also more severe in that the blood perfusion immediately post-surgery was an average of 15.95 ± 0.91% for all of the mice. At day -2 post-injection, the average blood perfusion had only increased to 33.51 ± 3.10%. In addition

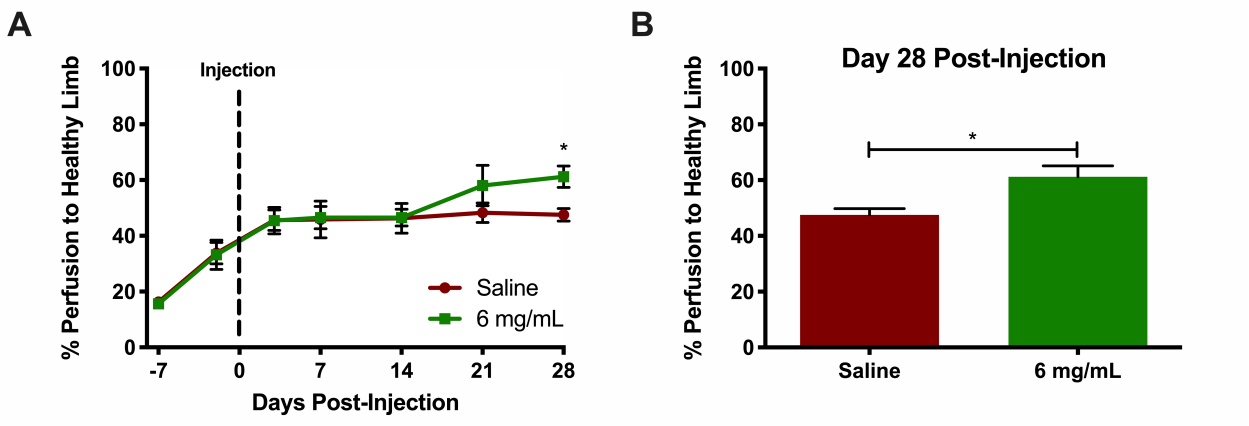

Figure 3.6 An aged mouse hindlimb ischemia model (n=6/group) was utilized, and blood perfusion measurements were acquired with LASCA imaging.Significant improvements in blood perfusion values were seen at 28 days post-injection. *p < 0.05 according to an unpaired Student's t-test at day 28 post-injection. Data are mean ± SEM.

to the necrosis seen in the mice, the slower improvement in restoring the blood perfusion indicated that the hindlimb ischemia surgery was more severe in the aged mice and impaired the natural regenerative process more so than the young rats. At day 21 post-injection, the ECM hydrogel-injected mice began improving more than the saline control, and by day 28 post-injection, the blood perfusion values for the ECM hydrogel group were significantly higher (Figure 3.6A, $p = 0.012$). The saline control reached a blood perfusion level of only $47.50 \pm 2.25\%$ at day 28 post-injection, but the ECM hydrogel increased the blood perfusion to $61.24 \pm 3.87\%$ (Figure 3.6B).

The previous published study, which investigated the 6 mg/mL ECM hydrogel in a young rat hindlimb ischemia model, showed significantly higher perfusion values at $80.21 \pm 3.85\%$ compared to the saline control at $69.06 \pm 2.63\%$ for day 35 post-injection.[7] Increases in the perfusion values began at day 14 post-injection and reached significance by day 21 for the young rat hindlimb ischemia study,[7] but the aged mice in this study did not show increases in perfusion until day 21 with significance achieved at day 28 post-injection. This delay in the restoration of the blood perfusion may also be attributed to age of the animals since studies have described age-related impairments in important regenerative processes like angiogenesis[22,23], vasculogenesis [23], and satellite cell activity [26-28]. The higher perfusion values for the rats relative to the aged mice could indicate impairments resulting from aging or could be associated with species differences. Injecting saline is known to cause an inflammatory response that could initiate some regeneration, but it was unable to increase perfusion beyond day 3 post-injection, or ~47% perfusion, in the aged mice. However, the administration of the 6 mg/mL ECM hydrogel restored the blood perfusion values to a higher value. The aged mice could be a more reliable model for detecting significant differences due to administration of the ECM hydrogels as the limited regeneration more accurately depicts the PAD and CLI patients

who may be aged or suffering from other comorbidities that would attenuate normal healing processes.

Conclusions

In summary, we have characterized the physical properties of three concentrations of a decellularized skeletal muscle ECM hydrogel and investigated the efficacy of these hydrogels in a hindlimb ischemia model. We demonstrated the importance of evaluating material retention and spreading *in vivo* as it may not change linearly with material concentration. Although the increasing concentrations of the ECM hydrogels corresponded to an increase in viscosity and mechanical strength, the spreading patterns and degradation rates impacted the *in vivo* efficacy, likely a result of differing biochemical cues amongst the various concentrations. The 6 mg/mL ECM hydrogel restored the blood perfusion to the highest value and was identified as the optimal concentration. Efficacy was further demonstrated in an aged mouse hindlimb ischemia model. Significant increases in blood perfusion were observed in the aged mice, which are more representative of the pathophysiology of the patient population. Overall, this study provides further proof-of-concept for the use of decellularized skeletal muscle ECM hydrogels for eventual translation to PAD patients. The following chapter will further evaluate the efficacy of this biomaterial in an additional skeletal muscle injury model.

Acknowledgements

This work was supported by the California Institute for Regenerative Medicine (TRAN1-09814). MJH was supported by a National Institutes of Health pre-doctoral fellowship (1F31HL132584). We would like to thank Martin Spang for performing the

scanning electron microscopy at the San Diego Nanotechnology Infrastructure (SDNI) of UCSD, a member of the National Nanotechnology Coordinated Infrastructure (NNCI), which is supported by the National Science Foundation (ECCS-1542148).

This chapter, in part, is currently being prepared for submission for publication of the material. The authors are Melissa J. Hernandez, Emma I. Zelus, Martin T. Spang, Rebecca L. Braden, and Karen L. Christman. The dissertation author was the primary investigator and author of this material.

References

1. Lawall H, Bramlage P, Amann B. Stem cell and progenitor cell therapy in peripheral artery disease. A critical appraisal. *Thromb Haemost* **103**, 696-709, doi:10.1160/TH09-10-0688 (2010).

2. Dormandy J, Heeck L, Vig S. The fate of patients with critical leg ischemia. *Semin Vasc Surg* **12**, 142-147 (1999).

3. Schillinger M, Sabeti S, Dick P, Amighi J, Mlekusch W, Schlager O, Loewe C, Cejna M, Lammer J, Minar E. Sustained benefit at 2 years of primary femoropopliteal stenting compared with balloon angioplasty with optional stenting. *Circulation* **115**, 2745-2749, doi:10.1161/CIRCULATIONAHA.107.688341 (2007).

4. Ungerleider JL, Christman KL. Concise review: injectable biomaterials for the treatment of myocardial infarction and peripheral artery disease: translational challenges and progress. *Stem Cells Transl Med* **3**, 1090-1099, doi:10.5966/sctm.2014-0049 (2014).

5. Hernandez MJ, Christman KL. Designing Acellular Injectable Biomaterial Therapeutics for Treating Myocardial Infarction and Peripheral Artery Disease. *JACC Basic Transl Sci* **2**, 212-226, doi:10.1016/j.jacbts.2016.11.008 (2017).

6. DeQuach JA, Lin JE, Cam C, Hu D, Salvatore MA, Sheikh F, Christman KL. Injectable skeletal muscle matrix hydrogel promotes neovascularization and muscle cell infiltration in a hindlimb ischemia model. *Eur Cell Mater* **23**, 400-412; discussion 412 (2012).

7. Ungerleider JL, Johnson TD, Hernandez MJ, Elhag DI, Braden RL, Dzieciatkowska M, Osborn KG, Hansen KC, Mahmud E, Christman KL. Extracellular Matrix Hydrogel Promotes Tissue Remodeling, Arteriogenesis, and Perfusion in a Rat Hindlimb Ischemia

Model. *JACC: Basic to Translational Science* **1**, 32-44, doi:10.1016/j.jacbts.2016.01.009 (2016).

8. Chekanov VS, Rayel R, Nikolaychik V, Kipshidze N, Baibekov I, Karakozov P, Bajwa T, Akhtar M. Direct fibrin injection to promote new collateral growth in hind limb ischemia in a rabbit model. *J Card Surg* **17**, 502-511; discussion 512 (2002).

9. Luyt CE, Meddahi-Pelle A, Ho-Tin-Noe B, Colliec-Jouault S, Guezennec J, Louedec L, Prats H, Jacob MP, Osborne-Pellegrin M, Letourneur D, Michel JB. Low-molecular-weight fucoidan promotes therapeutic revascularization in a rat model of critical hindlimb ischemia. *J Pharmacol Exp Ther* **305**, 24-30, doi:10.1124/jpet.102.046144 (2003).

10. Hussey GS, Dziki JL, Badylak SF. Extracellular matrix-based materials for regenerative medicine. *Nature Reviews Materials* **3**, 159-173, doi:10.1038/s41578-018-0023-x (2018).

11. Mecham RP. Overview of extracellular matrix. *Curr Protoc Cell Biol* **Chapter 10**, Unit 10 11, doi:10.1002/0471143030.cb1001s57 (2012).

12. Li F, Li W, Johnson S, Ingram D, Yoder M, Badylak S. Low-molecular-weight peptides derived from extracellular matrix as chemoattractants for primary endothelial cells. *Endothelium* **11**, 199-206, doi:10.1080/10623320490512390 (2004).

13. Badylak SF, Park K, Peppas N, McCabe G, Yoder M. Marrow-derived cells populate scaffolds composed of xenogeneic extracellular matrix. *Exp Hematol* **29**, 1310-1318 (2001).

14. Numata S, Fujisato T, Niwaya K, Ishibashi-Ueda H, Nakatani T, Kitamura S. Immunological and histological evaluation of decellularized allograft in a pig model: comparison with cryopreserved allograft. *J Heart Valve Dis* **13**, 984-990 (2004).

15. Zantop T, Gilbert TW, Yoder MC, Badylak SF. Extracellular matrix scaffolds are repopulated by bone marrow-derived cells in a mouse model of achilles tendon reconstruction. *J Orthop Res* **24**, 1299-1309, doi:10.1002/jor.20071 (2006).

16. Rieder E, Nigisch A, Dekan B, Kasimir MT, Muhlbacher F, Wolner E, Simon P, Weigel G. Granulocyte-based immune response against decellularized or glutaraldehyde cross-linked vascular tissue. *Biomaterials* **27**, 5634-5642, doi:10.1016/j.biomaterials.2006.06.020 (2006).

17. Reing JE, Zhang L, Myers-Irvin J, Cordero KE, Freytes DO, Heber-Katz E, Bedelbaeva K, McIntosh D, Dewilde A, Braunhut SJ, Badylak SF. Degradation products of

extracellular matrix affect cell migration and proliferation. *Tissue Eng Part A* **15**, 605-614, doi:10.1089/ten.tea.2007.0425 (2009).

18. Beattie AJ, Gilbert TW, Guyot JP, Yates AJ, Badylak SF. Chemoattraction of progenitor cells by remodeling extracellular matrix scaffolds. *Tissue Eng Part A* **15**, 1119-1125, doi:10.1089/ten.tea.2008.0162 (2009).

19. Rao N, Agmon G, Tierney MT, Ungerleider JL, Braden RL, Sacco A, Christman KL. Engineering an Injectable Muscle-Specific Microenvironment for Improved Cell Delivery Using a Nanofibrous Extracellular Matrix Hydrogel. *ACS Nano* **11**, 3851-3859, doi:10.1021/acsnano.7b00093 (2017).

20. Eraso LH, Fukaya E, Mohler ER, 3rd, Xie D, Sha D, Berger JS. Peripheral arterial disease, prevalence and cumulative risk factor profile analysis. *Eur J Prev Cardiol* **21**, 704-711, doi:10.1177/2047487312452968 (2014).

21. Grounds MD. Age-associated changes in the response of skeletal muscle cells to exercise and regeneration. *Ann N Y Acad Sci* **854**, 78-91 (1998).

22. Rivard A, Fabre JE, Silver M, Chen D, Murohara T, Kearney M, Magner M, Asahara T, Isner JM. Age-dependent impairment of angiogenesis. *Circulation* **99**, 111-120 (1999).

23. Shimada T, Takeshita Y, Murohara T, Sasaki K, Egami K, Shintani S, Katsuda Y, Ikeda H, Nabeshima Y, Imaizumi T. Angiogenesis and vasculogenesis are impaired in the precocious-aging klotho mouse. *Circulation* **110**, 1148-1155, doi:10.1161/01.CIR.0000139854.74847.99 (2004).

24. Carlson BM. Factors influencing the repair and adaptation of muscles in aged individuals: satellite cells and innervation. *J Gerontol A Biol Sci Med Sci* **50 Spec No**, 96-100 (1995).

25. Delbono O. Neural control of aging skeletal muscle. *Aging Cell* **2**, 21-29 (2003).

26. Conboy IM, Conboy MJ, Wagers AJ, Girma ER, Weissman IL, Rando TA. Rejuvenation of aged progenitor cells by exposure to a young systemic environment. *Nature* **433**, 760-764, doi:10.1038/nature03260 (2005).

27. Brack AS, Conboy MJ, Roy S, Lee M, Kuo CJ, Keller C, Rando TA. Increased Wnt signaling during aging alters muscle stem cell fate and increases fibrosis. *Science* **317**, 807-810, doi:10.1126/science.1144090 (2007).

28. Le Grand F, Rudnicki MA. Skeletal muscle satellite cells and adult myogenesis. *Curr Opin Cell Biol* **19**, 628-633, doi:10.1016/j.ceb.2007.09.012 (2007).

29. Carlson BM, Faulkner JA. Muscle transplantation between young and old rats: age of host determines recovery. *American Journal of Physiology - Cell Physiology* **256**, C1262-C1266 (1989).

30. Goldspink G, Fernandes K, Williams PE, Wells DJ. Age-related changes in collagen gene expression in the muscles of mdx dystrophic and normal mice. *Neuromuscul Disord* **4**, 183-191 (1994).

31. Ungerleider JL, Johnson TD, Rao N, Christman KL. Fabrication and characterization of injectable hydrogels derived from decellularized skeletal and cardiac muscle. *Methods* **84**, 53-59, doi:10.1016/j.ymeth.2015.03.024 (2015).

32. Hernandez MJ, Yakutis GE, Zelus EI, Hill RC, Dzieciatkowska M, Hansen KC, Christman KL. Manufacturing considerations for producing and assessing decellularized extracellular matrix hydrogels. *Methods*, doi:10.1016/j.ymeth.2019.09.015 (2019).

33. Roustit M, Millet C, Blaise S, Dufournet B, Cracowski JL. Excellent reproducibility of laser speckle contrast imaging to assess skin microvascular reactivity. *Microvasc Res* **80**, 505-511, doi:10.1016/j.mvr.2010.05.012 (2010).

34. Senarathna J, Rege A, Li N, Thakor NV. Laser Speckle Contrast Imaging: theory, instrumentation and applications. *IEEE Rev Biomed Eng* **6**, 99-110, doi:10.1109/RBME.2013.2243140 (2013).

35. Lee KY, Bouhadir KH, Mooney DJ. Controlled degradation of hydrogels using multi-functional cross-linking molecules. *Biomaterials* **25**, 2461-2466 (2004).

36. Burdick JA, Chung C, Jia X, Randolph MA, Langer R. Controlled degradation and mechanical behavior of photopolymerized hyaluronic acid networks. *Biomacromolecules* **6**, 386-391, doi:10.1021/bm049508a (2005).

37. Suarez SL, Rane AA, Munoz A, Wright AT, Zhang SX, Braden RL, Almutairi A, McCulloch AD, Christman KL. Intramyocardial injection of hydrogel with high interstitial spread does not impact action potential propagation. *Acta Biomater* **26**, 13-22, doi:10.1016/j.actbio.2015.08.004 (2015).

38. Record RD, Hillegonds D, Simmons C, Tullius R, Rickey FA, Elmore D, Badylak SF. In vivo degradation of 14C-labeled small intestinal submucosa (SIS) when used for urinary bladder repair. *Biomaterials* **22**, 2653-2659, doi:10.1016/s0142-9612(01)00007-2 (2001).

39. Singelyn JM, Christman KL. Modulation of material properties of a decellularized myocardial matrix scaffold. *Macromol Biosci* **11**, 731-738, doi:10.1002/mabi.201000423 (2011).

40. Wassenaar JW, Braden RL, Osborn KG, Christman KL. Modulating In Vivo Degradation Rate of Injectable Extracellular Matrix Hydrogels. *J Mater Chem B* **4**, 2794-2802, doi:10.1039/C5TB02564H (2016).

41. Costa A, Naranjo JD, Turner NJ, Swinehart IT, Kolich BD, Shaffiey SA, Londono R, Keane TJ, Reing JE, Johnson SA, Badylak SF. Mechanical strength vs. degradation of a biologically-derived surgical mesh over time in a rodent full thickness abdominal wall defect. *Biomaterials* **108**, 81-90, doi:10.1016/j.biomaterials.2016.08.053 (2016).

42. Faber JE, Zhang H, Lassance-Soares RM, Prabhakar P, Najafi AH, Burnett MS, Epstein SE. Aging causes collateral rarefaction and increased severity of ischemic injury in multiple tissues. *Arterioscler Thromb Vasc Biol* **31**, 1748-1756, doi:10.1161/ATVBAHA.111.227314 (2011).

43. Wang JS, Liu X, Xue ZY, Alderman L, Tilan JU, Adenika R, Epstein SE, Burnett MS. Effects of aging on time course of neovascularization-related gene expression following acute hindlimb ischemia in mice. *Chin Med J (Engl)* **124**, 1075-1081 (2011).

44. Westvik TS, Fitzgerald TN, Muto A, Maloney SP, Pimiento JM, Fancher TT, Magri D, Westvik HH, Nishibe T, Velazquez OC, Dardik A. Limb ischemia after iliac ligation in aged mice stimulates angiogenesis without arteriogenesis. *J Vasc Surg* **49**, 464-473, doi:10.1016/j.jvs.2008.08.077 (2009).

45. Anderson EM, Silva EA, Hao Y, Martinick KD, Vermillion SA, Stafford AG, Doherty EG, Wang L, Doherty EJ, Grossman PM, Mooney DJ. VEGF and IGF Delivered from Alginate Hydrogels Promote Stable Perfusion Recovery in Ischemic Hind Limbs of Aged Mice and Young Rabbits. *J Vasc Res* **54**, 288-298, doi:10.1159/000479869 (2017).

46. Bosch-Marce M, Okuyama H, Wesley JB, Sarkar K, Kimura H, Liu YV, Zhang H, Strazza M, Rey S, Savino L, Zhou YF, McDonald KR, Na Y, Vandiver S, Rabi A, Shaked Y, Kerbel R, Lavallee T, Semenza GL. Effects of aging and hypoxia-inducible factor-1 activity on angiogenic cell mobilization and recovery of perfusion after limb ischemia. *Circ Res* **101**, 1310-1318, doi:10.1161/CIRCRESAHA.107.153346 (2007).

47. Zhuo Y, Li SH, Chen MS, Wu J, Kinkaid HY, Fazel S, Weisel RD, Li RK. Aging impairs the angiogenic response to ischemic injury and the activity of implanted cells: combined consequences for cell therapy in older recipients. *J Thorac Cardiovasc Surg* **139**, 1286-1294, 1294 e1281-1282, doi:10.1016/j.jtcvs.2009.08.052 (2010).

Chapter 4. Evaluation of the Therapeutic Window for Decellularized Skeletal Muscle Extracellular Matrix Hydrogels in a Chronic Rotator Cuff Model

Introduction

In the United States, 75,000 surgical rotator cuff repairs are performed annually with 86% of these repairs being done on patients over the age of 44 years.[1,2] Several surgical techniques, including arthroscopic tendon repair, tendon transfer, or shoulder replacement, are available for patients with rotator cuff tears (RCTs), yet the recurrence rate ranges between 17 and 94%.[3-12] Following a RCT, rotator cuff muscles experience unloading, which subsequently initiates a remodeling response in the skeletal muscle. Although skeletal muscle is one of the few organs to possess regenerative capabilities, this chronic unloading will ultimately cause contractile tissue to be replaced with non-contractile tissue. These negative remodeling events include fibrosis, muscle fiber atrophy, fatty infiltration, and muscle degeneration, which have been observed in patients with RCTs.[13,14] The injured skeletal muscle represents an important part of a RCT injury since the impaired function of the damaged muscle likely contributes to the high rates of tendon retearing.

Existing surgical procedures mainly aim to treat the torn tendon, yet fatty infiltration, atrophy, and muscle degeneration continue to worsen following tendon repair.[15-19] As a result, researchers have begun to investigate therapies to address the negative remodeling within the skeletal muscle. Several cell types, perivascular stem cells and fibro-adipogenic progenitors, have been transplanted to induce muscle regeneration.[20,21] In a mouse model of RCT, the intramuscular injection of pericytes or adventitial cells led to higher muscle masses, higher fiber cross-sectional areas (CSA), and less fibrosis.[20] Similarly, beige adipose fibro-adipogenic progenitors were injected intramuscularly into a mouse RCT model and resulted in reduced

fibrosis, fatty infiltration, and atrophy, while increasing vascularization and shoulder function according to gait analyses.[21] Tellier et al. sought to investigate the effects of microparticles loaded with a growth factor, stromal cell-derived factor-1α, in a rat RCT model.[22] Results suggested a shift towards a more pro-remodeling environment in the injected muscle, but further studies would be necessary to confirm efficacy. Platelet-rich plasma has also been injected into the supraspinatus muscle in a rat model of RCT in which fatty infiltration was attenuated.[23] Lastly, a transforming growth factor-β small molecular inhibitor SB431542 was delivered intraperitoneally in a mouse RCT model, which led to reduced fibrosis, fatty infiltration, and muscle loss.[24] Although these studies demonstrated promise for RCT, murine models inaccurately depict human pathophysiology, and many researchers include nerve transection to increase the severity of the model. In addition, growth factor and cell therapies must overcome delivery challenges, including retention and off-target effects, and these products are often expensive to manufacture.

Decellularized skeletal muscle extracellular matrix (ECM) hydrogels have also been investigated for skeletal muscle repair applications.[25,26] An injectable, porcine-derived skeletal muscle ECM hydrogel was injected in a rat hindlimb ischemia model of peripheral artery disease.[26] In this acute injury model, the ECM hydrogel improved blood perfusion restoration and increased the density of large diameter arterioles relative to a saline control. Muscle fiber cross-sectional areas also more closely resembled healthy muscle, and the density of $Pax7^+$ satellite cells was significantly increased shortly after injection of the ECM hydrogel.

Here we sought to investigate a decellularized skeletal muscle ECM hydrogel in a chronic rabbit model of RCT. The skeletal muscle ECM hydrogel has not been evaluated in a chronic model of disease or a larger animal model. Nonetheless, we hypothesized the skeletal muscle ECM hydrogel would maintain similar efficacy by promoting muscle regeneration and remodeling in this skeletal muscle application. Therapeutics for RCT are often administered at

the time of tendon repair, but we sought to examine the effects of the ECM hydrogel when injecting at the time of repair and at a delayed time point.

Materials and Methods

All experiments in this study were performed in accordance with the guidelines established by the Institutional Animal Care and Use Committee at the University of California San Diego and the American Association for Accreditation of Laboratory Animal Care.

Material production

Skeletal muscle ECM hydrogels were processed according to previously published methods.[27,28] Briefly, longissimus dorsi muscles (pork loins) were harvested from Yorkshire farm pigs (4-7 months old, S&S Farms) at the UC San Diego Medical School. The muscles were immediately frozen for a minimum of 24 hours at -20°C, chopped into ~0.5 cm^3 pieces, decellularized in 1% wt/vol sodium docecyl sulfate, delipidized in isopropanol, and rinsed in water. The decellularized material was then lyophilized and milled into a fine powder. Prior to use, the ECM powder was partially pepsin digested for 48 hours and then adjusted to physiological pH and salt conditions at a final concentration of 6 mg/mL. Aliquots of the ECM hydrogel were lyophilized and stored at -80°C until injections were performed.

Preparation of ECM hydrogel for injections

To resuspend the lyophilized ECM aliquots, an appropriate volume of sterile water was added to each microcentrifuge tube, and the material was gently pipetted up and down to solubilize the ECM without introducing air bubbles. The ECM hydrogel was left on ice for ~10 minutes and a 25G needle was then used for shearing the material to ensure all ECM particulates had been fully solubilized. All injections were performed with a 27G needle.

Tenotomy surgery

Female New Zealand white rabbits (~6 months, 32 total, Western Oregon Rabbit Company, Philomath, OR) were anesthetized with a subcutaneous injection of ketamine and xylazine (35 mg/kg ketamine/5 mg/kg xylazine, MWI Veterinary Supply, Boise, ID). Following intubation, 2-4% isoflurane (VetOne, Boise, ID) was utilized to keep the animals under anesthesia for the duration of the surgery. The surgical site was disinfected, and an incision was made through the skin and deltoid muscle overlying the rotator cuff. After exposing the supraspinatus tendon, a unilateral tenotomy was performed by transecting the tendon at its footprint on the greater tubercle of the humerus. Surrounding soft tissues were bluntly dissected to permit unobstructed retraction of the tendon. To avoid the formation of tissue adhesions, a Penrose drain (Medline, Northfield, IL) was sutured to the tendon stump. The muscle and skin layers were subsequently sutured and stapled closed, and the animals were allowed to recover. Tenotomies were only performed on one shoulder to maintain the contralateral shoulder as an internal control. An E-collar was placed on the animals to prevent suture ripping, and after 14 days, the collar and any remaining staples were removed.

Tendon repair surgery

After 8 weeks, the animals underwent an additional surgery to repair the transected supraspinatus tendon. An injection of ketamine and xylazine (35 mg/kg ketamine/5 mg/kg xylazine, MWI Veterinary Supply, Boise, ID) was once again administered subcutaneously to anesthetize the animals, and 2-4% isoflurane was used for the remainder of the surgery. Another incision was made through the skin and deltoid muscle to expose the tendon stump and attached Penrose drain. The tendon stump was reattached to the retracted tendon with suture, and the Penrose drain was removed. After closing the muscle and skin with suture and staples, the animals were allowed to recover. Similar to the tenotomy surgery, animals were fitted with an E-collar for 14 days before removing the collar and remaining staples.

Administration of ECM hydrogel

Injections of the skeletal muscle ECM hydrogel or a saline control were performed at the time of tendon repair (n=17 total) or 12 days post-repair (n=15 total). At the time of repair, the injections were administered after the final incision had been closed. Using a 27G needle, a total of 1 mL of saline or ECM hydrogel was distributed via 10 equally spaced injections of 100 µL along the supraspinatus muscle. For the delayed injections, the animals were anesthetized with a subcutaneous injection of ketamine and xylazine (35 mg/kg ketamine/5 mg/kg xylazine, MWI Veterinary Supply, Boise, ID), and the injections were performed in the same manner as the immediate injections.

Muscle harvesting

At the conclusion of the study, animals were euthanized at two time points. Supraspinatus muscles from animals with an immediate injection were harvested at 1 week post-repair/1 week post-injection (saline: n=5, ECM: n=4) and 8 weeks post-repair/8 weeks post-injection (n=4/group). Animals with a delayed injection were euthanized at ~3 weeks post-repair/1 week post-injection (saline: n=3, ECM: n=4) and 8 weeks post-repair/~6 weeks post-injection (n=4/group). At the specified time points, animals were euthanized with an intravenous overdose of pentobarbital (Beuthanasia, 120 mg/kg, MWI Veterinary Supply, Boise, ID). The supraspinatus muscles from both shoulders were harvested and divided into four regions with the central tendon serving as the muscle midline between the anterior and posterior sides of the muscle. These four regions included anterior lateral (A1), posterior lateral (P1), anterior medial (A2), and posterior medial (P2), and one full-muscle thickness fragment was harvested from each location. The harvested muscles were pinned to *in vivo* length and flash frozen in liquid nitrogen-chilled isopentane for storage at -80°C. For this particular study, only the P1 region was utilized since the severity of the RCT model is highest in that region.

Histology

Frozen segments of the supraspinatus muscles were embedded in Tissue-Tek® O.C.T. Compound (Sakura Finetek, Torrance, CA) and cryosectioned with a Leica CM3050 S cryostat (Leica Biosystems, Wetzlar, Germany) into 10 μm axial and longitudinal sections. Tissue sections were stained with hematoxylin and eosin (H&E) to assess overall muscle health. In addition, DAPI (VECTASHIELD® Antifade Mounting Medium, Vector Laboratories, Burlingame, CA) and wheat germ agglutinin conjugated with Alexa Fluor 594 (1:2000, ThermoFisher Scientific, Waltham, MA) were utilized to quantify CSA and the percentage of centralized nuclei as indicators of muscle remodeling. Average muscle fiber areas for each individual animal were used for statistical analyses. Ten randomly selected 10x magnification regions were imaged on a Leica CTR 6500 confocal microscope (Leica Microsystems, Wetzlar, Germany) fit with a Leica DFC365 FX CCD microscope camera (Leica Microsystems, Wetzlar, Germany) and analyzed with a custom ImageJ macro.

Quantitative PCR

In addition to the muscle segments harvested from the supraspinatus muscles for histology, approximately 30-50 mg of muscle tissue was collected from each region and homogenized in bead tubes (Navy, Next Advance, Troy, NY) with TRIzol™ (ThermoFisher Scientific, Waltham, MA). The manufacturer's protocol for RNeasy spin columns (Qiagen, Hilden, Germany) was followed to isolate RNA. Complimentary DNA was then synthesized with 1 μg RNA, SuperScript IV reverse transcriptase (ThermoFisher Scientific, Waltham, MA), and random hexamers. Primers for qPCR were designed with NCBI Primer Blast for three muscle transcription factors (Pax7, Myf5, and myogenin), embryonic myosin heavy chain (MYH3), a skeletal muscle metabolic regulator (mTOR), and a housekeeping gene (GAPDH). The primers for Pax7 were as follows: forward 5'-CTGGCGGACGTGGAGAATAA-3' and reverse 5'-

CCAGACTGTTGCCTCGCTTA-3'. The primers for Myf5 were as follows: forward 5'-GCATGCCTGAATGCAACAGC-3' and reverse 5'-GTTGCTCTGAGGAGGTGATCC-3'. The primers for myogenin were as follows: forward 5'-GTGTAAGAGGAAGTCAGTGTCCAT-3' and reverse 5'-TGCAAGCATATGGTCTCCTGG-3'. The primers for MYH3 were as follows: forward 5'-ACAACCTACAGCGGGTCAAG-3' and reverse 5'-CTGGGACACGATGCTTTCCT-3'. The primers for mTOR were as follows: forward 5'-GGGACCTCTTCAATGCTGCT-3' and reverse 5'-AGAGACTCCAAAATGGCGGG-3'. The primers for GAPDH were as follows: forward 5'-ATTGCCCTCAATGACCACTTTG-3' and reverse 5'-TCTTACTCCTTGGAGGCCATGT-3'. All PCR reactions included cDNA (1:20 dilution), Forget-Me-Not™ EvaGreen® qPCR Master Mix (Biotium, Hayward, CA), and 1 μM forward and reverse primers. Each PCR plate was run on a CFX96 Touch™ Real-Time PCR Detection System (Bio-Rad, Hercules, CA) and included the housekeeping gene to avoid inter-plate variability. All fold changes were normalized to the saline control.

Statistical analysis

Results are displayed as mean ± standard error of the mean (SEM). Two-way ANOVAs with a Sidak's multiple comparison test were performed to examine the effects of the two time points and treatments. At each individual time point, a Student's t-test was used for the centralized nuclei and arteriole data, and a Mann-Whitney test was applied to the muscle fiber cross-sectional area data. Cycle values from the PCR experiments were analyzed with the delta delta C_t method, and a Student's t-test was used for the individual genes at each time point. Prism 8 (GraphPad Software, San Diego, CA) was utilized for all statistical analyses with statistical significance accepted at $p < 0.05$.

Results and Discussion

Overall muscle health

At 1 week post-injection for both injection schemes, areas of hypercellularity were visualized (Figure 4.1). Tissue samples collected from animals with no treatment (repair alone) contained regions of interstitial fibrosis, and the muscle fibers appeared atrophied relative to healthy muscle. Similarly, the immediate injections of either saline or ECM also induced fibrosis and atrophy, but the inflammatory response was much more apparent, based on the high density of cell nuclei. The delayed injection produced a response most similar to the repair alone group, and the heightened inflammatory response was largely absent in these animals.

At 8 weeks post-repair (8 weeks post-injection for immediate injection, ~6 weeks post-injection for delayed injection), the repair alone and delayed injection experimental groups resembled healthy skeletal muscle, but some interstitial fibrosis was observed (Figure 4.1). With the delayed injections, the muscle fiber sizes were largely consistent across the two time points, but, at 6 weeks post-injection (8 weeks post-repair), very small fibers were visualized, which could indicate muscle remodeling. The animals that received injections at the time of repair still had a small degree of inflammation present at 8 weeks post-injection (8 weeks post-repair), and interstitial fibrosis was also seen. In addition, some of the muscle fibers appeared hypertrophied, which was only prevalent in the animals with the immediate injection.

Following the repair surgery, an inflammatory cascade was initiated, which would consist of infiltrating neutrophils for the first few days followed by the migration and proliferation of macrophages, T cells, mast cells, and other inflammatory cells for approximately two weeks.[29] In addition to the inflammatory response from the reloading of the muscle, a secondary inflammatory response was induced by the injection of saline or the ECM hydrogel. Both injections cause inflammation due to mechanical damage caused by the physical injection of the bolus to the muscle. The ECM hydrogel additionally stimulates cell migration into the material.

As a result, the immediate injection produced a larger inflammatory response due to the concurrent inflammation from the repair surgery and material injections. The residual inflammation at 8 weeks post-injection for the immediate experimental group further indicated

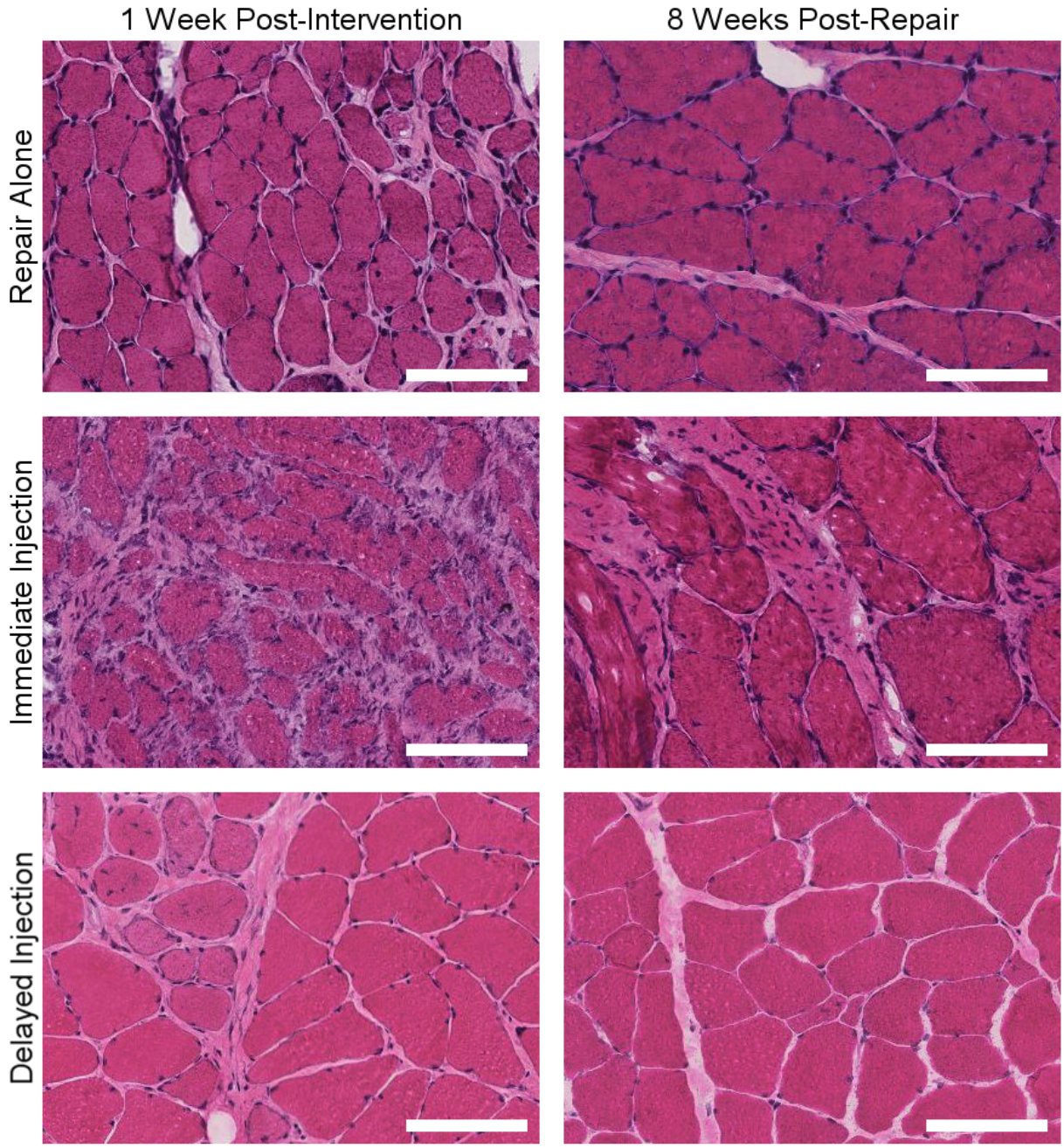

Figure 4.1 Representative hematoxylin and eosin (H&E) staining for tissue samples from the P1 regions of animals injected at the time of repair and 12 days post-injection and a repair alone control.

the need to delay the intramuscular injections to allow the initial inflammation from the surgery to subside.

3.1 Muscle fiber morphology and remodeling

To investigate the atrophy and muscle fiber morphology more thoroughly, the muscle fiber areas were quantified for the two experimental groups at each time point (Figure 4.2). For animals injected at the time of repair (Figure 4.2A), the CSA values for the ECM hydrogel-treated animals (3575 ± 627 μm^2) at 1 week post-injection closely resembled healthy supraspinatus muscle, which averages approximately 3500 μm^2. However, the saline group was more atrophied, although not significantly, with an average CSA of 3084 ± 157 μm^2. By 8 weeks post-injection and post-repair, the ECM hydrogel-treated animals remained constant with an average CSA of 3599 ± 307 μm^2, but the average CSA for the saline animals had markedly increased to 5361 ± 848 μm^2. This hypertrophy response, which was more prevalent in the saline animals, was also visualized in the H&E images (Figure 4.1) and confirmed in the quantitative assessment for CSA. A two-way ANOVA indicated significant differences due to the

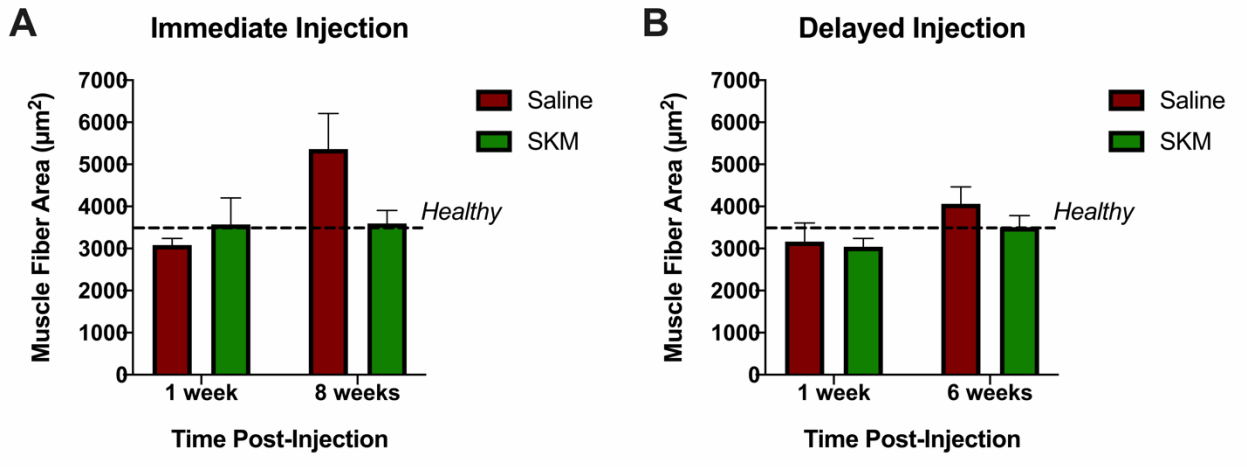

Figure 4.2 Cross-sectional area (CSA) measurements for both injection schemes (n=3-5/group). The ECM hydrogel did not produce significant improvements over the saline control. Data are mean ± SEM.

time points, but no statistical differences were detected between the interventions based on the two-way ANOVA or separate Mann-Whitney tests for each time point.

With the delayed injection scheme, the CSA averages for the saline and ECM-hydrogel treated groups were reduced at 1 week post-injection (~3 weeks post-repair) relative to the healthy average at 3164 ± 444 μm^2 and 3040 ± 202 μm^2, respectively. Both CSA averages slightly increased at ~6 weeks post-injection (8 weeks post-repair) with the saline group improving to 4065 ± 399 μm^2, and the ECM hydrogel group reaching 3509 ± 275 μm^2. No significant differences were detected amongst the groups or time points based on a two-way ANOVA or individual Mann-Whitney tests. Compared to the immediate injections, the saline control did not produce a hypertrophy response with the delayed injections. However, the effects from the ECM hydrogel were not different for either injection approach.

In addition to quantifying the CSA for muscle fiber morphology, the centralized nuclei were also assessed as a metric for muscle remodeling (Figure 4.3). Healthy muscle contains ~5% centralized nuclei, and injuries to skeletal muscle induce muscle damage and/or remodeling, which leads to an increased number of centralized nuclei.[30] The administration of saline or the ECM hydrogel increased the number of centralized nuclei to a greater extent with

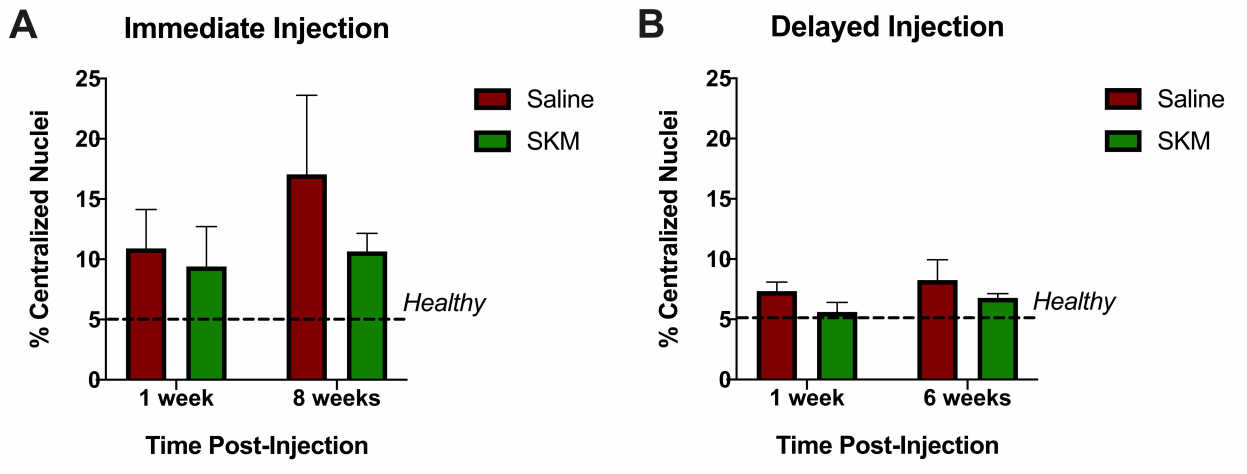

Figure 4.3 The percentage of centralized nuclei was quantified to assess the muscle remodeling for both injection schemes (n=3-5/group). No significant differences were detected. Data are mean ± SEM.

the immediate injection (Figure 4.3A). The ECM hydrogel injection yielded 9.4 ± 3.3% centralized nuclei at 1 week post-injection (1 week post-repair) and slightly increased to 10.7 ±1.5% at 8 weeks post-injection (8 weeks post-repair). Conversely, the saline-treated animals had a similar percentage of centralized nuclei at 1 week post-injection (1 week post-repair) with 10.9 ± 3.2% but increased more noticeably to 17.0 ± 6.6% at 8 weeks post-injection (8 weeks post-repair). The larger increase in percentage centralized nuclei for the saline group relative to the ECM hydrogel could be attributed to the heightened inflammatory response observed with the immediate injections since centralized nuclei can indicate damaged fibers.[30] Higher variability for the percentage of centralized nuclei was also seen with the immediate injection, which may have resulted from the varying degrees of inflammation in the animals. However, no significant differences were detected amongst the time points or experimental groups.

For the delayed injections, the percentages of centralized nuclei for both groups at each time point were closer to healthy levels. The saline control had slightly higher percentages than the ECM hydrogel group at 1 and ~6 weeks post-injection with 7.3 ± 0.8% and 8.3 ± 1.7%, respectively. The ECM hydrogel-treated animals resembled healthy tissue with 5.6 ± 0.8% at 1 week post-injection (~3 weeks post-repair) and 6.8 ± 0.3% at ~6 weeks post-injection (8 weeks post-repair). Statistical differences were not identified from individual unpaired Student's t-tests or a two-way ANOVA. Due to the reduced inflammatory response from the delayed injections, the percentage of centralized nuclei decreased relative to the immediate injections, and therefore, muscle remodeling also appeared to be minimal. This data corresponded to the average CSA values for the delayed injections as those values were also similar to the healthy average.

The delayed injection of saline or the skeletal muscle ECM hydrogel reduced the inflammation in the supraspinatus muscle based on the H&E images, but this also led to less muscle remodeling based on the lower percentages of centralized nuclei. Saline injections are

expected to produce an inflammatory response but will not induce regeneration; however, studies have demonstrated the therapeutics effects of the skeletal muscle ECM hydrogel for muscle remodeling.[26] The lack of improvements from the ECM hydrogel in this study could be due to the use of a chronic animal model or an insufficient dose of the biomaterial. The skeletal muscle ECM hydrogel has only been evaluated in acute animal models, which avoid the development of fibrosis and fatty infiltration. In effect, a biomaterial-alone approach may not be sufficient in a chronic model for skeletal muscle repair where non-contractile tissue, including fibrosis, fatty infiltration, and muscle degeneration, has already replaced contractile tissue. The ECM hydrogel also degrades in approximately 3-4 weeks; therefore, additional therapeutic effects beyond this time point are unlikely. Consequently, multiple sequential injections of the ECM hydrogels should be evaluated to determine whether an ECM hydrogel may be efficacious in a chronic RCT model.

3.2 Expression of key muscle-related genes

To investigate the muscle regeneration of the ECM hydrogels more closely, the expression levels of several key muscle-related genes were quantified and normalized to the saline control (Figure 4.4). Pax7, Myf5, and myogenin are muscle transcription factors in which Pax7 denotes quiescent satellite cells, Myf5 represents activated satellite cells, and myogenin is a marker of differentiating satellite cells. Myosin heavy chain 3 (MYH3), also known as embryonic myosin heavy chain, indicates newly formed muscle fibers, and mammalian target of rapamycin (mTOR) is a master regulator for skeletal muscle metabolism. At 1 week post-injection (1 week post-repair) for the animals injected immediately, no significant differences were found between the saline and ECM hydrogel groups (Figure 4.4A). This was likely due to the extensive inflammation present in all of these animals at this time point. However, with the delayed injection and resulting decrease in inflammation, several genes, including Pax7, Myf5, and mTOR were significantly upregulated, and MYH3 was trending with $p = 0.065$. These

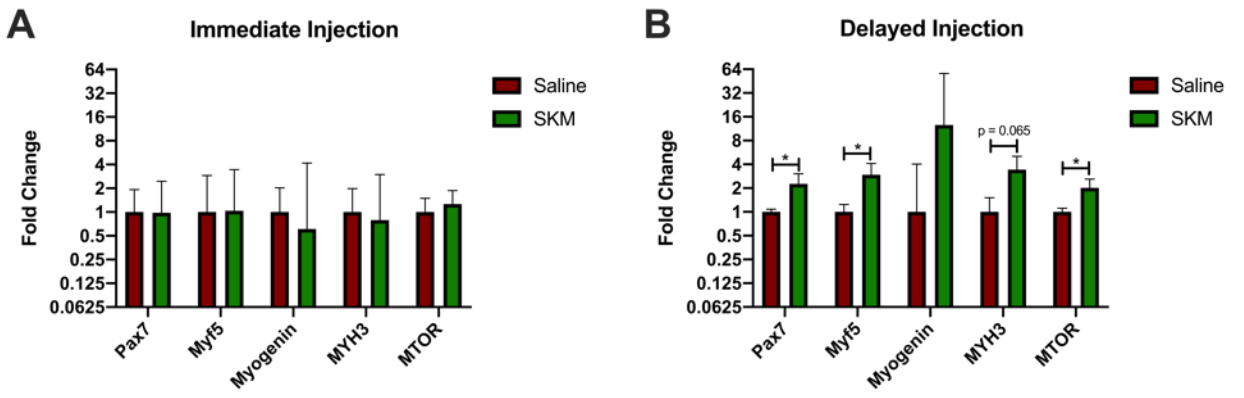

Figure 4.4 Gene expression levels at 1 week post-injection for several muscle transcription factors (Pax7, Myf5, myogenin), embryonic myosin heavy chain (MYH3), and a skeletal muscle metabolic regulator (MTOR). Delaying the intramuscular injections led to an upregulation of several genes related to muscle regeneration with the ECM hydrogel group (n=3-5/group). *p < 0.05 according to unpaired Student's t-tests for each individual gene.

results indicated an upregulation of pathways related to muscle regeneration, but the changes in gene expression levels did not translate to tissue-level improvements. Fold changes were also quantified at 8 weeks post-repair, but no significant differences were identified for either injection scheme. This was expected since previous studies with these decellularized ECM hydrogels have displayed little differential gene expression after 1 week post-injection.[26,31] Regardless, these results validated the efficacy of the skeletal muscle ECM hydrogel to initiate the process of muscle regeneration, but further studies, as mentioned previously, are required to optimize the therapeutic benefits of the material.

Conclusions

RCT represents a significant health burden for the United States, and patients often experience a significant decrease in quality of life as a result of the injury. Several surgical procedures are available for patients with RCTs, and many researchers are investigating injectable therapies for the torn tendons. However, the damage to the unloaded and then reloaded muscle has been largely neglected. We sought to evaluate a decellularized skeletal

muscle ECM hydrogel with injections performed at two different time points to determine the therapeutic efficacy of the material. By delaying the material injections, the initial inflammation from the repair surgery diminished, and the secondary immune response from the material injections initiated some muscle regeneration. No significant differences were detected from quantitative muscle fiber assessments with either injection scheme, which could be attributed to an insufficient dose of the ECM hydrogel resulting from its degradation rate. However, significant upregulation of several important muscle-related genes was observed from the skeletal muscle ECM hydrogel at 1 week post-injection with the delayed injection approach. The upregulation of these genes suggested the ECM hydrogel injection stimulated muscle regeneration pathways, but was insufficient for altering tissue level metrics. This failure to provide a therapeutic effect is likely due to the concurrent environment of fibrosis, fatty infiltration, and degeneration. One promising way to improve the efficacy of ECM hydrogels in a chronic RCT model would be sequential delivery of the biomaterial, where serial injection/material degradation cycles may induce a more robust pro-remodeling response. Nonetheless, this study indicates the importance of assessing the timing of delivering therapeutics in an RCT model to avoid interrupting the inherent natural regenerative processes of the skeletal muscle. To augment the material by including additional therapeutics, the following chapter will assess the ECM hydrogel as a delivery vehicle.

Acknowledgements

This work was supported by the National Institutes of Health (5R21AR072523). This chapter, in part, is currently being prepared for submission for publication of the material. Melissa J. Hernandez, Michael C. Gibbons, Holly L. Sullivan, Emma I. Zelus, Jessica L. Ungerleider, Mary C. Esparza, Shanelle Dorn, Karen L. Christman, Samuel R. Ward. The dissertation author was the primary investigator and author of this material.

References

1. Vitale MA, Vitale MG, Zivin JG, Braman JP, Bigliani LU, Flatow EL. Rotator cuff repair: an analysis of utility scores and cost-effectiveness. *J Shoulder Elbow Surg* **16**, 181-187, doi:10.1016/j.jse.2006.06.013 (2007).

2. Jain NB, Higgins LD, Losina E, Collins J, Blazar PE, Katz JN. Epidemiology of musculoskeletal upper extremity ambulatory surgery in the United States. *BMC Musculoskelet Disord* **15**, 4, doi:10.1186/1471-2474-15-4 (2014).

3. Gerber C, Fuchs B, Hodler J. The results of repair of massive tears of the rotator cuff. *J Bone Joint Surg Am* **82**, 505-515, doi:10.2106/00004623-200004000-00006 (2000).

4. Galatz LM, Ball CM, Teefey SA, Middleton WD, Yamaguchi K. The outcome and repair integrity of completely arthroscopically repaired large and massive rotator cuff tears. *J Bone Joint Surg Am* **86**, 219-224, doi:10.2106/00004623-200402000-00002 (2004).

5. Zumstein MA, Jost B, Hempel J, Hodler J, Gerber C. The clinical and structural long-term results of open repair of massive tears of the rotator cuff. *J Bone Joint Surg Am* **90**, 2423-2431, doi:10.2106/JBJS.G.00677 (2008).

6. Park JY, Lhee SH, Oh KS, Moon SG, Hwang JT. Clinical and ultrasonographic outcomes of arthroscopic suture bridge repair for massive rotator cuff tear. *Arthroscopy* **29**, 280-289, doi:10.1016/j.arthro.2012.09.008 (2013).

7. Chung SW, Huong CB, Kim SH, Oh JH. Shoulder stiffness after rotator cuff repair: risk factors and influence on outcome. *Arthroscopy* **29**, 290-300, doi:10.1016/j.arthro.2012.08.023 (2013).

8. Berdusco R, Trantalis JN, Nelson AA, Sohmer S, More KD, Wong B, Boorman RS, Lo IK. Arthroscopic repair of massive, contracted, immobile tears using interval slides: clinical and MRI structural follow-up. *Knee Surg Sports Traumatol Arthrosc* **23**, 502-507, doi:10.1007/s00167-013-2683-9 (2015).

9. Barth J, Fotiadis E, Barthelemy R, Genna S, Saffarini M. Ultrasonic evaluation of the repair integrity can predict functional outcomes after arthroscopic double-row rotator cuff repair. *Knee Surg Sports Traumatol Arthrosc* **23**, 376-385, doi:10.1007/s00167-015-3505-z (2015).

10. Wang E, Wang L, Gao P, Li Z, Zhou X, Wang S. Single-versus double-row arthroscopic rotator cuff repair in massive tears. *Med Sci Monit* **21**, 1556-1561, doi:10.12659/MSM.893058 (2015).

11. Heuberer PR, Kolblinger R, Buchleitner S, Pauzenberger L, Laky B, Auffarth A, Moroder P, Salem S, Kriegleder B, Anderl W. Arthroscopic management of massive rotator cuff tears: an evaluation of debridement, complete, and partial repair with and without force couple restoration. *Knee Surg Sports Traumatol Arthrosc* **24**, 3828-3837, doi:10.1007/s00167-015-3739-9 (2016).

12. Godeneche A, Freychet B, Lanzetti RM, Clechet J, Carrillon Y, Saffarini M. Should massive rotator cuff tears be reconstructed even when only partially repairable? *Knee Surg Sports Traumatol Arthrosc* **25**, 2164-2173, doi:10.1007/s00167-016-4105-2 (2017).

13. Melis B, Nemoz C, Walch G. Muscle fatty infiltration in rotator cuff tears: descriptive analysis of 1688 cases. *Orthop Traumatol Surg Res* **95**, 319-324, doi:10.1016/j.otsr.2009.05.001 (2009).

14. Melis B, DeFranco MJ, Chuinard C, Walch G. Natural history of fatty infiltration and atrophy of the supraspinatus muscle in rotator cuff tears. *Clin Orthop Relat Res* **468**, 1498-1505, doi:10.1007/s11999-009-1207-x (2010).

15. Gladstone JN, Bishop JY, Lo IK, Flatow EL. Fatty infiltration and atrophy of the rotator cuff do not improve after rotator cuff repair and correlate with poor functional outcome. *Am J Sports Med* **35**, 719-728, doi:10.1177/0363546506297539 (2007).

16. Gerber C, Schneeberger AG, Hoppeler H, Meyer DC. Correlation of atrophy and fatty infiltration on strength and integrity of rotator cuff repairs: a study in thirteen patients. *J Shoulder Elbow Surg* **16**, 691-696, doi:10.1016/j.jse.2007.02.122 (2007).

17. Jo CH, Shin JS. Changes in appearance of fatty infiltration and muscle atrophy of rotator cuff muscles on magnetic resonance imaging after rotator cuff repair: establishing new time-zero traits. *Arthroscopy* **29**, 449-458, doi:10.1016/j.arthro.2012.10.006 (2013).

18. Fabbri M, Ciompi A, Lanzetti RM, Vadala A, Lupariello D, Iorio C, Serlorenzi P, Argento G, Ferretti A, De Carli A. Muscle atrophy and fatty infiltration in rotator cuff tears: Can surgery stop muscular degenerative changes? *J Orthop Sci* **21**, 614-618, doi:10.1016/j.jos.2016.06.001 (2016).

19. Hamano N, Yamamoto A, Shitara H, Ichinose T, Shimoyama D, Sasaki T, Kobayashi T, Kakuta Y, Osawa T, Takagishi K. Does successful rotator cuff repair improve muscle atrophy and fatty infiltration of the rotator cuff? A retrospective magnetic resonance imaging study performed shortly after surgery as a reference. *J Shoulder Elbow Surg* **26**, 967-974, doi:10.1016/j.jse.2016.10.016 (2017).

20. Eliasberg CD, Dar A, Jensen AR, Murray IR, Hardy WR, Kowalski TJ, Garagozlo CA, Natsuhara KM, Khan AZ, McBride OJ, Cha PI, Kelley BV, Evseenko D, Feeley BT,

McAllister DR, Peault B, Petrigliano FA. Perivascular Stem Cells Diminish Muscle Atrophy Following Massive Rotator Cuff Tears in a Small Animal Model. *J Bone Joint Surg Am* **99**, 331-341, doi:10.2106/JBJS.16.00645 (2017).

21. Lee C, Liu M, Agha O, Kim HT, Liu X, Feeley BT. Beige fibro-adipogenic progenitor transplantation reduces muscle degeneration and improves function in a mouse model of delayed repair of rotator cuff tears. *J Shoulder Elbow Surg*, doi:10.1016/j.jse.2019.09.021 (2019).

22. Tellier LE, Krieger JR, Brimeyer AL, Coogan AC, Falis AA, Rinker TE, Schudel A, Thomas SN, Jarrett CD, Willett NJ, Botchwey EA, Temenoff JS. Localized SDF-1alpha Delivery Increases Pro-Healing Bone Marrow-Derived Cells in the Supraspinatus Muscle Following Severe Rotator Cuff Injury. *Regen Eng Transl Med* **4**, 92-103, doi:10.1007/s40883-018-0052-4 (2018).

23. Takase F, Inui A, Mifune Y, Sakata R, Muto T, Harada Y, Ueda Y, Kokubu T, Kurosaka M. Effect of platelet-rich plasma on degeneration change of rotator cuff muscles: In vitro and in vivo evaluations. *J Orthop Res* **35**, 1806-1815, doi:10.1002/jor.23451 (2017).

24. Davies MR, Liu X, Lee L, Laron D, Ning AY, Kim HT, Feeley BT. TGF-beta Small Molecule Inhibitor SB431542 Reduces Rotator Cuff Muscle Fibrosis and Fatty Infiltration By Promoting Fibro/Adipogenic Progenitor Apoptosis. *PLoS One* **11**, e0155486, doi:10.1371/journal.pone.0155486 (2016).

25. DeQuach JA, Lin JE, Cam C, Hu D, Salvatore MA, Sheikh F, Christman KL. Injectable skeletal muscle matrix hydrogel promotes neovascularization and muscle cell infiltration in a hindlimb ischemia model. *Eur Cell Mater* **23**, 400-412; discussion 412 (2012).

26. Ungerleider JL, Johnson TD, Hernandez MJ, Elhag DI, Braden RL, Dzieciatkowska M, Osborn KG, Hansen KC, Mahmud E, Christman KL. Extracellular Matrix Hydrogel Promotes Tissue Remodeling, Arteriogenesis, and Perfusion in a Rat Hindlimb Ischemia Model. *JACC: Basic to Translational Science* **1**, 32-44, doi:10.1016/j.jacbts.2016.01.009 (2016).

27. Ungerleider JL, Johnson TD, Rao N, Christman KL. Fabrication and characterization of injectable hydrogels derived from decellularized skeletal and cardiac muscle. *Methods* **84**, 53-59, doi:10.1016/j.ymeth.2015.03.024 (2015).

28. Hernandez MJ, Yakutis GE, Zelus EI, Hill RC, Dzieciatkowska M, Hansen KC, Christman KL. Manufacturing considerations for producing and assessing decellularized extracellular matrix hydrogels. *Methods*, doi:10.1016/j.ymeth.2019.09.015 (2019).

29. Smith C, Kruger MJ, Smith RM, Myburgh KH. The inflammatory response to skeletal muscle injury: illuminating complexities. *Sports Med* **38**, 947-969, doi:10.2165/00007256-200838110-00005 (2008).

30. Wroblewski R, Edstrom L, Mair WG. Five different types of centrally nucleated muscle fibres in man: elemental composition and morphological criteria. A study of myopathies, fetal tissue and muscle spindle. *J Submicrosc Cytol* **14**, 377-387 (1982).

31. Wassenaar JW, Gaetani R, Garcia JJ, Braden RL, Luo CG, Huang D, DeMaria AN, Omens JH, Christman KL. Evidence for Mechanisms Underlying the Functional Benefits of a Myocardial Matrix Hydrogel for Post-MI Treatment. *J Am Coll Cardiol* **67**, 1074-1086, doi:10.1016/j.jacc.2015.12.035 (2016).

Chapter 5. Decellularized Extracellular Matrix Hydrogels as a Delivery Platform for MicroRNA and Extracellular Vesicle Therapeutics

Introduction

Therapeutics, particularly growth factor–based and cell-based, have been extensively investigated for many clinical applications including, but not limited to, cardiovascular disease,[1,2] cancer,[3,4] and autoimmune diseases.[5,6] With mechanisms regulating essential biological processes such as neovascularization, extracellular matrix remodeling, and inflammation, many growth factor–based and cell-based therapies have been pursued in clinical trials, but translation to the clinic has been largely unsuccessful, as mentioned in Chapter 2.[7-9] Along with a lack of demonstrated efficacy in patients, manufacturing difficulties, like shortened shelf life and high production costs, hinder the feasibility of utilizing cell and growth factor–based approaches. Although engineered growth factors have recently been introduced to overcome many of these obstacles from growth factor therapeutics,[10,11] researchers have been exploring alternative biologics, including microRNAs (miRNAs) and extracellular vesicles (EVs).

MiRNAs, short 20–22 base pair oligonucleotides, have emerged as a promising therapeutic for many applications, including cardiovascular disease,[12] inflammatory disease,[13] metabolic disease,[14] and cancer.[15,16] These therapies harness the ability of miRNAs to regulate post-transcriptional gene expression, which occurs via complementary binding with a target messenger RNA. Chemical modifications have been implemented to produce miRNA mimics and inhibitors with increased stability and more favorable pharmacokinetics,[17,18] which have contributed to multiple miRNA therapeutics progressing to clinical trials.[19]

Another class of biologic products that is emerging as a potent cellular mediator in numerous physiological and pathological processes is EVs. EVs, cell-derived vesicles comprising exosomes and microvesicles, have been shown to play a major role in cell to cell

communication, allowing cells to exchange proteins, lipids, and genetic materials, including mRNAs and,noncoding RNAs such as miRNAs, thus making them effective regulators of tissue homeostasis and repair.[20,21] EVs have been shown to play a major role in many processes including cell signaling,[22,23] immunity,[5,24] cancer development and progression,[25,26] protein clearance,[27] and infection.[28,29] Due to their broad repertoire of bioactive molecules and biological functions,[21,30] EVs have been investigated in many therapeutic applications including organ regeneration,[30-32] cancer,[33,34] immune-based diseases,[35,36] and neurodegenerative diseases.[37]

Although miRNA and EV therapeutics have resulted in significant therapeutic outcomes in many preclinical studies,[19,38] these benefits are hindered by poor delivery strategies and rapid clearance soon after administration. Intravenous delivery is the main delivery route employed by these therapies, and direct injections have also been utilized; however, both of these approaches fail to capitalize on the full therapeutic potential of miRNAs and EVs. Current delivery methods, which often require large payloads, could yield undesired side effects from unspecific binding of miRNAs. In addition, degradation by endogenous nucleases and rapid diffusion represent significant obstacles.[12] Consequently, improved delivery strategies are greatly needed.

Several groups have begun exploring the use of hydrogels as a delivery platform for miRNA and EV therapies,[39,40] but natural materials alone (i.e., without the addition of chemical crosslinkers or modifications) have not been investigated. Unlike most synthetic materials, natural materials can better mimic the *in vivo* environment, but, in particular, decellularized extracellular matrix (ECM), one type of naturally derived biomaterial, successfully maintains biochemical cues of the native tissue microenvironment, as discussed in Chapter 2. Decellularized ECM has several beneficial properties, which include promoting cellular influx,[41] and its degradation products are angiogenic,[42] chemoattractant,[42,43] and promote cell migration and proliferation.[44] In addition, previous studies in a myocardial infarction model have confirmed the benefits of using cardiac-derived ECM hydrogels as a delivery platform for growth factors

with increased arteriogenesis compared to growth factor alone and ECM hydrogel alone controls.[11,45] These ECM hydrogels have also been used for cell delivery in a hindlimb ischemia model of peripheral artery disease, which increased cell engraftment and survival, stimulated neovascularization and could also potentially be used for cell transplantation into the myocardium.[46,47] Along with the efficacy of these decellularized materials, the hydrogels can be delivered minimally invasively, as has been shown via catheter in the heart or a direct injection for the skeletal muscle.[46,48-50] With a complex mixture of proteins, we anticipated that an ample supply of binding sites would be present to facilitate the binding of nucleic acids and EVs. Additionally, ECM hydrogels could ensure localization of both miRNAs and EVs, and the nanoscale and microscale architecture of these hydrogels could promote a slow release of the payload.

Here we evaluated the use of porcine-derived decellularized ECM hydrogels as a

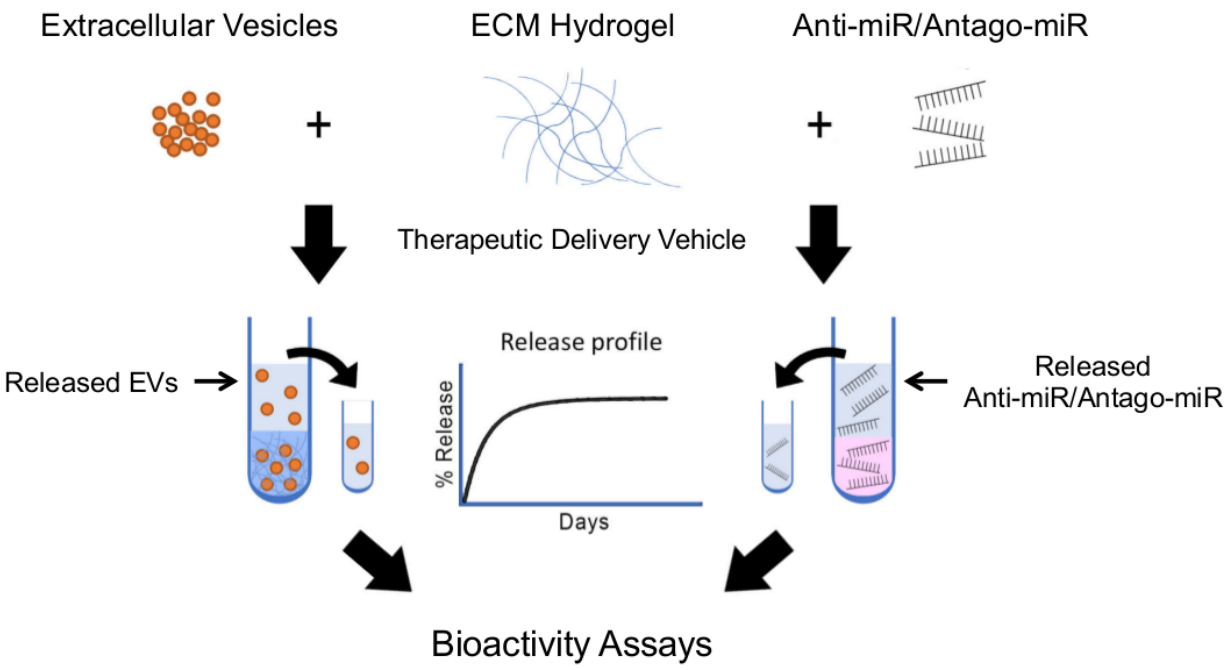

Figure 5.1 Schematic of the workflow for assessing decellularized ECM hydrogels as a delivery platform for miRNA and EV therapeutics. Anti-miRs, antago-miRs, and EVs were encapsulated in ECM hydrogels, and the release profiles were first generated. Antago-miR and EV release samples were then further analyzed to ensure the biologics remained bioactive.

platform for the delivery of model miRNAs and EVs (Figure 5.1). We performed assessments of our ECM hydrogels to provide a slow release profile and maintain bioactivity of miRNA and EV therapeutics, demonstrating that these biomaterials could be a potential delivery platform for such newer generation biologics.

Experimental Section

Extracellular Matrix Preparation: Porcine-derived extracellular matrix (ECM) was prepared as previously described.[51,52] Briefly, tissue from Yorkshire farm pigs was chopped into small cubes (2–5 mm) and decellularized with detergent for 3–5 days. Myocardial ECM, skeletal muscle ECM, and lung ECM was derived from porcine left ventricular myocardium, psoas muscle, and lung, respectively. For both the myocardial and skeletal muscle ECM hydrogels, decellularization was accomplished using 1% sodium dodecyl sulfate, while lung ECM hydrogels were decellularized with 0.1% sodium dodecyl sulfate. Skeletal muscle ECM hydrogels also required an additional isopropyl alcohol step to remove remaining lipids. Following decellularization, the tissue was then lyophilized and milled into a fine powder for long-term storage. Prior to use, the milled powder was partially digested with pepsin (Sigma-Aldrich) at a concentration of 10 mg ECM per 1 mL pepsin solution (1 mg pepsin per 1 mL 0.1 M HCl) for at least 48 h and then neutralized to physiological pH and salt conditions. Finally, the concentration of the ECM hydrogel was adjusted to 6 mg/mL with 1x phosphate buffered saline (PBS) and then lyophilized once again for storage at −80°C.

Cell Culture: All cell lines were preserved in a humidified incubator at 37°C, 5% CO_2 and atmospheric O_2. Human cardiac progenitor cells (hCPCs)[53] and human coronary artery endothelial cells (HCAECs) were used between passages 17–23 and 7–14, respectively. hCPCs were cultured as previously described.[54] Briefly, cells were cultured in 0.1% porcine gelatin (Sigma-Aldrich) coated flasks in growth media consisting of 10% fetal bovine serum

(Thermo Fisher Scientific), 22% EBM2 (Lonza) complemented with EGM2 single quotes (Lonza) in Medium 199 (Corning), 1x nonessential amino acids (Lonza), and 1x penicillin-streptomycin (Life Technologies). HCAECs were grown in MesoEndo cell growth media (Cell Applications).

MiRNA Preparation: Anti-miR and antago-miR oligonucleotides were synthesized with the following sequence: 5' – ACU GCC UGU CUG UGC CUG CUG T – 3' (Eurofins Genomics). Both oligonucleotides were designed with 2' O-methylation, 4 PTO-linkages on the 3' end, and 2 PTO linkages on the 5' end. The antago-miR was further modified with a 3' cholesterol group. For release experiments requiring miRNA detection via fluorescence measurements, a Cy3 dye molecule was conjugated to the 5' end. All lyophilized anti-miR or antago-miR aliquots were resuspended with RNase-free water (Life Technologies) to a final concentration of 100 μM.

Anti-miR and Antago-miR Release: Decellularized ECM hydrogels were prepared by resuspending lyophilized aliquots to a final concentration of 6 mg/mL with RNase-free water or a mixture of RNase-free water and miRNA inhibitors. Cy3-labeled anti-miR (4 μg, n = 3 per ECM type) or antago-miR (4 μg, n = 3 per ECM type) was mixed into the ECM hydrogels.[55] Hydrogels (200 μL total) were formed in microcentrifuge tubes by incubating at 37°C overnight. Larger volume gels were used for the anti-miR and antago-miR release compared to the EVs release, since concentrated amounts of the antago-miR did affect gelation *in vitro*. All ECM hydrogels were initially rinsed with RNase-free 1x PBS (250 μL, Alfa Aesar) to remove any unincorporated anti-miR or antago-miR. After RNase-free 1x PBS (250 μL) was added to each gel, all gels were incubated at 37 °C on a shaker plate. Every 24 ± 2 h for 15 days, the PBS supernatant (200 μL) was collected for quantification of miRNA release. On day 15 following collection of the PBS supernatant, bacterial collagenase (200 μL, Worthington Biomedical Corporation) at 100 U/mL in a 0.1 M Tris-base, 0.25 M CaCl2 solution, pH 7.4 was added to degrade the hydrogels. For complete degradation, gels were incubated at 37°C for 4 h. Then, collagenase samples (200 μL) were collected, and 1.5 M NaCl solution (200 μL) was added to dissociate residual electrostatic interactions between the miRNAs and ECM hydrogels. Gels were allowed to

incubate at 37°C for 1 h prior to sample collection. The miRNA content in each of the release samples was quantified using a BioTek Synergy 4 Multi-Mode Microplate Reader. The Cy3 dye molecules were detected using an emission spectrum with a constant excitation at 547 nm and an emission ranging from 577 to 597 nm. Known amounts of the Cy3-labeled anti-miR or antago-miR were mixed with supernatant from empty ECM hydrogels to construct individual standard curves. These standard curves were then used to determine the amount of released miRNAs. Release samples were stored at −80°C for later analysis.

Antago-miR Bioactivity—Tube Formation Assay: Growth factor reduced Matrigel (10 µL, Corning) was carefully pipetted into individual wells in a µ-slide angiogenesis (Ibidi) and allowed to gel at 37°C for approximately 45 min. In the meantime, HCAECs were collected, and the mixture was then concentrated to 400,000 cells per mL in MesoEndo growth media for a total amount of 10,000 cells per well. In separate microcentrifuge tubes, samples were prepared to yield 50 µL total per well. Each sample tube contained sample (25 µL) and cells in media (25 µL). The sample volume was taken directly from tubes containing the collected release from days 1 and 3 and the PBS supernatant at day 15 prior to collagenase and 1.5 M NaCl treatments. The experiment was done in triplicate, and data was analyzed using the MATLAB AngioQuant toolbox.

EV Isolation: hCPCs from three different donors were used for EV isolation. CPCs were cultured in EV-free growth media until 80% confluency was reached, and the media was collected for EV isolation. To prepare EV free growth media, 33% FBS in Medium 199 was centrifuged at 100,000 x g for 16 h at 4°C (Optima L-80 XP Ultracentrifuge) and sterile filtered. The supernatant was used to prepare growth media as described earlier. hCPC-conditioned media was collected and centrifuged at 2000 x g for 15 min at 4 °C (Eppendorf Centrifuge 5810R) to pellet dead cells and debris. The supernatant was then centrifuged at 10,000 x g for 30 min at 4°C to pellet larger vesicles. The EV pellet was obtained in the last centrifuge step at 100,000 x g at 4 °C for 60 min, sterile filtered, resuspended in PBS, and stored at 4°C when

used the next day or at −80 °C for long-term storage. EV concentration was measured using the Micro BCA Protein Assay Kit (Thermo Scientific). Bovine serum albumin (BSA) standards were prepared within the range of 0.5 μg/mL to 200 μg/mL. Both standards and EV samples were incubated with Micro BCAWorking Reagent at 37°C for 2 h and analyzed with a BioTek Synergy 4 Multi-ModeMicroplate Reader at 562 nm. EV concentration was determined by comparing the values of the EV samples with the known concentrations of the standards.

EV Labeling: EVs were fluorescently labeled with 2 x 10^{-6} M PKH26 red fluorescent dye (Sigma; PKH26 Red Fluorescent cell linker mini-kit for general cell membrane labeling, MINI26-1KT) according to the manufacturer's protocol. The labeling reaction was stopped by adding 33% EV-free FBS in M199 (3 mL) and ultracentrifuged as described earlier. After centrifugation, the pellet was resuspended in PBS at a concentration of 0.5 μg/μL and used for encapsulation experiments.

EV Detection: EV release from decellularized myocardial (n=4), skeletal muscle (n = 3), and lung (n = 3) ECM hydrogels was measured using an EV capture method with antibody-coated magnetic beads. Samples were incubated with anti-CD63-coated magnetic beads (ExoCap, JSR Life Sciences) overnight and washed by aspiration on the magnet and adding 2% BSA in PBS (washing buffer). Secondary CD63-Alexa647 antibody in PBS (BD Biosciences) was added and incubated for 2 h at room temperature while shaking. Beads were washed with washing buffer and resuspended in 0.25% BSA in PBS. Mean fluorescent intensity of the samples was measured by FACS (Canto).

EV Bioactivity—Stimulation of pERK Expression: In a flat bottom 24 well plate, 100,000 HCAECs were plated in MesoEndo cell growth media. After 24 h, the cells were starved by replacing media with Medium 199 for 3 h. Following starvation, HCAECs were incubated with myocardial ECM hydrogel-conditioned PBS (200 μL) from gels with or without encapsulated EVs. Samples from days 1 (n=4 per group), 3 (n=3 per group), and 7 (n = 4 per group) were examined. Cells were lysed with cOmplete Lysis-Mbuffer (Roche) on ice for 5 min. Lysate was

centrifuged at 14,000 x g for 10 min at 4 °C, and the supernatant was stored at −80°C. To prepare the samples for gel electrophoresis, HCAEC lysate (24 µL) was combined with 4x NuPAGE LDS Sample Buffer (10 µL, Thermo Fisher Scientific) and 10x NuPAGE Sample Reducing Agent (4 µL, Thermo Fisher Scientific). The samples were then heated for 10 min at 70°C. A NuPAGE 4–12% Bis-Tris Protein Gel (Thermo Fisher Scientific) was loaded with sample (40 µL) and PageRuler Prestained Protein Ladder (15 µL, Thermo Fisher Scientific). The gel was placed in the XCell SureLockMini-Cell Electrophoresis System (Thermo Fisher Scientific), and the chambers were filled with 1x NuPAGE MOPS SDS Running Buffer (Thermo Fisher Scientific). In addition, Nu-PAGE Antioxidant (500 µL, Thermo Fisher Scientific) was added to the inner chamber. Electrophoresis was performed at 200 volts for 50 min. Western blot was performed using the XCell SureLock Mini-Cell Electrophoresis System filled with 1x NuPAGE Transfer Buffer (Thermo Fisher Scientific) in 10% methanol in deionized water. Proteins were transferred from the gel onto a 0.45 µm nitrocellulose membrane (Bio-Rad Laboratories) at 35 volts for 1 h on ice. The membrane was blocked in 5% BSA (Gemini Bio) in TBS for 1 h at room temperature, followed by incubation with primary antibodies 1:500 phospho-p44/42 MAPK (Thr202/Tyr204; Cell Signal) or 1:750 p42/44 MAPK (ERK1/2; Cell Signaling Technology) in 0.5% BSA in TBS for 1 h at room temperature. The membrane was then incubated with secondary antibody 1:1000 goat anti-rabbit IgG HRP (Abcam) in 5% milk 0.1% Tween in TBS for 1 h at room temperature. Prior to imaging, the membrane was incubated with Pierce ECL Western Blotting Substrate (Thermo Fisher Scientific) for 1 min and imaged with a Bio-Rad ChemiDoc MP System using Image Lab 3.0 software. Total ERK was evaluated on the same membrane used for phospho-p44/42 MAPK. To remove primary and secondary pERK antibodies, the membrane was incubated in stripping buffer (1.5% glycine, 0.1% SDS, 1% Tween 20 in H_2O at pH2.2; 2 x 7.5 min) followed by washing in PBS (2 x 10 min) and TBS (2 x 10 min) and stained as described earlier.

EV Bioactivity—Antiapoptotic Effect: A 96-well plate was coated with 0.1% porcine

gelatin, and 7,500 hCPCs per well were seeded and incubated in growth media overnight. After 24 h, the media was replaced by 10% alamarBlue Cell Viability Reagent (Invitrogen) in growth media and incubated for 4 h at 37°C. AlamarBlue was transferred to a flat bottom 96-well plate (100 µL per well), and baseline values were measured in a BioTek Synergy 4 Multi-Mode Microplate Reader at 550 nm excitation and 585 nm emission. After baseline measurements, cells were incubated with 25 µM H_2O_2 in myocardial ECM hydrogel-conditioned PBS from gels with or without encapsulated EVs for 16 h at 37°C followed by incubation with 10% alamarBlue in growth media for 4 h at 37°C. AlamarBlue was again transferred to a flat bottom 96-well plate (100 µL per well), and the final values were measured with the microplate reader.

Statistical Analysis: Results are displayed as mean ± standard error of the mean (SEM). GraphPad Prism 6 was used for statistical analyses with significance accepted at $p < 0.05$ for all experiments. For the miRNA release experiments, individual standard curves were generated each day for the anti-miR and antago-miR using PBS supernatant collected from empty ECM hydrogels. The amount of miRNA rinsed away on day 0 was subtracted from the original 4 µg and used as the total amount for calculating the cumulative percent released. Some of the error bars are too small to be seen on the miRNA release study graphs. A sample size of three gels was used for both miRNA antagonists and each ECM type (18 gels total). Images taken for assessing the bioactivity of the released antagomiRs were analyzed with the MATLAB AngioQuant toolbox. Each experimental group was done in triplicate, and values for the tubule length and number of junctions were normalized to the PBS supernatant group. For comparisons between the antago-miR release samples and PBS supernatant control, a one-way ANOVA with a Dunnett's post hoc test was used. For the EV release study, standard curves were generated using known amounts of EVs, and EV detection was done as described previously. A total of four hydrogels were evaluated for the myocardial ECM, and three hydrogels were tested for the skeletal muscle and lung ECM. To analyze the results from the pERK expression studies, ImageJ software was utilized to quantify the intensity of the bands (n

= 3 per group for day 3, n = 4 per group for days 1 and 7) with respect to total ERK. Values were normalized to the PBS supernatant group for each time point and then compared with an unpaired Student's t-test. Cell survival for the apoptosis experiment was measured as percentage of viable cells compared to baseline measurements. Six and seven replicates were performed for day 1 and day 3 samples, respectively. An unpaired Student's t-test was used to determine statistical significance.

Supporting Information

Residual dsDNA content: To isolate the residual dsDNA content in the ECM hydrogels, a NucleoSpin® Tissue kit (Macherey-Nagal) was used according to the manufacturer's protocol. Lyophilized aliquots of the ECM (1 mg) post-digestion and neutralization were used for this experiment. Once isolated, the amount of dsDNA (n=3/ECM type) was quantified with a Quant-iT™ PicoGreen™ dsDNA Assay Kit (Invitrogen). All samples and standards were prepared according to the manufacturer's protocol. A BioTek Synergy™ 4 Multi-Mode Microplate Reader was used for fluorescent detection. Data was analyzed with a one-way AVOVA and Tukey's post hoc test using GraphPad Prism 6 software. Significance was accepted at $p < 0.05$. Results are shown as mean ± SEM.

Unlabeled miRNA release: Decellularized myocardial ECM hydrogels were prepared by resuspending lyophilized aliquots to a final concentration of 6 mg/ml with RNase-free water or a mixture of RNase-free water and miRNA inhibitors. Unlabeled anti-miR (4 μg, n=3) or antago-miR (4 μg, n=3) was mixed into the myocardial ECM hydrogels. Hydrogels (200 μL total) were formed in microcentrifuge tubes by incubating at 37°C overnight. The ECM hydrogels were initially rinsed with RNase-free 1X PBS (250 μL, Alfa Aesar) to remove any unincorporated anti-miR or antago-miR. After, RNase-free 1X PBS (250 μL) was added to each gel, all gels were incubated at 37°C on a shaker plate. Every 24 ± 2 hours for 3 days, the PBS supernatant (200

μL) was collected for quantification of miRNA release. The miRNA content in each of the release samples was quantified using the Quant-iT™ RiboGreen™ RNA Assay Kit (Invitrogen) according to the manufacturer's protocol. A BioTek Synergy™ 4 Multi-Mode Microplate Reader was then used for fluorescent detection. Known amounts of the unlabeled anti-miR or antago-miR were mixed with supernatant from empty ECM hydrogels to construct individual standard curves. These standard curves were then used to determine the amount of released miRNAs. Significant differences between the Cy3-labeled and unlabeled miRNAs were compared using unpaired Student's t-tests for each individual day. Significance was accepted at $p < 0.05$. Results are shown as mean ± SEM.

Global proteomics: A previously published protocol was followed to prepare the samples for LC-MS/MS. Milled ECM was chemically digested in 100 mM CNBr in 86% TFA (400 μL) for 24 hours at room temperature and subsequently neutralized with 1M Tris-HCl pH 8.0. Samples (50 μg) were then further digested according to the FASP protocol using a 10 kDa molecular weight cutoff filter. A Gemini-NH C18, 50 x 2 mm column was used for high pH reversed phase chromatography with 20 mM ammonium bicarbonate (pH 10) as mobile phase (A) and 20 mM ammonium bicarbonate and 75% acetonitrile (pH) as mobile phase (B). Global LC-MS/MS was performed on 6 fractions using the LTQ-FT Ultra Hybrid ion cyclotron resonance mass spectrometer (Thermo Fisher Scientific), and nano-flow reverse phase LC-MS/MS was performed using a capillary Agilent 1200 HPLC System. Acquired data for the ECM samples was searched against the *Sus scrofa* protein sequence database from the UniProtKB/Swiss-Prot database. Unique peptide identifications were accepted based on the following conditions: 95.0% minimum peptide threshold, 99.0% minimum protein threshold, contain at least 2 unique peptides, 0.9% peptide FDR (Prophet), and 0.0% protein FDR (Prophet). The top 20 most abundant identified proteins were compared between the three different types of ECM.

Results and Discussion

Due to the earlier success with delivering growth factors and cells with tissue-derived hydrogels,[11,45-47] we hypothesized that the ECM hydrogels would also provide an enhanced delivery platform for model miRNAs and EVs. Specifically, we expected the ECM hydrogels would prolong the release of miRNAs and EVs but would not affect the bioactivity of either therapeutic. To first evaluate retention, model miRNAs and EVs were mixed with three different types of decellularized ECM hydrogels. Specifically, myocardial, skeletal muscle, and lung ECM hydrogels were used due to differences in the composition of ECM proteins[48,51] (Table 5.1, Supporting Information) and to demonstrate potential broad applications of this delivery platform. Although these hydrogels were derived from a xenogeneic tissue source, a very low amount of residual dsDNA was detected (Figure 5.2), indicating adequate decellularization. Cardiac progenitor cell (CPC)-derived EVs[56] and miRNA antagonists for miR-214,[55] an anti-miR and antago-miR, were used as model therapeutics for these studies since they have been evaluated considerably and showed promising results in many therapeutic applications.[31,57,58]

Table 5.1 Global proteomics of ECM hydrogel

Proteins	Myocardium	Skeletal Muscle	Lung
Basement Membrane			
Collagen alpha-1(IV) chain	X	X	X
Collagen alpha-2(IV) chain	X	X	X
Collagen alpha-4(IV) chain			X
Laminin subunit beta-2	X	X	X
Laminin subunit beta-3			X
Laminin subunit gamma-1	X	X	X
Laminin subunit gamma-2			X
Perlecan	X	X	X
Cytoskeletal			
Alpha-1,4 glucan phosphorylase	X		
Desmoplakin	X		
Filamin-C	X		
Myosin-binding protein C, cardiac	X		
Myosin-binding protein C, fast-type		X	
Myosin-1		X	
Myosin-7	X	X	
Phosphorylase		X	
Spectrin alpha chain	X		
ECM Regulator			
Protein-glutamine gamma-glutamyltransferase 2			X
FACIT Collagen			
Collagen alpha1(XIV) chain		X	
Fibrillar Collagen			
Collagen alpha-1(I) chain	X	X	X
Collagen alpha-2(I) chain	X	X	X
Collagen alpha-1(II) chain			X
Collagen alpha-1(III) chain	X	X	X
Collagen alpha-1(V) chain	X	X	X
Collagen alpha-2(V) chain	X	X	X
Collagen alpha-3(V) chain		X	
Matricellular			
Collagen alpha-2(VI) chain	X	X	X
Collagen alpha-3(VI) chain	X	X	X
Emilin 1			X
Fibronectin	X	X	X
Structural ECM			
Fibrillin-1	X	X	X

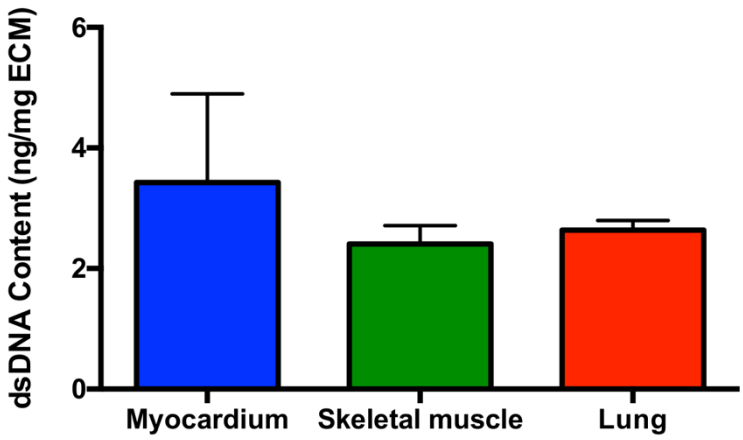

Figure 5.2 Residual dsDNA content is low and does not vary significantly between ECM hydrogels (n=3/gel type). Data are represented as mean ± SEM.

MicroRNAs

For model miRNAs therapeutics, an anti-miR and antago-miR against miR-214 were used, which have been shown to recover neovascularization through the regulation of angiogenic factors.[55] Since decellularized ECM also has angiogenic properties,[42] this miRNA target was chosen since the combination of these therapies could potentially enhance neovascularization processes in later *in vivo* applications. The release profiles from the three ECM hydrogels were evaluated for the miRNA inhibitors up to 15 days (Figure 5.3). Comparing the anti-miR and antago-miR, the release profiles varied significantly, likely due to hydrophobic interactions caused by the presence of a cholesterol group on the 3' end of the antago-miR. In fact, over 50% of the anti-miR was released from the ECM hydrogels by day 2 (Figure 5.3A), but the antago-miR did not reach 50% until around day 10 (Figure 5.3B). Moreover, the anti-miR was virtually completely released by day 10, but the antago-miR was not fully released until the additions of first collagenase to degrade the collagen in the ECM hydrogels and then 1.5 M NaCl to dissociate residual antago-miRs. The rate of release was likely heavily facilitated by hydrophobic interactions, as indicated by the further release of antago-miR, but not anti-miR, following the addition of 1.5 M NaCl. The amount of amines present in the ECM hydrogels could

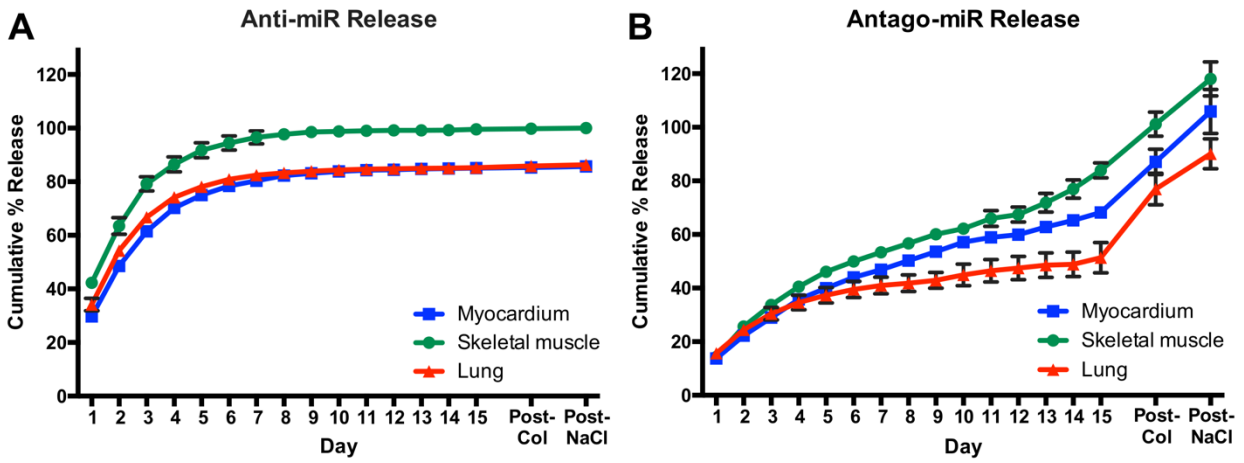

Figure 5.3 Release profiles for miRNA inhibitors of miR-214, an anti-miR and antago-miR. Values were obtained from fluorescence measurements using the Cy3 dye molecule conjugated to each miRNA. A) The anti-miR yielded a more rapid release rate, likely due to the absence of a cholesterol group, which is present on the antago-miR. B) The cholesterol group introduces hydrophobic interactions, which appear to affect the release rate. Some of the error bars are too small to be visualized at each time point. n = 3 per gel type. Data are mean ± SEM.

also contribute to modulating the release profile, since there are some differences present amongst the tissue sources. Despite being very similar, the relative composition of the different ECM proteins differs among the different hydrogels (Table 5.1). Specifically, the lung ECM hydrogel shows a broader composition of basement membrane proteins or different isoforms compared to the myocardial or skeletal muscle hydrogels, which in turn differ in the relative composition of the fibrillar collagen components. Moreover, the relative abundance of these ECM proteins, which was not investigated in the current study, could also play a fundamental role in regulating the release of the encapsulated therapeutic products.

Although some release profiles did not reach 100%, it is unlikely this was due to degradation since the chemical modifications made to the miRNA inhibitors provide added stability, and RNases-free solutions were used for all experiments. For those values above 100%, this was likely due to the gels slightly breaking down toward the end of the 15 days, particularly with the antago-miR, which may have resulted in samples containing larger amounts of the miRNA inhibitors. Unlabeled miRNA antagonists were also examined out to day 3 with the

myocardial ECM hydrogel, which demonstrated that the Cy3 dye did not affect the release profiles (Figure 5.4).

Since a prolonged release over a period of 1–2 weeks would likely be preferred, only the antago-miR was investigated for the *in vitro* studies. In addition, only the myocardial ECM hydrogel was studied further due to the relevance of this particular model miRNA inhibitor in applications of cardiovascular disease, like myocardial infarction. Although the incorporation of the antagomiR into the ECM hydrogels yielded prolonged release profiles, it was necessary to assess whether the ECM hydrogels interfered with the inherent bioactivity of the encapsulated antago-miR. To evaluate the bioactivity of the released antago-miRs, supernatant collected from myocardial ECM hydrogels at days 1 and 3 was tested in a Matrigel tube formation assay with human coronary artery endothelial cells (HCAECs), since miR-214 is known to affect angiogenic-related processes (Figure 5.5).[55] As a control, PBS supernatant obtained from hydrogels at day 15 was used since this likely contained the maximum amount of ECM soluble factors, which could also potentially have angiogenic effects. After incubating the cells with miRNA-conditioned media for 12 h, visual differences were observed in the degree of tube formation (Figure 5.5A). Compared to the PBS supernatant controls, released samples from

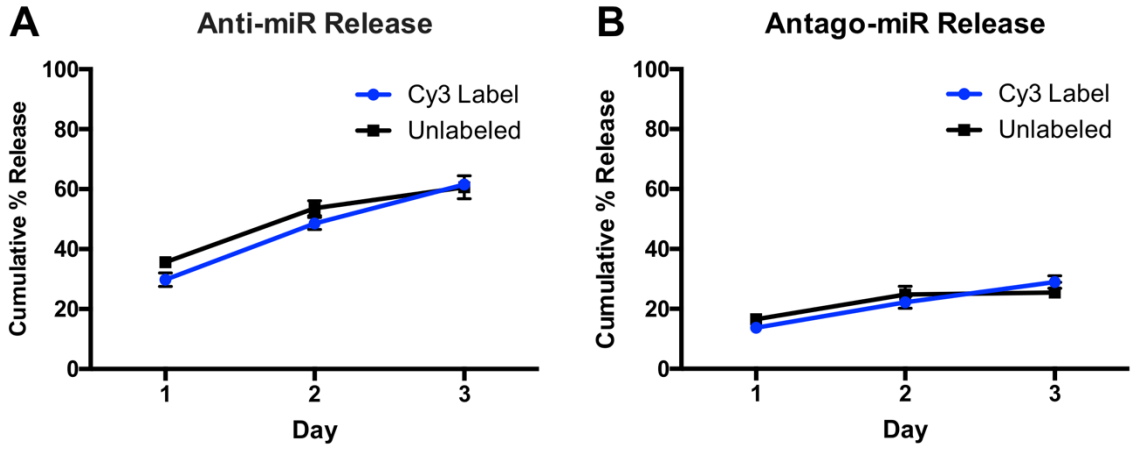

Figure 5.4 A brief release study with unlabeled anti-miR (n=3) and antago-miR (n=3) in myocardial ECM hydrogels did not show any significant differences when compared to the Cy3-labeled miRNAs used in the full release profiles. Data are represented as mean ± SEM.

days 1 and 3 yielded more organized tubes with significantly less cell clustering. When normalized to the PBS supernatant group, the total length increased to 1.53 ± 0.15 for day 1 and 1.42 ± 0.08 for day 3, and the number of junctions increased to 1.84 ± 0.12 and 1.71 ± 0.19 for days 1 and 3, respectively (Figure 5.5B). Although, the extent of tube formation did slightly decrease at day 3 relative to day 1, this was likely due to using a fixed amount of sample for each well, which contained less released antago-miR for day 3. These results demonstrated that the antago-miR largely maintained bioactivity following release from ECM hydrogels; however, it was not possible to determine what fraction of the antago-miRs remained bioactive.

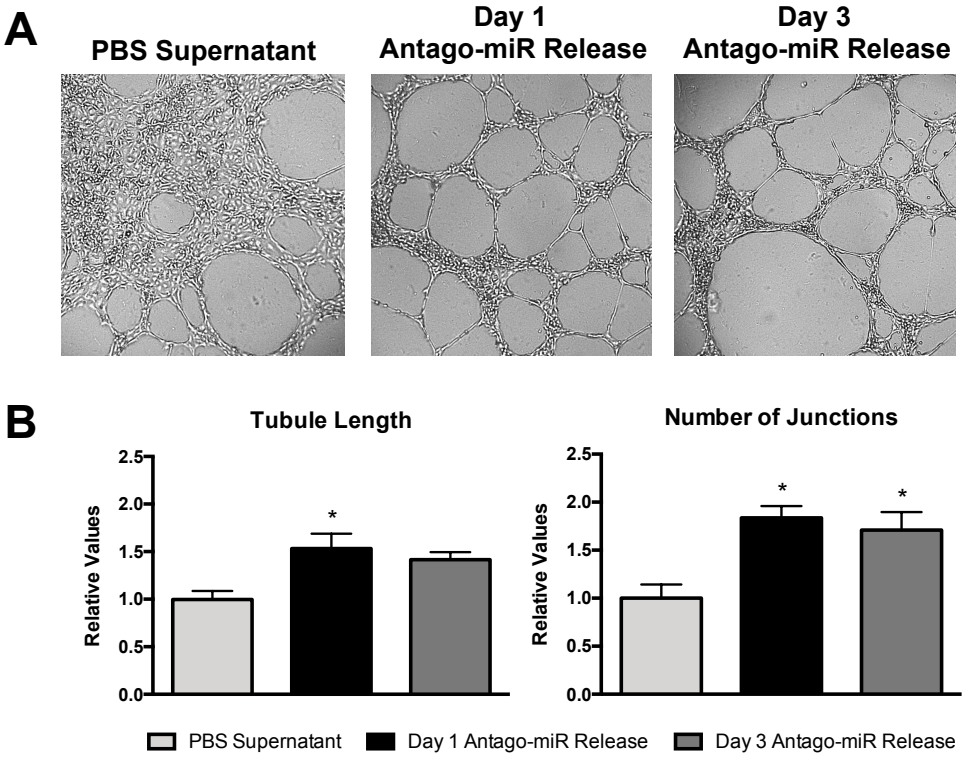

Figure 5.5 Bioactivity of released antago-miRs in a Matrigel tube formation assay. A) Representative images are shown for the tube formation of HCAECs on Matrigel. Since ECM soluble factors are present in the PBS supernatant group, some tube formation is seen but with a large degree of cell clustering. However, released samples from days 1 and 3 produce more organized tubes that yield relative increases in B) tubule length and the number of junctions over the PBS control (n = 3 per group). *$p < 0.05$ compared to the PBS supernatant control using a one-way ANOVA with a Dunnett's post hoc test. Data are mean ± SEM.

Further experiments would be necessary to investigate this.

Overall, the use of the ECM hydrogels prolonged the release of the miRNA inhibitors, particularly the antago-miR, without impairing the bioactivity. This slower release rate would likely be favored for many therapeutic applications, and antago-miRs have been engineered to enhance efficacy *in vivo*. Specifically, the conjugation of the cholesterol group is thought to increase cellular uptake and improve *in vivo* stability.[18,59] By combining this optimized biologic with a decellularized ECM hydrogel, the beneficial outcomes from these therapies could be further augmented.

Extracellular Vesicles

Similar to miRNAs, EVs have also been increasingly studied for many disease applications. In the present study, EVs derived from human cardiac progenitor cells (hCPCs)[56] were used for all experiments, as they have been shown to exert a protective effect on damaged myocardium by reducing cardiomyocyte apoptosis[58] and increasing cardiac function.[60] EVs were encapsulated into three different hydrogels and their release profile from the different scaffolds was evaluated at days 1, 3, and 7 (Figure 5.6). After 7 days, approximately 40%, 45%, and 25% of EVs were released from the myocardial, skeletal, and lung ECM hydrogels, respectively. Of the released EVs, the majority were detected 1 day after encapsulation, ranging from ~30% in the myocardial and skeletal matrix hydrogels to ~20% in the lung ECM hydrogels (Figure 5.6A). Most of the remaining EVs were released by day 3, and only a minimal increase was observed at day 7, indicating that a high amount of EVs were still retained in the gel. This was also indirectly confirmed by labeling the encapsulated EVs with PKH26 red fluorescent dye. A washing step after EV labeling and before EV encapsulation was also performed to remove excess dye, thus minimizing potential artifacts from free dye. The encapsulation of labeled EVs

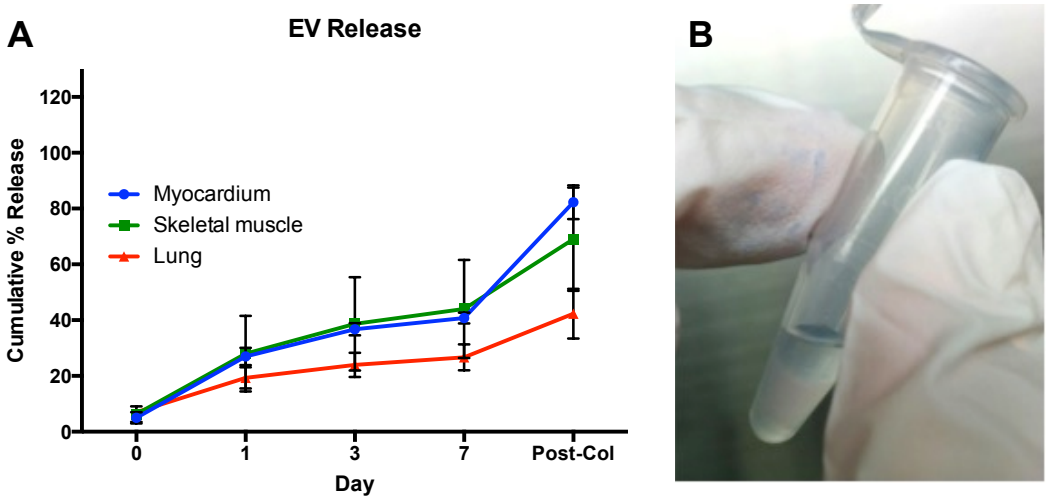

Figure 5.6 Cumulative release of hCPC-derived EVs from porcine ECM hydrogels. A) Conditioned PBS was collected at days 0, 1, 3, and 7, and the concentration of detected EVs is shown as a percentage of the mean fluorescent intensity of untreated EVs. Fluorescent intensities were determined with magnetic bead capture flow cytometry. Myocardial ECM hydrogels (n = 4), skeletal muscle ECM hydrogels (n = 3), and lung ECM hydrogels (n = 3) were examined. B) PKH26-labeled EVs confer a pink color to the gels, which is still visible after 7 days and indicates the presence of the encapsulated EVs. Data are mean ± SEM.

in the hydrogels conferred a pink coloration, which was still visible at the end of the release study, indicative of the presence of the encapsulated EVs (Figure 5.6B). We also quantified the remaining EVs by digesting the hydrogels with collagenase, confirming that indeed the majority of EVs were still encapsulated, with some differences among the different hydrogels. In particular, the cumulative study showed that after collagenase treatment, we were able to detect ~80%, 70%, and 45% of the encapsulated EVs in the myocardial, skeletal, and lung ECM hydrogels, respectively. Since we were not able to detect all of the encapsulated EVs, we evaluated the effects of the collagenase treatment on EV detection shortly after encapsulation. EVs were encapsulated within the different hydrogels, and after hydrogel gelation, the gels were immediately treated with collagenase and compared with the same amount of nonencapsulated EVs. Our analysis showed that only ~60% of the encapsulated EVs (58.75 ± 23.4%) were detected, indicating that the collagenase treatment negatively affected the EV detection, thus explaining the reason for not being able to recover all encapsulated EVs. However, we cannot

exclude that some of the released EVs degraded due to experimental conditions, since it has been previously demonstrated that EVs are degraded when stored at 37°C.[61] Moreover, since our detection method is based on CD63 expression on the EV membrane, it is possible that the expression of this receptor is influenced by our experimental conditions, thus affecting the total detection of the encapsulated EVs; however, this is unlikely. We also observed some degree of variability among different experiments when using the same tissue source. A possible reason could be due to slight differences in the ECM fibrous network between different experiments or potential differences in EV size between isolations, which could influence the kinetics of the EV release.

All ECM hydrogels provided a slow release of the encapsulated EV therapeutics; however, some differences were observed on the extent of the EV release between the different tissue sources. The level of released EVs detected in the EV-conditioned media from the lung ECM hydrogels was considerably lower than the values of the myocardial ECM and the skeletal muscle ECM hydrogels. A possible explanation could be that the composition of the lung ECM hydrogels allowed for a more sustained encapsulation of the EVs compared to the muscle tissue–derived ECM hydrogels. It is possible that a combination of physical entrapment, noncovalent interactions, or specific binding domains all contributed to the release profile of the encapsulated EVs. The combination of tissue-specific ECM molecules (Table 5.1), which can affect the mechanical properties, pore size, and electrostatic properties of the hydrogel, could explain the differences observed among the different tissue sources.[62] Another possible mechanism behind the rate of EV release from the ECM hydrogels is the presence of matrix metalloproteinases (MMPs) in cardiac progenitor cell-derived extracellular vesicles.[53] These enzymes are generally known to induce ECM remodeling by degrading certain ECM molecules, which could modulate the degradation rate of ECM hydrogels *in vivo*.

We next evaluated if encapsulation could negatively impact the bioactivity of the

released EVs and if the released EVs would still assert their beneficial effects once released from the hydrogels. Conditioned media from EVs encapsulated in hydrogels was used to stimulate the phosphorylation of the ERK 1/2 pathway in target HCAECs and compared to the PBS supernatant collected from empty hydrogels. Western blot analysis showed that the EVs released 1 and 3 days after encapsulation significantly increased the phosphorylation of the

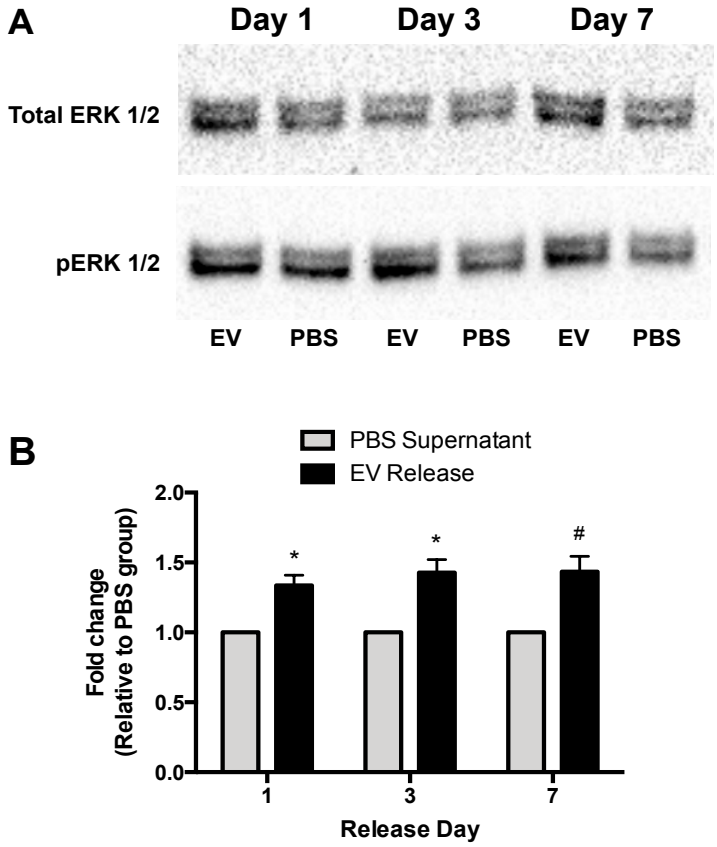

Figure 5.7 The effect of CPC-derived EVs released from myocardial ECM hydrogels on pERK 1/2 levels in HCAECs. Cells were incubated with conditioned PBS collected at days 1 (n = 3 per group), 3 (n = 3 per group), and 7 (n = 3 per group). The expression of pERK 1/2 was determined with A) western blot analysis and B) normalized to total ERK content and relative to conditioned PBS from empty ECM hydrogels. *$p < 0.05$ and #$p = 0.059$ compared to PBS supernatant using an unpaired Student's t-test. Data are mean ± SEM.

ERK 1/2 proteins when compared to the PBS supernatant controls (1.33 ± 0.07 and 1.42 ± 0.09 fold increase, respectively), and a trend was seen when the EV-conditioned media collected 7 days after encapsulation was used (1.43 ± 0.11 fold increase, p = 0.058; Figure 5.7). The reduced bioactivity of the released EVs 1 week after encapsulation could likely be due to the lower amount of EVs released after the first days. However, the minimal observed release or reduced bioactivity of the EV-conditioned media released at day 7 could also partly be due to EV degradation in the experimental conditions, as mentioned earlier.

Since the EVs' therapeutic efficacy is in part mediated by exerting antiapoptotic effects on the targeted cells,[63] we then investigated whether released EVs were also able to preserve cell survival in the presence of reactive oxygen species. Based on the pERK activation data, we only evaluated EVs released 1 and 3 days after encapsulation. A significant increase in cell

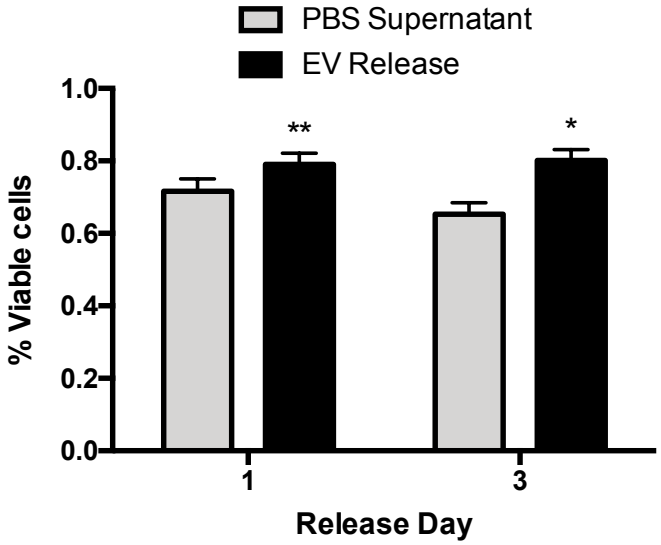

Figure 5.8 The protective effect of CPC-derived EVs released from myocardial ECM hydrogels on H2O2-induced apoptosis of hCPCs. Cells were incubated with conditioned PBS, collected at days 1 (n = 6 per group) and 3 (n = 7 per group) in combination with 25 μm H_2O_2. The survival rate was determined with an alamarBlue cell viability assay and normalized to alamarBlue baseline values. *p < 0.05 and **p < 0.01 compared to PBS supernatant using an unpaired Student's t-test. Data are mean ± SEM.

survival was observed with both EV-conditioned medias when compared to the PBS supernatants (EVs: 79.07 ± 3.03% at day 1 and 80.08 ± 3.06% at day 3; PBS: 71.64 ± 3.40% at day 1 and 65.26 ± 3.22% at day 3; Figure 5.8). The modest increase in cell survival observed using EVs released after 1 day could be explained by the protective effects also exerted by the hydrogel alone, as has been previously shown both *in vitro*[47] and *in vivo*[64]. It is possible that small ECM molecules that do not form the fibrous network of the hydrogel were released soon after PBS incubation, thus mitigating the pro-survival effects observed using EVs released 1 day after encapsulation.

Conclusion and Outlook

The discovery of miRNAs and EVs as potent mediators of cellular function and tissue homeostasis has led many researchers to investigate their potential use for a wide variety of disease pathways. However, similar to cells, growth factors, or small molecules, their delivery is hampered by rapid clearance soon after administration, therefore potentially limiting their therapeutic effects. The use of decellularized ECM hydrogels has been proposed as an alternative approach to modulate the release rate of model miRNA and EV therapeutics. Our data collectively indicated that these hydrogels successfully retained the encapsulated biologics over a prolonged period of time with some differences between the therapeutics or hydrogel tissue source. Samples collected for the release profiles were also further investigated with bioactivity assays, and both the antago-miR and EVs remained bioactive after being released from the ECM hydrogels. This study demonstrates that decellularized ECM hydrogels may represent a platform for slow delivery of miRNAs and EVs due to their ability to induce a pro-regenerative response in the damaged tissue, the possibility of utilizing minimally invasive catheter delivery, and an established path to clinical translation. Since the myocardial ECM hydrogel has already been injected via catheter in the hearts of myocardial infarction patients in

a Phase I trial (clinicaltrials.gov identifier NCT02305602), and several other xenogeneic ECM products have been safely used in patients,[65,66] this suggests the clinical applicability of using injectable ECM hydrogels to deliver miRNAs and EVs in a wide array of disease applications, including peripheral artery disease. With the ability to potentially utilize the ECM hydrogels as a stand-alone therapy or as a delivery platform for including additional therapeutics, the feasibility for manufacturing was evaluated in the following chapter.

Acknowledgements

M.J.H. and R.G. contributed equally to this work. This work was supported by the NIH NHLBI (R01HL113468). M.J.H. was supported by the NHLBI (F31HL132584, T32HL105373). J.P.G.S. and E.M. are supported by Horizon2020 ERC-2016-COG EVICARE (725229), the Project SMARTCARE-II of the BioMedicalMaterials Institute, co-funded by the ZonMw-TAS program (#116002016), the Dutch Ministry of Economic Affairs, Agriculture and Innovation and the Netherlands CardioVascular Research Initiative (CVON): the Dutch Heart Foundation, Dutch Federations of University Medical Centers, the Netherlands Organization for Health Research and Development, and the Royal Netherlands Academy of Sciences.

This chapter, in part, is a reprint of the material as it appears in Advanced Therapeutics 2018. The authors are Melissa J. Hernandez, Roberto Gaetani, Vera M. Peiters, Nathan W. Ng, Audrey E. Chang, Taylor R. Martin, Eva van Ingen, Emma A. Mol, Monika Dzieciatkowska, Kirk C. Hansen, Joost P.G. Sluijter, and Karen L. Christman. The dissertation author was a primary investigator of this material.

References

1. Segers VF, Lee RT. Stem-cell therapy for cardiac disease. *Nature* **451**, 937-942, doi:10.1038/nature06800 (2008).

2. Hastings CL, Roche ET, Ruiz-Hernandez E, Schenke-Layland K, Walsh CJ, Duffy GP. Drug and cell delivery for cardiac regeneration. *Adv Drug Deliv Rev* **84**, 85-106, doi:10.1016/j.addr.2014.08.006 (2015).

3. Woodburn JR. The epidermal growth factor receptor and its inhibition in cancer therapy. *Pharmacol Ther* **82**, 241-250 (1999).

4. Tugues S, Koch S, Gualandi L, Li X, Claesson-Welsh L. Vascular endothelial growth factors and receptors: anti-angiogenic therapy in the treatment of cancer. *Mol Aspects Med* **32**, 88-111, doi:10.1016/j.mam.2011.04.004 (2011).

5. Robbins PD, Morelli AE. Regulation of immune responses by extracellular vesicles. *Nat Rev Immunol* **14**, 195-208, doi:10.1038/nri3622 (2014).

6. Munir H, McGettrick HM. Mesenchymal Stem Cell Therapy for Autoimmune Disease: Risks and Rewards. *Stem Cells Dev* **24**, 2091-2100, doi:10.1089/scd.2015.0008 (2015).

7. Trounson A, McDonald C. Stem Cell Therapies in Clinical Trials: Progress and Challenges. *Cell Stem Cell* **17**, 11-22, doi:10.1016/j.stem.2015.06.007 (2015).

8. Feyen DAM, Gaetani R, Doevendans PA, Sluijter JPG. Stem cell-based therapy: Improving myocardial cell delivery. *Adv Drug Deliv Rev* **106**, 104-115, doi:10.1016/j.addr.2016.04.023 (2016).

9. Sluijter JPG, Davidson SM, Boulanger CM, Buzas EI, de Kleijn DPV, Engel FB, Giricz Z, Hausenloy DJ, Kishore R, Lecour S, Leor J, Madonna R, Perrino C, Prunier F, Sahoo S, Schiffelers RM, Schulz R, Van Laake LW, Ytrehus K, Ferdinandy P. Extracellular vesicles in diagnostics and therapy of the ischaemic heart: Position Paper from the Working Group on Cellular Biology of the Heart of the European Society of Cardiology. *Cardiovasc Res* **114**, 19-34, doi:10.1093/cvr/cvx211 (2018).

10. Liu CJ, Jones DS, 2nd, Tsai PC, Venkataramana A, Cochran JR. An engineered dimeric fragment of hepatocyte growth factor is a potent c-MET agonist. *FEBS Lett* **588**, 4831-4837, doi:10.1016/j.febslet.2014.11.018 (2014).

11. Sonnenberg SB, Rane AA, Liu CJ, Rao N, Agmon G, Suarez S, Wang R, Munoz A, Bajaj V, Zhang S, Braden R, Schup-Magoffin PJ, Kwan OL, DeMaria AN, Cochran JR, Christman KL. Delivery of an engineered HGF fragment in an extracellular matrix-derived hydrogel prevents negative LV remodeling post-myocardial infarction. *Biomaterials* **45**, 56-63, doi:10.1016/j.biomaterials.2014.12.021 (2015).

12. van Rooij E, Olson EN. MicroRNA therapeutics for cardiovascular disease: opportunities and obstacles. *Nat Rev Drug Discov* **11**, 860-872, doi:10.1038/nrd3864 (2012).

13. Dai R, Ahmed SA. MicroRNA, a new paradigm for understanding immunoregulation, inflammation, and autoimmune diseases. *Transl Res* **157**, 163-179, doi:10.1016/j.trsl.2011.01.007 (2011).

14. Rottiers V, Naar AM. MicroRNAs in metabolism and metabolic disorders. *Nat Rev Mol Cell Biol* **13**, 239-250, doi:10.1038/nrm3313 (2012).

15. Chen Y, Gao DY, Huang L. In vivo delivery of miRNAs for cancer therapy: challenges and strategies. *Adv Drug Deliv Rev* **81**, 128-141, doi:10.1016/j.addr.2014.05.009 (2015).

16. Kasinski AL, Slack FJ. Epigenetics and genetics. MicroRNAs en route to the clinic: progress in validating and targeting microRNAs for cancer therapy. *Nat Rev Cancer* **11**, 849-864, doi:10.1038/nrc3166 (2011).

17. Lennox KA, Behlke MA. Chemical modification and design of anti-miRNA oligonucleotides. *Gene Ther* **18**, 1111-1120, doi:10.1038/gt.2011.100 (2011).

18. Krutzfeldt J, Rajewsky N, Braich R, Rajeev KG, Tuschl T, Manoharan M, Stoffel M. Silencing of microRNAs in vivo with 'antagomirs'. *Nature* **438**, 685-689, doi:10.1038/nature04303 (2005).

19. van Rooij E, Purcell AL, Levin AA. Developing microRNA therapeutics. *Circ Res* **110**, 496-507, doi:10.1161/CIRCRESAHA.111.247916 (2012).

20. Pitt JM, Kroemer G, Zitvogel L. Extracellular vesicles: masters of intercellular communication and potential clinical interventions. *J Clin Invest* **126**, 1139-1143, doi:10.1172/JCI87316 (2016).

21. van Niel G, D'Angelo G, Raposo G. Shedding light on the cell biology of extracellular vesicles. *Nat Rev Mol Cell Biol*, doi:10.1038/nrm.2017.125 (2018).

22. Valadi H, Ekstrom K, Bossios A, Sjostrand M, Lee JJ, Lotvall JO. Exosome-mediated transfer of mRNAs and microRNAs is a novel mechanism of genetic exchange between cells. *Nat Cell Biol* **9**, 654-659, doi:10.1038/ncb1596 (2007).

23. Cossetti C, Iraci N, Mercer TR, Leonardi T, Alpi E, Drago D, Alfaro-Cervello C, Saini HK, Davis MP, Schaeffer J, Vega B, Stefanini M, Zhao C, Muller W, Garcia-Verdugo JM, Mathivanan S, Bachi A, Enright AJ, Mattick JS, Pluchino S. Extracellular vesicles from

neural stem cells transfer IFN-gamma via Ifngr1 to activate Stat1 signaling in target cells. *Mol Cell* **56**, 193-204, doi:10.1016/j.molcel.2014.08.020 (2014).

24. Robbins PD, Dorronsoro A, Booker CN. Regulation of chronic inflammatory and immune processes by extracellular vesicles. *J Clin Invest* **126**, 1173-1180, doi:10.1172/JCI81131 (2016).

25. Kosaka N, Yoshioka Y, Fujita Y, Ochiya T. Versatile roles of extracellular vesicles in cancer. *J Clin Invest* **126**, 1163-1172, doi:10.1172/JCI81130 (2016).

26. Naito Y, Yoshioka Y, Yamamoto Y, Ochiya T. How cancer cells dictate their microenvironment: present roles of extracellular vesicles. *Cell Mol Life Sci* **74**, 697-713, doi:10.1007/s00018-016-2346-3 (2017).

27. Yuyama K, Sun H, Mitsutake S, Igarashi Y. Sphingolipid-modulated exosome secretion promotes clearance of amyloid-beta by microglia. *J Biol Chem* **287**, 10977-10989, doi:10.1074/jbc.M111.324616 (2012).

28. Bukong TN, Momen-Heravi F, Kodys K, Bala S, Szabo G. Exosomes from hepatitis C infected patients transmit HCV infection and contain replication competent viral RNA in complex with Ago2-miR122-HSP90. *PLoS Pathog* **10**, e1004424, doi:10.1371/journal.ppat.1004424 (2014).

29. Wiley RD, Gummuluru S. Immature dendritic cell-derived exosomes can mediate HIV-1 trans infection. *Proc Natl Acad Sci U S A* **103**, 738-743, doi:10.1073/pnas.0507995103 (2006).

30. S ELA, Mager I, Breakefield XO, Wood MJ. Extracellular vesicles: biology and emerging therapeutic opportunities. *Nat Rev Drug Discov* **12**, 347-357, doi:10.1038/nrd3978 (2013).

31. Mol EA, Goumans MJ, Sluijter JPG. Cardiac Progenitor-Cell Derived Exosomes as Cell-Free Therapeutic for Cardiac Repair. *Adv Exp Med Biol* **998**, 207-219, doi:10.1007/978-981-10-4397-0_14 (2017).

32. Jing H, He X, Zheng J. Exosomes and regenerative medicine: state of the art and perspectives. *Transl Res* **196**, 1-16, doi:10.1016/j.trsl.2018.01.005 (2018).

33. Tickner JA, Urquhart AJ, Stephenson SA, Richard DJ, O'Byrne KJ. Functions and therapeutic roles of exosomes in cancer. *Front Oncol* **4**, 127, doi:10.3389/fonc.2014.00127 (2014).

34. Vader P, Breakefield XO, Wood MJ. Extracellular vesicles: emerging targets for cancer therapy. *Trends Mol Med* **20**, 385-393, doi:10.1016/j.molmed.2014.03.002 (2014).

35. Borger V, Bremer M, Ferrer-Tur R, Gockeln L, Stambouli O, Becic A, Giebel B. Mesenchymal Stem/Stromal Cell-Derived Extracellular Vesicles and Their Potential as Novel Immunomodulatory Therapeutic Agents. *Int J Mol Sci* **18**, doi:10.3390/ijms18071450 (2017).

36. Tan L, Wu H, Liu Y, Zhao M, Li D, Lu Q. Recent advances of exosomes in immune modulation and autoimmune diseases. *Autoimmunity* **49**, 357-365, doi:10.1080/08916934.2016.1191477 (2016).

37. Quek C, Hill AF. The role of extracellular vesicles in neurodegenerative diseases. *Biochem Biophys Res Commun* **483**, 1178-1186, doi:10.1016/j.bbrc.2016.09.090 (2017).

38. Akyurekli C, Le Y, Richardson RB, Fergusson D, Tay J, Allan DS. A systematic review of preclinical studies on the therapeutic potential of mesenchymal stromal cell-derived microvesicles. *Stem Cell Rev* **11**, 150-160, doi:10.1007/s12015-014-9545-9 (2015).

39. Hernandez MJ, Christman KL. Designing Acellular Injectable Biomaterial Therapeutics for Treating Myocardial Infarction and Peripheral Artery Disease. *JACC Basic Transl Sci* **2**, 212-226, doi:10.1016/j.jacbts.2016.11.008 (2017).

40. Curtin CM, Castano IM, O'Brien FJ. Scaffold-Based microRNA Therapies in Regenerative Medicine and Cancer. *Adv Healthc Mater* **7**, doi:10.1002/adhm.201700695 (2018).

41. Rieder E, Nigisch A, Dekan B, Kasimir MT, Muhlbacher F, Wolner E, Simon P, Weigel G. Granulocyte-based immune response against decellularized or glutaraldehyde cross-linked vascular tissue. *Biomaterials* **27**, 5634-5642, doi:10.1016/j.biomaterials.2006.06.020 (2006).

42. Li F, Li W, Johnson S, Ingram D, Yoder M, Badylak S. Low-molecular-weight peptides derived from extracellular matrix as chemoattractants for primary endothelial cells. *Endothelium* **11**, 199-206, doi:10.1080/10623320490512390 (2004).

43. Beattie AJ, Gilbert TW, Guyot JP, Yates AJ, Badylak SF. Chemoattraction of progenitor cells by remodeling extracellular matrix scaffolds. *Tissue Eng Part A* **15**, 1119-1125, doi:10.1089/ten.tea.2008.0162 (2009).

44. Reing JE, Zhang L, Myers-Irvin J, Cordero KE, Freytes DO, Heber-Katz E, Bedelbaeva K, McIntosh D, Dewilde A, Braunhut SJ, Badylak SF. Degradation products of

extracellular matrix affect cell migration and proliferation. *Tissue Eng Part A* **15**, 605-614, doi:10.1089/ten.tea.2007.0425 (2009).

45. Seif-Naraghi SB, Horn D, Schup-Magoffin PJ, Christman KL. Injectable extracellular matrix derived hydrogel provides a platform for enhanced retention and delivery of a heparin-binding growth factor. *Acta Biomater* **8**, 3695-3703, doi:10.1016/j.actbio.2012.06.030 (2012).

46. Rao N, Agmon G, Tierney MT, Ungerleider JL, Braden RL, Sacco A, Christman KL. Engineering an Injectable Muscle-Specific Microenvironment for Improved Cell Delivery Using a Nanofibrous Extracellular Matrix Hydrogel. *ACS Nano* **11**, 3851-3859, doi:10.1021/acsnano.7b00093 (2017).

47. Gaetani R, Yin C, Srikumar N, Braden R, Doevendans PA, Sluijter JP, Christman KL. Cardiac-Derived Extracellular Matrix Enhances Cardiogenic Properties of Human Cardiac Progenitor Cells. *Cell Transplant* **25**, 1653-1663, doi:10.3727/096368915X689794 (2016).

48. Ungerleider JL, Johnson TD, Hernandez MJ, Elhag DI, Braden RL, Dzieciatkowska M, Osborn KG, Hansen KC, Mahmud E, Christman KL. Extracellular Matrix Hydrogel Promotes Tissue Remodeling, Arteriogenesis, and Perfusion in a Rat Hindlimb Ischemia Model. *JACC: Basic to Translational Science* **1**, 32-44, doi:10.1016/j.jacbts.2016.01.009 (2016).

49. Singelyn JM, Sundaramurthy P, Johnson TD, Schup-Magoffin PJ, Hu DP, Faulk DM, Wang J, Mayle KM, Bartels K, Salvatore M, Kinsey AM, Demaria AN, Dib N, Christman KL. Catheter-deliverable hydrogel derived from decellularized ventricular extracellular matrix increases endogenous cardiomyocytes and preserves cardiac function post-myocardial infarction. *J Am Coll Cardiol* **59**, 751-763, doi:10.1016/j.jacc.2011.10.888 (2012).

50. Seif-Naraghi SB, Singelyn JM, Salvatore MA, Osborn KG, Wang JJ, Sampat U, Kwan OL, Strachan GM, Wong J, Schup-Magoffin PJ, Braden RL, Bartels K, DeQuach JA, Preul M, Kinsey AM, DeMaria AN, Dib N, Christman KL. Safety and efficacy of an injectable extracellular matrix hydrogel for treating myocardial infarction. *Sci Transl Med* **5**, 173ra125, doi:10.1126/scitranslmed.3005503 (2013).

51. Merna N, Fung KM, Wang JJ, King CR, Hansen KC, Christman KL, George SC. Differential beta3 Integrin Expression Regulates the Response of Human Lung and Cardiac Fibroblasts to Extracellular Matrix and Its Components. *Tissue Eng Part A* **21**, 2195-2205, doi:10.1089/ten.TEA.2014.0337 (2015).

52. Ungerleider JL, Johnson TD, Rao N, Christman KL. Fabrication and characterization of injectable hydrogels derived from decellularized skeletal and cardiac muscle. *Methods* **84**, 53-59, doi:10.1016/j.ymeth.2015.03.024 (2015).

53. Vrijsen KR, Sluijter JP, Schuchardt MW, van Balkom BW, Noort WA, Chamuleau SA, Doevendans PA. Cardiomyocyte progenitor cell-derived exosomes stimulate migration of endothelial cells. *J Cell Mol Med* **14**, 1064-1070, doi:10.1111/j.1582-4934.2010.01081.x (2010).

54. Smits AM, van Vliet P, Metz CH, Korfage T, Sluijter JP, Doevendans PA, Goumans MJ. Human cardiomyocyte progenitor cells differentiate into functional mature cardiomyocytes: an in vitro model for studying human cardiac physiology and pathophysiology. *Nat Protoc* **4**, 232-243, doi:10.1038/nprot.2008.229 (2009).

55. van Mil A, Grundmann S, Goumans MJ, Lei Z, Oerlemans MI, Jaksani S, Doevendans PA, Sluijter JP. MicroRNA-214 inhibits angiogenesis by targeting Quaking and reducing angiogenic growth factor release. *Cardiovasc Res* **93**, 655-665, doi:10.1093/cvr/cvs003 (2012).

56. Vrijsen KR, Maring JA, Chamuleau SA, Verhage V, Mol EA, Deddens JC, Metz CH, Lodder K, van Eeuwijk EC, van Dommelen SM, Doevendans PA, Smits AM, Goumans MJ, Sluijter JP. Exosomes from Cardiomyocyte Progenitor Cells and Mesenchymal Stem Cells Stimulate Angiogenesis Via EMMPRIN. *Adv Healthc Mater* **5**, 2555-2565, doi:10.1002/adhm.201600308 (2016).

57. Aurora AB, Mahmoud AI, Luo X, Johnson BA, van Rooij E, Matsuzaki S, Humphries KM, Hill JA, Bassel-Duby R, Sadek HA, Olson EN. MicroRNA-214 protects the mouse heart from ischemic injury by controlling Ca(2)(+) overload and cell death. *J Clin Invest* **122**, 1222-1232, doi:10.1172/JCI59327 (2012).

58. Chen L, Wang Y, Pan Y, Zhang L, Shen C, Qin G, Ashraf M, Weintraub N, Ma G, Tang Y. Cardiac progenitor-derived exosomes protect ischemic myocardium from acute ischemia/reperfusion injury. *Biochem Biophys Res Commun* **431**, 566-571, doi:10.1016/j.bbrc.2013.01.015 (2013).

59. Krutzfeldt J, Kuwajima S, Braich R, Rajeev KG, Pena J, Tuschl T, Manoharan M, Stoffel M. Specificity, duplex degradation and subcellular localization of antagomirs. *Nucleic Acids Res* **35**, 2885-2892, doi:10.1093/nar/gkm024 (2007).

60. Barile L, Lionetti V, Cervio E, Matteucci M, Gherghiceanu M, Popescu LM, Torre T, Siclari F, Moccetti T, Vassalli G. Extracellular vesicles from human cardiac progenitor cells inhibit cardiomyocyte apoptosis and improve cardiac function after myocardial infarction. *Cardiovasc Res* **103**, 530-541, doi:10.1093/cvr/cvu167 (2014).

61. Sokolova V, Ludwig AK, Hornung S, Rotan O, Horn PA, Epple M, Giebel B. Characterisation of exosomes derived from human cells by nanoparticle tracking analysis and scanning electron microscopy. *Colloids Surf B Biointerfaces* **87**, 146-150, doi:10.1016/j.colsurfb.2011.05.013 (2011).

62. Johnson TD, Lin SY, Christman KL. Tailoring material properties of a nanofibrous extracellular matrix derived hydrogel. *Nanotechnology* **22**, 494015, doi:10.1088/0957-4484/22/49/494015 (2011).

63. Arslan F, Lai RC, Smeets MB, Akeroyd L, Choo A, Aguor EN, Timmers L, van Rijen HV, Doevendans PA, Pasterkamp G, Lim SK, de Kleijn DP. Mesenchymal stem cell-derived exosomes increase ATP levels, decrease oxidative stress and activate PI3K/Akt pathway to enhance myocardial viability and prevent adverse remodeling after myocardial ischemia/reperfusion injury. *Stem Cell Res* **10**, 301-312, doi:10.1016/j.scr.2013.01.002 (2013).

64. Wassenaar JW, Gaetani R, Garcia JJ, Braden RL, Luo CG, Huang D, DeMaria AN, Omens JH, Christman KL. Evidence for Mechanisms Underlying the Functional Benefits of a Myocardial Matrix Hydrogel for Post-MI Treatment. *J Am Coll Cardiol* **67**, 1074-1086, doi:10.1016/j.jacc.2015.12.035 (2016).

65. Badylak SF. Xenogeneic extracellular matrix as a scaffold for tissue reconstruction. *Transpl Immunol* **12**, 367-377, doi:10.1016/j.trim.2003.12.016 (2004).

66. Badylak SF. Decellularized allogeneic and xenogeneic tissue as a bioscaffold for regenerative medicine: factors that influence the host response. *Ann Biomed Eng* **42**, 1517-1527, doi:10.1007/s10439-013-0963-7 (2014).

Chapter 6. Manufacturing Considerations for Producing and Assessing Decellularized Extracellular Matrix Hydrogels

Introduction

Biomaterials derived from decellularized extracellular matrices (ECM) have been extensively studied in a wide variety of medical applications ranging from myocardial infarction to orthopedic injuries.[1,2] Although many of these materials still require further evaluation in the pre-clinical stage, numerous decellularized products have become commercially available.[3] The majority of these products are derived from human, porcine, or bovine tissue sources, and they are most commonly manufactured into a sheet form. However, implantation of decellularized sheets requires more invasive procedures compared to injectable forms of decellularized materials. In particular, ECM hydrogels have been increasingly studied due to the ability to deliver them minimally invasively, and the gelled form of these materials is advantageous for filling abnormally shaped defects. Unlike the sheet form of decellularized ECM materials, only one injectable hydrogel, a decellularized myocardial matrix from Ventrix, Inc. (ClinicalTrials.gov identifier NCT02305602), has reached clinical trials.[4] As a result, manufacturing standards are not well established for injectable ECM hydrogels.

When designing biomaterials for regenerative medicine applications, including decellularized ECMs, it is important to consider implications for manufacturing, including increased costs, availability of raw materials, or difficulty of production.[5] While relevant manufacturing considerations have not been thoroughly discussed in the literature for decellularized materials, several official monographs from the United States Pharmacopoeia are available for decellularized ECM sheets. These monographs include documentation for scaffold bovine dermis, scaffold human dermis, scaffold porcine bladder, and scaffold porcine small intestinal submucosa. However, the evaluations required for each of these materials is not

uniform, regardless of all being decellularized sheets. For instance, all materials require some degree of histological evaluation, identification of key proteins, and sterility assessments. Conversely, though, mechanical strength testing is only specified for the scaffold bovine dermis and scaffold porcine bladder, and bioactivity evaluations are only listed for the scaffold small intestinal submucosa. Although these official monographs do provide some basis for assessing decellularized ECM hydrogels, there is still a lack of uniform standards, and various manufacturing parameters have not been examined.

In this article, we first discuss detailed methods for evaluating the effects of animal-to-animal variability of the tissue source, the addition of a bioburden reduction step, and the quality of tissue obtained under different harvesting conditions (Figure 6.1). When generating material for a manufacturing-scale batch, a certain number of animals or donors are necessary to eliminate batch effects; therefore, we sought to identify the degree of animal-to-animal variability within a single laboratory-scale batch. In addition, we investigated the effects of including a bioburden reducing reagent. For porcine tissue, the exterior of the tissue could be contaminated with bacteria, which could induce a negative immune response once delivered. To add this additional step in manufacturing, the final product must be evaluated for any changes in material

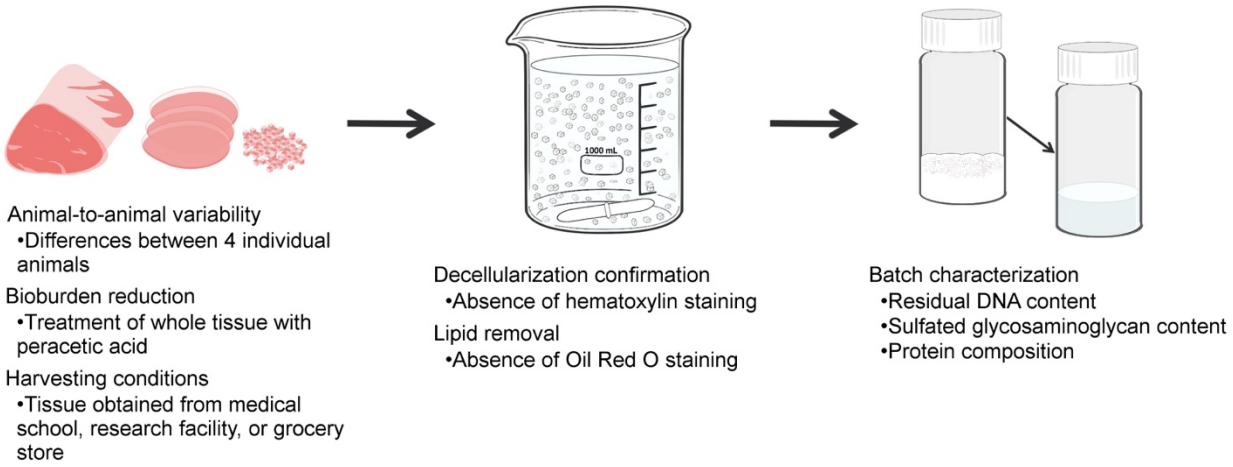

Figure 6.1 *Graphical Abstract***.** Overview of a decellularization process for skeletal muscle and accompanying experimental design considerations for the manufacturing of decellularized extracellular matrix hydrogels.

properties. Furthermore, several harvesting conditions for the tissue were examined to simulate the manufacturing decision of selecting raw material to reduce costs but maintain the quality of the final product. This article focuses on a decellularized skeletal muscle ECM hydrogel (SKM), but these concepts are applicable to various tissue sources.

Materials and Methods

Material production

All porcine derived skeletal muscle tissue was decellularized according to a previously published protocol.[6] Briefly, longissimus dorsi muscle, more commonly known as pork loin, was harvested, frozen overnight at minimum to increase the ease of chopping, and then chopped into ~0.5 cm^3 pieces. Each laboratory scale batch included at least 5 1-L beakers with ~40 g of tissue per beaker. For each subsequent solution change, the beakers were placed on a stir plate at ~125 rpm at room temperature. The tissue was decellularized for 4-5 days with 800 mL of solution consisting of 1% wt/vol sodium dodecyl sulfate (SDS) in 1X phosphate buffered saline (PBS). Solution changes were performed daily, and 4 mL of 10,000 U penicillin/streptomyocin (ThermoFisher Scientific, Waltham, MA) was added after each change to avoid contamination. After full decellularization was achieved, indicated by a fully white appearance, the tissue was rinsed in ultrapure water to remove residual SDS. Then, all beakers were pooled together, and 400 mL of isopropanol was added and tissue rinsed for 16-24 h to remove remaining lipids. The tissue was then rinsed in ultrapure water for another 24 h before being strained and frozen in 50 mL conicals at −80°C. A couple of pieces of tissue were collected periodically throughout the entire process and frozen in a microbeaker with Tissue-Tek® O.C.T. (Sakura Finetek, Torrance, CA) for later histological analyses.

Once the decellularized tissue had been frozen, the conicals were lyophilized with a FreeZone 2.5 Liter Benchtop Freeze Dry System (Labconco, Kansas City, MO) for ~72 h. After,

the tissue was ground into a fine powder with a Wiley Mini-Mill and immediately passed through a #60 filter to yield a uniform powder (Thomas Scientific, Swedesboro, NJ). The filtered and unfiltered ECM was stored at −80°C in 20 mL scintillation vials wrapped with parafilm and in desiccant for long-term storage. Prior to performing subsequent experiments, 25-30 mg of filtered, milled ECM was weighed into a new 20 mL scintillation vial, and a partial pepsin digestion was performed over 48 h. This was accomplished by dissolving pepsin (Sigma-Aldrich, St. Louis, MO) with 0.1 M HCl to 1 mg/mL and then adding the solution to milled ECM at a final concentration of 10 mg ECM/1mL pepsin in 0.1 M HCl. Once the ECM was solubilized, the mixture was adjusted to physiological pH and salt conditions, and a final concentration of 6 mg/mL was reached. The mixture was aliquoted into 1 mg or 2 mg aliquots in microcentrifuge tubes, frozen at −80°C, and then relyophilized for ~48 h. To resuspend the ECM, the appropriate volume of ultrapure water for a 6 mg/mL concentration was added to the microcentrifuge tube, and the pellet was briefly pipetted up and down before allowing to sit on ice for at least 10 min. After that time, the mixture was then mixed again by pipetting up and down to yield a well-mixed ECM solution.

Animal-to-animal variability

Longissimus dorsi muscles from 4 different pigs were used to evaluate animal-to-animal variability. Skeletal muscle for these experiments was obtained from Yorkshire farm pigs (4-7 months old) from S & S Farms, a company which breeds pigs for biomedical research purposes. After undergoing procedures for surgical practice at the UC San Diego medical school, the loins were excised from the pigs, immediately frozen at −20°C, and stored for up to 1 month prior to use. Decellularization of the tissue was performed as described above with 5 1-L beakers of tissue for each pig (SKM-1, SKM-2, SKM-3, SKM-4). All pigs were kept separate throughout the entire process, including milling and the partial pepsin digestion. However, to compare to a full batch of material, the 4 unfiltered portions from each pig were combined and then remilled

together with the #60 filter. This yielded a batch with all 4 pigs and was designated as SKM-UCSD. Characterization assays were then performed for the five experimental groups as described below.

Bioburden reduction

To reduce the bioburden on the surface of the skeletal muscle tissue, peracetic acid (PAA) was used. PAA is a biocide with bactericidal, fungicidal, and sporicidal properties and is hypothesized to employ mechanisms similar to peroxides and oxidizing agents.[7-10] PAA is also another common reagent utilized in decellularization processes to remove DNA content without damaging ECM composition.[11] Longissimus dorsi muscles were obtained from 2 Yorkshire farm pigs (4-7 months old) from the UC San Diego medical school and frozen as described in the previous section. This freezing step was crucial to ensure minimal thawing of the tissue due to the PAA treatment. Before beginning the decellularization, 2 L of 600 ppm PAA (Pfaltz and Bauer, Waterbury, CT) was made by combining 1.5 mL 35% PAA per 1 L of ultrapure water. The whole, fully frozen muscle was placed into a 4 L beaker containing the PAA solution for 10 min and promptly removed. Any muscle that had thawed during the process was trimmed away and discarded. To ensure residual PAA was successfully removed, the remaining muscle was soaked in ultrapure water for 10 min and then chopped into ~0.5 cm^3 pieces. Decellularization was subsequently completed as normal based on the protocol described in section 2.1 above, and the material generated from the 2 pigs was pooled together for further analysis. For the accompanying characterization assays, the PAA-treated material (+PAA) was compared to a pooled material consisting of equal parts of SKM-3 and SKM-4 (-PAA) to account for animal-to-animal variability.

Harvesting conditions

To compare skeletal muscle obtained under different harvesting conditions, the decellularization protocol from section 2.1 above was followed. Longissimus dorsi muscles were obtained from Yorkshire pigs (4-7 months old) undergoing surgical practice at the UC San Diego medical school (SKM-UCSD, SKM-3, and SKM-4 only), cross-bred pigs (Yorkshire, Landrace, and Duroc breeds, ~6 months old) from Midwest™ Research Swine, another company which provides swine for biomedical research (SKM-RF), and boneless pork loin chops (no saline injected, unknown age) from a grocery store (SKM-GS). Tissue obtained from UC San Diego and the swine research facility was harvested immediately after euthanasia and then quickly frozen. However, the porcine breed, harvesting time, shipment time, and refrigeration time were unknown for the grocery store tissue. All materials were milled and partially pepsin digested according to section 2.1, and methodology for the characterization assays will be discussed in the following sections.

Material characterization

Decellularization yield

Prior to freezing the decellularized tissue for lyophilization and milling, the tissue was weighed. This final decellularization mass was then compared to the combined masses of the fresh tissue from each beaker. To calculate the decellularization yield, the final decellularization mass was divided by the starting fresh tissue mass, and the fraction was then multiplied by 100 to yield a percentage. Since the yield was calculated from each batch individually, there were no replicates and therefore no error bars on these plots.

Histology

Frozen samples were removed from the microbeakers, and a cryostat (Leica Biosystems, Buffalo Grove, IL) was used to yield 10 μm thick sections for mounting on a

microscope slide. Slides for each sample were stained with hematoxylin and eosin (H&E), Hoechst 33342, and Oil Red O to assess muscle morphology, residual DNA content, and lipid content, respectively. For the Hoechst 33342 staining, slides were first fixed in acetone for 1.5 min and then rinsed three times in 1X PBS for 5 min. After, slides were placed in a humidity chamber for 10 min with a Hoechst solution consisting of 1 µL of Hoechst 33342 (ThermoFisher Scientific, Waltham, MA) in 10 mL of deionized (DI) water. The slides were subsequently washed in 1X PBS as before, and then cover slips were mounted with Fluoromount™ Aqueous Mounting Medium (Sigma-Aldrich, St. Louis, MO). For the Oil Red O staining, slides were rinsed twice for 5 min in propylene glycol and then placed in Oil Red O stain for 7 min at 60°C. The tissue was then rinsed in 85% propylene glycol in DI water for 3 min before being rinsed twice in pure DI water. After, the slides were placed in a 1:3 dilution of Harris hematoxylin in DI water for 1 min and then rinsed with tap water twice. The slides were then dipped in Bluing solution 20 times and finally rinsed twice in tap water followed by 2 rinses in DI water. All slides were subsequently coverslipped with Fluoromount™ Aqueous Mounting Medium (Sigma-Aldrich, St. Louis, MO). H&E and Oil Red O slides were imaged on an Aperio ScanScope CS2 (Leica Biosystems, Buffalo Grove, IL) with 20x magnification, and Hoechst slides were imaged with an Axio Observer D1 (Carl Zeiss AG, Oberkochen, Germany) with 10x magnification and a constant exposure time.

Gel electrophoresis

To qualitatively assess protein content, SDS-polyacrylamide gel electrophoresis (SDS-PAGE) was performed for all samples based on a previously published protocol.[6] Briefly, 1 mg of digested, lyophilized ECM was resuspended with 167 µL of DI water to reach a concentration of 6 mg/mL. ECM samples were prepared up to 15 µL total with the following ratios: 50% sample, 25% NuPAGE™ LDS Sample Buffer (4X, ThermoFisher Scientific, Waltham, MA), 10% NuPAGE™ Reducing Agent (10X, ThermoFisher Scientific, Waltham, MA), and 15% DI water.

ECM samples diluted 1:2 (25% sample and 40% DI water) were also included adjacent to the undiluted ECM if empty wells were available. Rat tail collagen I (2.5 mg/mL, Corning, Corning, NY) was used as a reference since the ECM hydrogels primarily consist of collagen.12 These collagen samples consisted of a ratio of 33% sample, 25% sample buffer, 10% reducing agent, and 32% DI water. Before loading the samples, all microcentrifuge tubes were placed in a heating block at 70°C for 10 min to denature the proteins. In the meantime, an XCell SureLock™ Mini-Cell Electrophoresis System (ThermoFisher Scientific, Waltham, MA) was assembled with a 10-well NuPAGE™ 4-12% Bis-Tris protein gel (ThermoFisher Scientific, Waltham, MA) and filled with a 1X solution of NuPAGE™ MOPS SDS running buffer (Thermo-Fisher Scientific, Waltham, MA). NuPAGE™ antioxidants (500 µL, ThermoFisher Scientific, Waltham, MA) were then added to the inner chamber. After denaturing the proteins, 10 µL of each sample were loaded into the protein gel along with 10 µL of Chameleon Duo Pre-Stained Protein Ladder (LI-COR Biosciences, Lincoln, NE) in an adjacent well. All gels were run at 200 V for ~50 min and then stained with Imperial™ Protein Stain (ThermoFisher Scientific, Waltham, MA) for ~18 h. Gels were then destained with DI water the following day for ~5-6 h and imaged between two sheets of plastic on a computer scanner.

Residual DNA content

To quantify residual dsDNA content, 1-mg digested, lyophilized ECM aliquots were resuspended in a proteinase K solution consisting of 25 µL of proteinase K (Roche Diagnostics, Mannheim, Germany) in buffer (150 mM NaCl, 10 mM Tris pH 8, 0.2% SDS) and 180 µL of buffer T1 from the NucleoSpin® Tissue kit (Macherey-Nagel, Bethlehem, PA). The samples were left on a heating block at 56°C overnight to digest the matrix. The following day, DNA was isolated according to the protocol from the NucleoSpin® Tissue kit (Macherey-Nagel, Bethlehem, PA). A Quant-iT™ PicoGreen™ dsDNA Assay kit (ThermoFisher Scientific, Waltham, MA) was then used to quantify the residual DNA, and a 96-well plate was prepared

according to the associated protocol. Fluorescent measurements were recorded on a Synergy 4 Multi-Mode Microplate Reader (BioTek Instruments, Winooski, VT) at 480 nm excitation and 520 nm emission to detect the PicoGreen™ dye, which fluoresces when bound to dsDNA. Those fluorescent values were then compared to a dsDNA standard from the kit, and the amount of residual dsDNA was calculated from a standard curve. The experiment was run in triplicate to determine statistical differences.

Sulfated glycosaminoglycan content

Sulfated glycosaminoglycan (sGAG) content was determined via a 1,9-dimethylmethylene blue (DMMB) dye assay based on previously published methods.[6] Digested, lyophilized ECM aliquots were resuspended to 6 mg/mL and then pipetted into 100 µL aliquots. Several solutions were made including an 8 M guanidine hydrochloride (GuHCl) solution (382 g GuHCl in 500 mL DI water), a formate solution (2.5 g sodium formate, 2.795 mL 85% formic acid, 240 mL 1 M GuHCl), and a vacuum-filtered DMMB solution (16 mg DMMB (Sigma-Aldrich, St. Louis, MO) in 25 mL ethanol). These solutions were then used to make a working solution (5 mL formate solution, 1.25 mL DMMB solution, 18.75 mL DI water) and a decomplexation solution (2.05 g sodium acetate, 250 mL 8 M GuHCl, 50 mL 1-propanol, 200 mL DI water). A 1-mg/mL chondroitin sulfate stock solution (25 mg chondroitin sulfate in 25 mL 1X PBS, MilliporeSigma, Burlington, MA) was used to make 6 serial dilutions for the following concentrations: 0, 2, 4, 6, 8, and 10 µg chondroitin sulfate/100 µL. Each standard tube contained 100 µL of each chondroitin sulfate solution. Working solution (1 mL) was added to each standard and ECM sample microcentrifuge tube, and the tubes were then vortexed (setting 3.5) for 30 min. All of the tubes were then centrifuged for 10 min at 12,000 rpm to promote pellet formation. The supernatant from each tube was carefully removed without disturbing the pellet, and 1 mL of decomplexation solution was then added to resuspend the pellet. The samples were vortexed (setting 3.5) again for 30 min to ensure a homogenous

solution. In a 96-well plate, 100 µL of each sample were pipetted into three wells per sample, and absorbance values at 656 nm were then recorded with a Synergy 4 Multi-Mode Microplate Reader (BioTek Instruments, Winooski, VT). A standard curve was generated with the serial dilutions of the chondroitin sulfate stock solution, and the sGAG content of the ECM samples was calculated from the standard curve. All ECM samples were run in triplicate.

Quantitative mass spectrometry

Based on a previously published protocol, milled ECM (~1 mg decellularized material) samples were prepared for liquid chromatography with tandem mass spectrometry (LC-MS/MS) as follows.[13] Samples were first chemically digested for 24 h at room temperature in 500 µL/mg of 100 mM CNBr in 86% TFA. After digestion, samples were dried and exchanged with water to reduce acid concentration, and this process was repeated 3 times. The samples were then neutralized with 0.1 M ammonium biocarbonate (ABC) buffer (pH 8.5). Equal volumes of each sample underwent further digestion with a 10 kDA molecular weight cutoff filter according to the FASP protocol. One pmol of $^{13}C_6$ Quantitative Concatamer (QconCAT) peptides, representing ECM and ECM-associated proteins,[14] was added to each sample prior to digestion. Briefly, samples were washed with 8 M urea and 0.1 M ABC pH 8.5, reduced with 10 mM DTT for 30 min at room temperature, and alkylated with 55 mM iodoacetamide for 30 min in the dark at room temperature with subsequent spins between each step. Samples were centrifuged once again and then washed with urea solution 3 times and 10 mM ABC pH 8.0 3 times. Sequencing grade modified trypsin (Promega, Madison, WI) at a concentration of 1/50 protease/protein (wt/wt) in 0.02% ProteaseMax surfactant (Promega, Madison, WI) was used to digest the proteins at 37°C overnight. Peptides were eluted with 10 mM ABC pH 8.0, dried on a Speed-Vac (ThermoFisher Scientific, Waltham, MA), and reconstituted with a known volume of control alcohol dehydrogenase peptide for quantitative normalization. Samples were kept frozen at −80°C until liquid chromatography-selected reaction monitoring (LC-SRM) analysis. To perform

LC-SRM, a QTRAP® 5500 triple quadrupole mass spectrometer (Sciex, Framingham, MA) was used coupled with a Dionex Ultimate 3000 UHPLC (ThermoFisher Scientific, Waltham, MA). Using a previously published protocol,[14] 8 µL of each sample was injected representing 100 fmol of SIL labeled QconCAT peptides per 5 µg total protein per run. To analyze the data, Skyline v4.2 software (MacCoss Lab Software, Seattle, WA) was utilized,[15] and manual validation was performed for transition quality, peak shape, and peak area boundaries. After incorporating Savitsy-Golay smoothing, the integrated peak areas were determined, and data was quantified by using a ratio of the ^{12}C peptide for the endogenous sample relative to the ^{13}C peptide from ECM targeted QconCATs. Previous studies were referenced to define the linear range, limit of detection, and limit of quantitation.[14] If peptides fell outside of those established parameters, they were excluded from the analysis.

Statistical analysis

Results are displayed as mean ± SEM. Statistical analyses were performed with Prism 8 (GraphPad Software, San Diego, CA), and statistical significance was accepted at $p < 0.05$. For characterization assays with only two experimental groups (bioburden reduction testing), an unpaired Student's t-test was used. Characterization assays with three or more experimental groups (animal-to-animal variability, harvesting conditions) were analyzed with a one-way ANOVA and a Tukey's post hoc test. For the LC-SRM analysis, the peak area ratios were normalized to an internal standard spike. Values are reported as mean ± SEM.

Results and Discussion

When designing biomaterials for regenerative medicine applications, manufacturing considerations are often unappreciated or disregarded, but to satisfy FDA requirements and produce large quantities of material, additional manufacturing steps could affect the efficacy of

the final product. To illuminate differences between laboratory-scale and manufacturing batches, we investigated the effects of animal-to-animal variability, bioburden reduction, and several harvesting conditions for a decellularized skeletal muscle ECM hydrogel.

Decellularization process

The decellularization procedure, excluding the addition of the bioburden reduction step, was similar for all muscle samples, although the timing of the decellularization step did vary amongst harvesting conditions. Skeletal muscle from UC San Diego required 5 days in the detergent to fully decellularize the tissue, whereas muscle from the research facility or grocery store only required 4 days in detergent. While the UC San Diego tissue was immediately frozen and only thawed prior to beginning the decellularization, the research facility or grocery store tissue may have undergone additional freeze-thaw cycles. This would explain the abbreviated decellularization timing since freeze-thaw represents another decellularization method.[16] A qualitative assessment of H&E staining and Hoechst staining did not yield obvious differences between any of the decellularized ECM batches (images not shown) and were similar to previous studies.[6] However, muscle from the research facility and grocery store had visibly larger amounts of fat present, and some beakers had fat floating on the surface following the first day in detergent. This was further supported by Oil Red O staining (Figure 6.2) in which fresh tissue from the UC San Diego medical school contained fewer regions with less concentrated lipids compared to the more intense lipid staining in the research facility and grocery store samples. Although little information is known for the grocery store tissue, differences in the fat content could be attributed to the strain or age of the pigs from which the tissue was obtained. The lipid content was reduced in all of the samples post-decellularization, but the IPA lipid removal step appeared insufficient for the grocery store skeletal muscle.

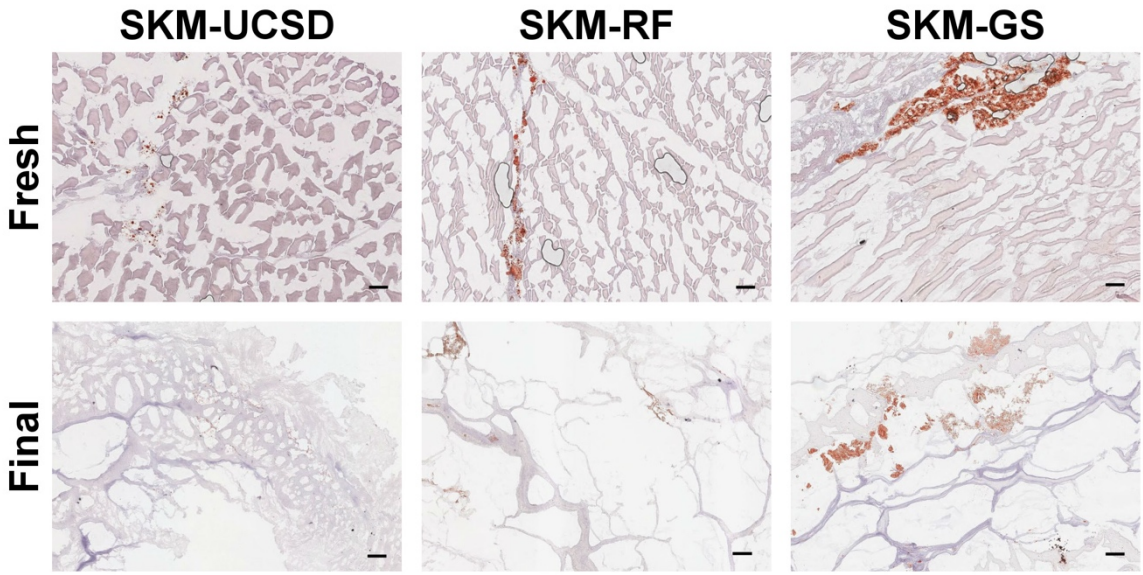

Figure 6.2 Representative images of lipid content for different harvesting conditions. Samples were collected at each time point, frozen, cryosectioned, and subsequently stained for Oil Red O. The tissue obtained from the UC San Diego medical school contained fewer lipids (red staining) compared to tissue from the research facility and grocery store. Scale bars are 100 μm.

Animal-to-animal variability

For any manufactured product, fabricating uniform batches is paramount; therefore, the variability between animals can become problematic when utilizing an animal, or even human, tissue source. Based on previous laboratory-scale batches, tissue from 4 pigs is typically combined to reduce animal-to-animal variability, but we sought to characterize the material derived from each animal separately. The decellularization processes were identical for all 4 animals (SKM-1,2,3,4), and the histological analyses (H&E, Hoechst, and Oil Red O) did not reveal any differences between pigs (images not shown). In addition, the material yield was similar amongst pigs (Figure 6.3). Some differences did exist among the pigs for the residual dsDNA content (0.12–1.17 ng dsDNA/mg ECM) and sGAG content (9.13–13.74 μg sGAGs/mg ECM), but values fell within the expected range of 0.1 to 5 ng dsDNA/mg ECM and 5 to 15 μg sGAGs/mg ECM, respectively, based on previously published methods (Figure 6.3).6 As a result, these significant differences are not concerning for the manufacturing process. For the

protein compositions of each batch for the separate animals, the SDS-PAGE gel did not reveal any band intensity differences between the animals (Figure 6.4). However, quantitative mass spectrometry results did generate some differences, but the largest fractions of ECM proteins classified by function were consistent across all animals (Table 6.1). Therefore, there appear to be minimal effects due to animal-to-animal variability, and the values for the batched material (SKM-UCSD) are representative of the averaged values for all 4 animals. The actual manufacturing of large batches of decellularized ECM hydrogels would require a large number of pigs, thereby further reducing batch-to-batch variability, but these discrepancies are still important to consider for continuity and reproducibility in a laboratory setting.

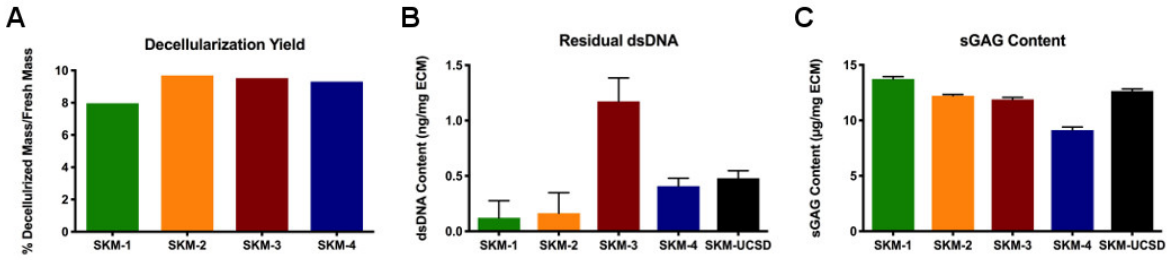

Figure 6.3 Animal-to-animal variability. Differences were detected amongst the 4 pigs (SKM-1, 2, 3, 4) and relative to the combined batch of all 4 pigs (SKM-UCSD) for the (A) material yield, (B) residual dsDNA content, and (C) sulfated glycosaminoglycan (sGAG) content. All values still fell within the expected ranges, and the values for the full batch closely resembled the average of the individual values.

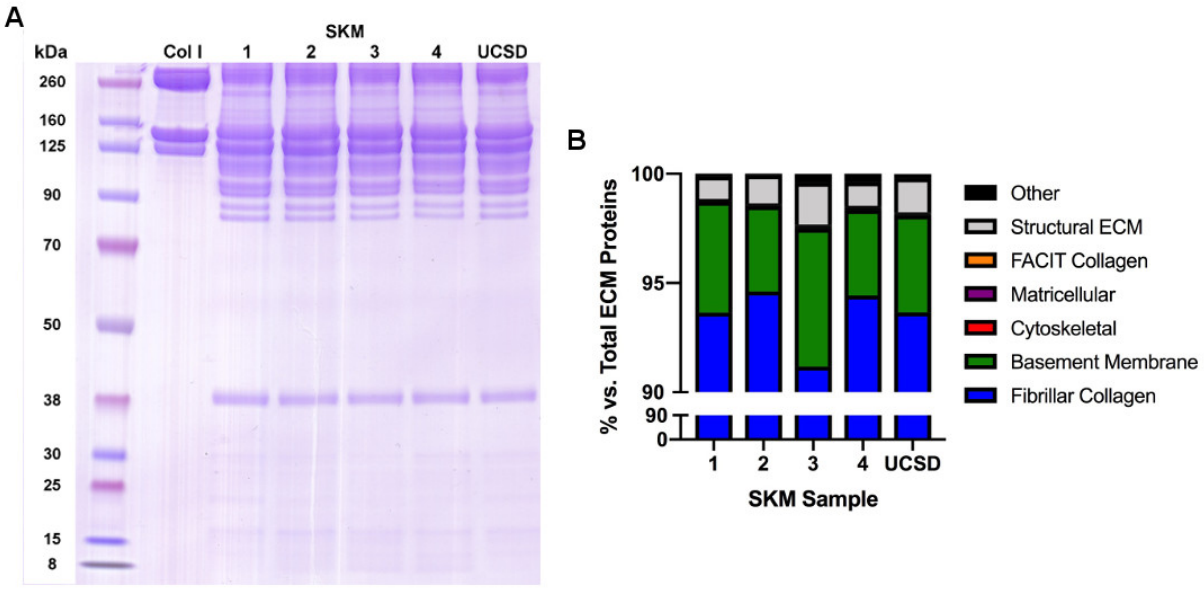

Figure 6.4 Protein composition for animal-to-animal variability. (A) The band intensities in the SDS-PAGE gel did not vary amongst the individual pigs, but the (B) the quantitative mass spectrometry did reveal some differences in the percentages for the ECM proteins according to function.

Table 6.1 Absolute protein quantification for decellularized skeletal muscle extracellular matrix (SKM) from four individual pigs.

Protein	Gene	Functional Classification	Protein Amount (nmol/g)				
			SKM-1	SKM-2	SKM-3	SKM-4	SKM-UCSD
Collagen alpha-1(IV) chain(Arresten/Core Protein)	COL4A1	Basement Membrane	11.129	12.315	12.489	9.744	12.309
Collagen alpha-1/5(IV) chain(Arresten/Core Protein)	COL4A1/5	Basement Membrane	19.281	10.911	16.665	12.669	15.216
Collagen alpha-2(IV) chain(Canstatin/Core Protein)	COL4A2	Basement Membrane	5.157	4.610	6.629	3.767	2.755
Perlecan	HSPG2	Basement Membrane	2.597	2.382	2.397	1.501	2.079
Laminin alpha-2	LAMA2	Basement Membrane	0.033	0.024	0.111	0.052	0.080
Laminin Beta-2	LAMB2	Basement Membrane		0.038			0.071
Laminin Gamma-1	LAMC1	Basement Membrane	0.611	0.058	0.031	0.951	0.062
Nidogen-1	NID1	Basement Membrane					
Actin (All Isoforms)	ACT	Cytoskeletal	0.153	0.135	0.316	0.579	0.222
Tubulin beta-4B chain(4b & 5 chain)	TUBB	Cytoskeletal	0.075	0.076	0.081	0.065	0.084
Vimentin	VIM	Cytoskeletal	0.096	0.100	0.113	0.078	0.080
Collagen alpha-1(XIV) chain	COL14A1	FACIT Collagen	0.278	0.277	0.375	0.364	0.326
Collagen alpha-1(I) chain	COL1A1	Fibrillar Collagen	315.607	325.871	252.482	337.088	332.136
Collagen alpha-1(I) chain(galglu modified K)	COL1A1	Fibrillar Collagen	205.213	178.623	125.532	158.075	153.219
Collagen alpha-2(I) chain	COL1A2	Fibrillar Collagen	183.938	220.534	169.945	186.547	195.874
Collagen alpha-1 (III) chain	COL3A1	Fibrillar Collagen	1.387	1.524	0.915	1.533	1.142
Collagen alpha-1(V) chain(C-term Propeptide)	COL5A1	Fibrillar Collagen	5.882	3.425	1.262	3.344	1.289
Collagen alpha-2(V) chain	COL5A2	Fibrillar Collagen	5.293	4.338	4.156	4.020	4.861
Fibulin 4	EFEMP2	Matricellular	0.112	0.053	0.073	0.067	0.142
Fibulin 5	FBLN5	Matricellular	0.104	0.087	0.083	0.071	0.063
Osteopontin	SPP1	Matricellular	0.091	0.065	0.086	0.100	0.088
Periostin	POSTN	Matricellular	0.082	0.087	0.105	0.077	0.098
Glyceraldehyde-3-phosphate dehydrogenase	GAPDH	Other Cellular	0.491	0.336	2.012	2.398	0.960
Histone 2A(H2A-A-K)	H2A	Other Cellular					0.159
Annexin A4	ANXA4	ECM-affiliated	0.110	0.053	0.133	0.148	0.038

Bioburden reduction

Upon treating the longissimus dorsi muscles with PAA and then subsequently removing the thawed tissue, no differences were observed between the untreated and treated tissue throughout the decellularization process. In addition, the material yield was nearly identical (Figure 6.5). No significant differences were calculated for the residual dsDNA content between the two groups (-PAA: 1.07 ± 0.43 ng dsDNA/mg ECM vs. +PAA: 0.84 ± 0.10 ng dsDNA/mg ECM; data not shown), but this result was expected since the outer layer of the tissue with likely the largest amount of bioburden was removed. Quantification of sGAG content also showed no effects from the addition of the PAA (-PAA: 10.93 ± 0.56 µg sGAGs/mg ECM vs. +PAA: 12.14 ± 0.16 µg sGAGs/mg ECM; Figure 6.5). The intensity of the bands in the SDS-PAGE gel did appear slightly weaker with the PAA treatment (Figure 6.6); however, these differences could be attributed to slight variations in the dilutions of the samples during sample preparation. Moreover, quantitative mass spectrometry showed similarities when comparing fractions based on ECM protein function classification (Figure 6.6, Table 6.2). The lack of differences between untreated and treated tissue was expected since any tissue that thawed during the PAA treatment was removed and discarded. This procedure was utilized to ensure that bioburden on the surface of the tissue was removed and to prevent residual acidic PAA from negatively affecting the ECM proteins. Regardless, further examination confirmed that including a PAA treatment step to reduce bioburden did not influence the final decellularized ECM product, and this methodology could represent a viable method for reducing exterior bacterial contamination. However, tissue obtained from the UC San Diego medical school likely has lower bioburden levels compared to a slaughterhouse, for instance, since the tissue is harvested in a sterile operating suite. Therefore, the efficiency of this bioburden reduction step would need to be verified on the raw product intended for manufacturing.

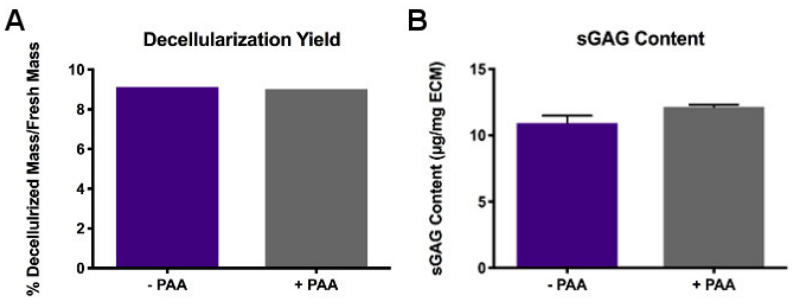

Figure 6.5 Bioburden reduction – PAA treatment. The addition of peracetic acid (PAA) did not have a significant effect on (A) material yield or (B) sulfated glycosaminoglycan (sGAG) content. This was not surprising since any tissue penetrated with PAA was removed prior to chopping.

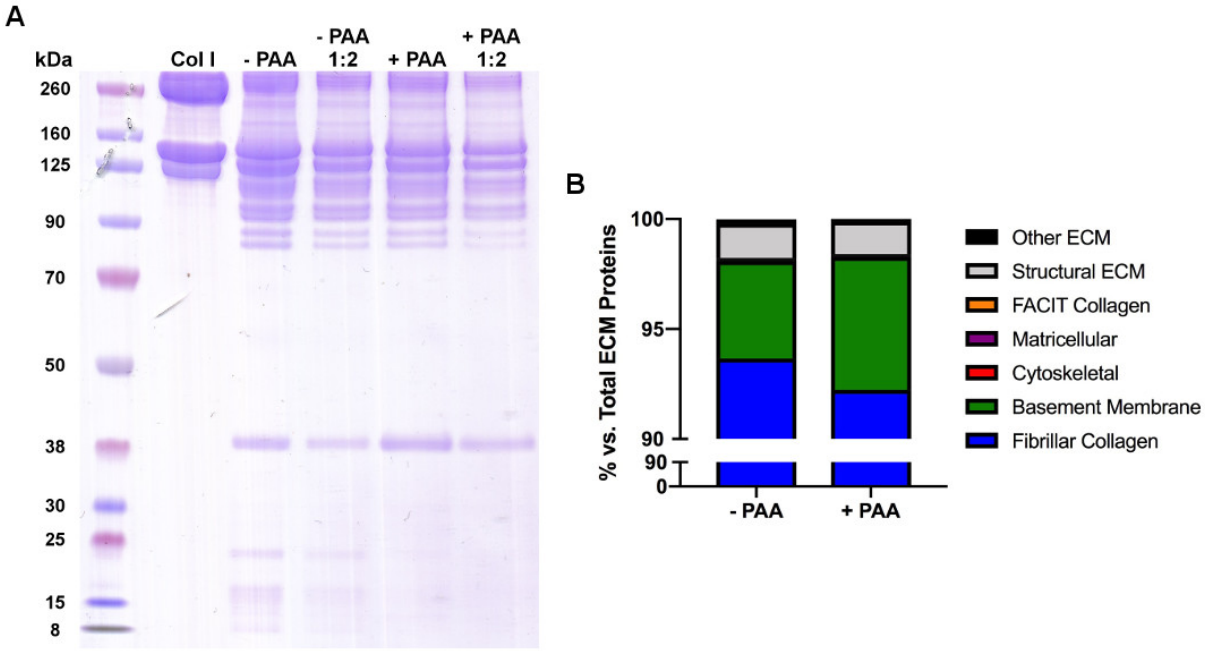

Figure 6.6 Protein composition for bioburden reducing step. Results from a (A) SDS-PAGE gel and (B) quantitative mass spectrometry did not reveal remarkable differences between the two groups, indicating minimal to no effects from the peracetic acid (PAA) treatment.

Table 6.2 Absolute protein quantification for decellularized skeletal muscle extracellular matrix treated with or without peracetic acid (PAA).

Protein	Gene	Functional Classification	Protein Amount (nmol/g)	
			- PAA	+ PAA
Collagen alpha-1(IV) chain(Arresten/Core Protein)	COL4A1	Basement Membrane	12.309	20.241
Collagen alpha-1/5(IV) chain(Arresten/Core Protein)	COL4A1/5	Basement Membrane	15.216	20.687
Collagen alpha-2(IV) chain(Canstatin/Core Protein)	COL4A2	Basement Membrane	2.755	9.105
Perlecan	HSPG2	Basement Membrane	2.079	2.140
Laminin alpha-2	LAMA2	Basement Membrane	0.080	0.074
Laminin Beta-2	LAMB2	Basement Membrane	0.071	
Laminin Gamma-1	LAMC1	Basement Membrane	0.062	1.146
Nidogen-1	NID1	Basement Membrane		
Actin (All Isoforms)	ACT	Cytoskeletal	0.222	0.199
Tubulin beta-4B chain(4b & 5 chain)	TUBB	Cytoskeletal	0.084	0.096
Vimentin	VIM	Cytoskeletal	0.080	0.077
Collagen alpha-1(XIV) chain	COL14A1	FACIT Collagen	0.326	0.364
Collagen alpha-1(I) chain	COL1A1	Fibrillar Collagen	332.136	372.211
Collagen alpha-1(I) chain(galglu modified K)	COL1A1	Fibrillar Collagen	153.219	198.873
Collagen alpha-2(I) chain	COL1A2	Fibrillar Collagen	195.874	233.623
Collagen alpha-1 (III) chain	COL3A1	Fibrillar Collagen	1.142	1.519
Collagen alpha-1(V) chain(C-term Propeptide)	COL5A1	Fibrillar Collagen	1.289	3.679
Collagen alpha-2(V) chain	COL5A2	Fibrillar Collagen	4.861	6.043
Fibulin 4	EFEMP2	Matricellular	0.142	0.128
Fibulin 5	FBLN5	Matricellular	0.063	
Osteopontin	SPP1	Matricellular	0.088	0.092
Periostin	POSTN	Matricellular	0.098	0.094
Glyceraldehyde-3-phosphate dehydrogenase	GAPDH	Other Cellular	0.960	0.554
Histone 2A(H2A-A-K)	H2A	Other Cellular	0.159	

Harvesting conditions

Although tissue obtained from the UC San Diego medical school yields potent and consistent batches of decellularized ECM hydrogels based on previous successful *in vivo* studies, this does not represent a viable source for large-scale manufacturing. Tissue from 1 or 2 pigs, which have undergone procedures for surgical practice, can often only be collected on a weekly basis, and the costs associated with the tissue and time required for veterinary staff to remove the tissue are substantial. In addition, the amount of tissue required for manufacturing would be significantly greater than 4 pigs per batch, and batches would need to be produced on

a much more frequent and regular basis. As a result, we aimed to compare UC San Diego batches of material to tissue obtained from a swine research facility specializing in providing tissue for biomedical purposes and a grocery store. For the grocery store tissue, though, the strain of the pigs, harvesting conditions, timing between harvesting and purchasing, and storage conditions were all unknown.

Based on these different harvesting conditions, the material yield was higher for the grocery store batch relative to the UC San Diego and research facility batches (UCSD: 0.38%, RF: 0.38%, GS: 0.49%; Figure 6.7). This was likely due to the insufficient removal of fat from the grocery store tissue, as discussed in section 3.1 above (Figure 6.2). No significant differences were observed between groups for the quantification of residual dsDNA content, but the grocery store tissue did retain the largest amount of dsDNA (UCSD: 0.01 ± 0.29 ng dsDNA/mg ECM, RF: 0.39 ± 0.21 ng dsDNA/mg ECM, GS: 1.38 ± 0.76 ng dsDNA/mg ECM; Figure 6.7). Unlike the UC San Diego and research facility tissue, which comes from biomedical research grade pigs and is promptly frozen after harvesting, the grocery store tissue was likely handled more extensively and was not kept frozen. In effect, this could produce a great amount of bioburden on the surface of the tissue, which could explain the higher residual DNA levels. For the sGAG content, there were also no differences between the three conditions (UCSD: 18.71 ± 0.51 µg sGAGs/mg ECM, RF: 18.35 ± 1.06 µg sGAGs/mg ECM, GS: 18.96 ± 0.98 µg sGAGs/mg ECM;

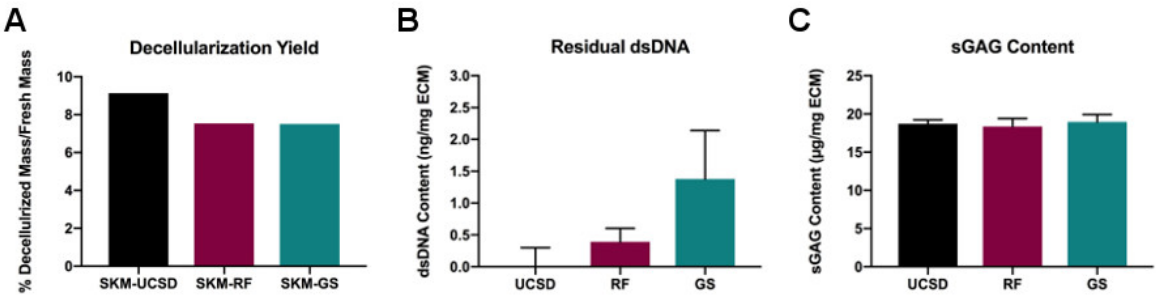

Figure 6.7 Effects of harvesting conditions. Skeletal muscle tissue was obtained from the UC San Diego medical school (UCSD), a swine research facility (RF), and a grocery store (GS). (A) Material yield was lower for the research facility and grocery store batches, but there were no statistically significant differences for (B) residual dsDNA content or (C) sulfated glycosaminoglycan (sGAG) content.

Figure 6.7). Differences did arise when qualitatively assessing SDS-PAGE, though (Figure 6.8). The UC San Diego and research facility batches had bands with similar intensities, but the grocery store batch was missing bands for peptides at ~80 and ~90 kDa. When investigating ECM proteins in this size range, collagen VI was identified as the possibly depleted protein, which was further confirmed when quantifying three isoforms of collagen VI (COL6A1, COL6A2, COL6A3; Table 6.3). The quantitative mass spectrometry data also revealed fewer differences between the UC San Diego and research facility decellularized tissue relative to the composition of the grocery store decellularized material (Figure 6.8, Table 6.3). In particular, the fibrillar collagen and other ECM percentages were higher for the grocery store material, while the fractions for the basement membrane and structural ECM categories were lower. This could be attributed to the decellularization process being harsher on the grocery store tissue relative to

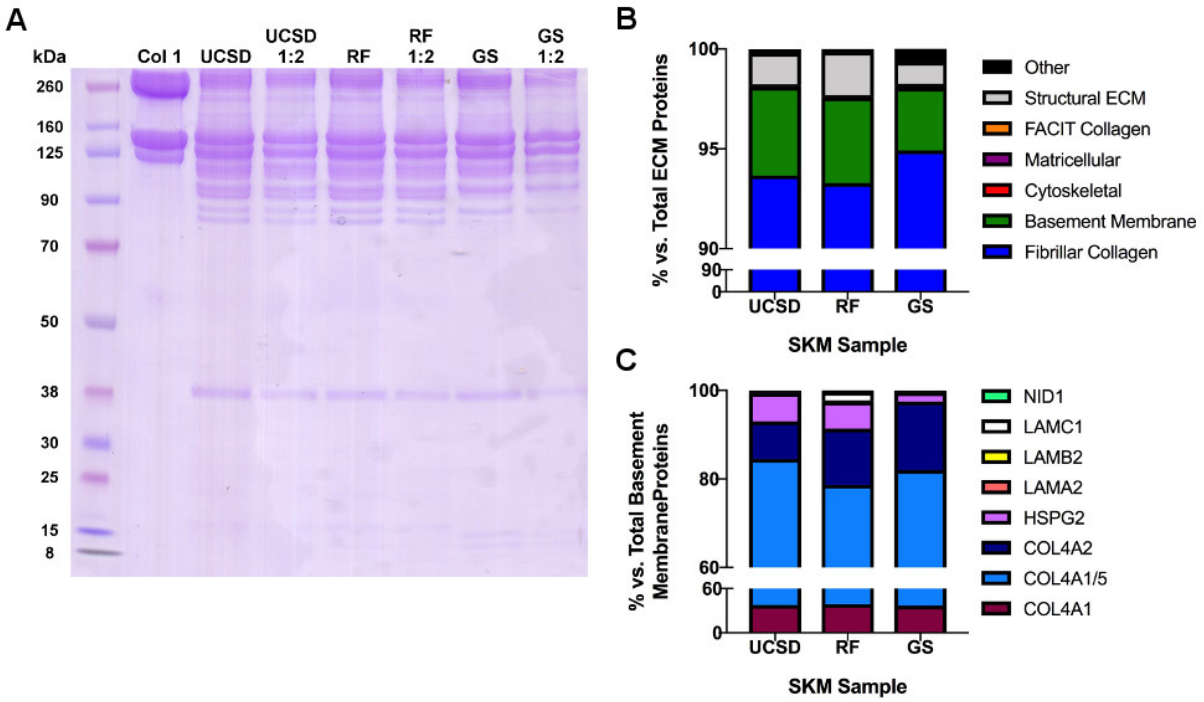

Figure 6.8 Protein compositions for various harvesting conditions. (A) Protein composition from a SDS-PAGE gel appeared similar between the UC San Diego (UCSD) and research facility (RF) batches, but certain proteins seemed depleted for the grocery store (GS) batch. (B) Differences were also detected with quantitative mass spectrometry in terms of percentages based on functional classes of ECM proteins and (C) particular basement membrane proteins.

the UCSD and research facility batches since excessive decellularization can yield a material containing nearly all fibrillar collagen. When the basement membrane fraction was more thoroughly explored, though, the grocery store decellularized material predominantly consisted of collagens compared to the larger assortment of proteins in the UC San Diego and research facility samples. In particular, various laminin isoforms are virtually undetectable in the grocery store batch, and the amount of perlecan (HSPG2) is reduced in the grocery store batch relative to the UCSD and research facility batches (Table 6.3). Laminin represents an important basement membrane protein for muscle regeneration and satellite cell function,[17-19] while perlecan is necessary for skeletal muscle development pathways.[20] For skeletal muscle applications, in particular, the basement membrane proteins are crucial for muscle regeneration.[21] Consequently, the basement membrane protein composition of an ECM

Table 6.3 Absolute protein quantification for decellularized skeletal muscle extracellular matrix harvested via three different conditions (SKM-UCSD, SKM-RF, SKM-GS).

Protein	Gene	Functional Classification	Protein Amount (nmol/g)		
			SKM-UCSD	SKM-RF	SKM-GS
Collagen alpha-1(IV) chain(Arresten/Core Protein)	COL4A1	Basement Membrane	12.309	12.842	5.380
Collagen alpha-1/5(IV) chain(Arresten/Core Protein)	COL4A1/5	Basement Membrane	15.216	13.215	6.572
Collagen alpha-2(IV) chain(Canstatin/Core Protein)	COL4A2	Basement Membrane	2.755	4.209	2.258
Perlecan	HSPG2	Basement Membrane	2.079	1.993	0.302
Laminin alpha-2	LAMA2	Basement Membrane	0.080	0.056	0.039
Laminin Beta-2	LAMB2	Basement Membrane	0.071	0.091	
Laminin Gamma-1	LAMC1	Basement Membrane	0.062	0.610	0.028
Nidogen-1	NID1	Basement Membrane		0.118	
Actin (All Isoforms)	ACT	Cytoskeletal	0.222	0.126	0.260
Tubulin beta-4B chain(4b & 5 chain)	TUBB	Cytoskeletal	0.084	0.071	0.074
Vimentin	VIM	Cytoskeletal	0.080	0.070	0.101
Collagen alpha-1(XIV) chain	COL14A1	FACIT Collagen	0.326	0.317	0.131
Collagen alpha-1(I) chain	COL1A1	Fibrillar Collagen	332.136	331.766	211.247
Collagen alpha-1(I) chain(galglu modified K)	COL1A1	Fibrillar Collagen	153.219	173.179	106.598
Collagen alpha-2(I) chain	COL1A2	Fibrillar Collagen	195.874	209.392	115.972
Collagen alpha-1 (III) chain	COL3A1	Fibrillar Collagen	1.142	1.313	0.925
Collagen alpha-1(V) chain(C-term Propeptide)	COL5A1	Fibrillar Collagen	1.289	2.020	2.752
Collagen alpha-2(V) chain	COL5A2	Fibrillar Collagen	4.861	4.633	2.931
Fibulin 4	EFEMP2	Matricellular	0.142	0.106	0.132
Fibulin 5	FBLN5	Matricellular	0.063	0.130	0.069
Osteopontin	SPP1	Matricellular	0.088	0.068	0.089
Periostin	POSTN	Matricellular	0.098	0.112	0.078
Glyceraldehyde-3-phosphate dehydrogenase	GAPDH	Other Cellular	0.960	0.805	2.664
Histone 2A(H2A-A-K)	H2A	Other Cellular	0.159		

hydrogel could influence the extent of muscle regeneration, although this would need to be explored with additional studies.

General Considerations and Hints for Troubleshooting

For preparing laboratory scale batches of material, it is important to maintain an aseptic environment to avoid contamination. All tools, equipment, and solutions should be sterilized when possible. If a batch has become contaminated, brown spots will often appear on the tissue, and the individual pieces will begin to aggregate in the beakers. Those batches should be discarded immediately.

When handling skeletal muscle for chopping prior to decellularization, thawed tissue will become sticky, which makes it more difficult to consistently chop the tissue. To avoid those inconsistencies, the tissue should be minimally thawed on ice (~1-2 h for 20 cm x 12 cm x 6 cm loin).

If the decellularized ECM fails to form a hydrogel upon incubation at 37°C, this could be attributed to poor lyophilization post-digestion. All material should form a well-defined pellet during lyophilization, and the vacuum pressure of the lyophilizer pump should not exceed 100mTorr. Additionally, too much residual fat can also affect gelation, and the timing of the IPA step may need to be altered.

For comparing data between particular experimental groups, all samples for a single characterization assay should be run on the same day. Each assay requires fresh preparation of certain solutions, which may introduce variability. However, data should still fall within the recommended range of 0.1 to 5 ng dsDNA/mg ECM for residual dsDNA content and 5 to 15 µg sGAGs/mg ECM for sGAG content for SKM.[6]

Conclusions

This paper describes the methodology for investigating three important manufacturing considerations – animal-to-animal variability, bioburden reduction, and harvesting conditions. Based on quality control assessments for residual DNA content, sGAG content, and overall protein composition, the variability amongst individual animals and the addition of a bioburden reducing agent did not affect the material properties of the final decellularized product, but harvesting conditions did appear to affect processing. Tissue obtained under various harvesting conditions yielded some differences in protein composition, which could ultimately impact *in vivo* efficacy. This indicates the importance of identifying a feasible raw tissue source and performing quality control experiments. By producing a material with low residual DNA content, the chances of initiating a negative immune response are likely lowered, and a pro-remodeling environment can instead be achieved.[22] Similarly, sufficient sGAG and protein composition likely contribute to the bioactivity and subsequent therapeutic effects of these materials.[23,24] Since this paper is limited to assessments for biochemical composition, further *in vitro* or *in vivo* testing would be necessary to fully evaluate the potency of each batch of material. Minimal changes were detected for several of the biochemical measurements, but results from a bioactivity assay could potentially enhance those differences. All in all, by investigating these parameters in a laboratory setting, decisions can be better informed for manufacturing decellularized ECM hydrogels.

Acknowledgements

This work was supported by the California Institute for Regenerative Medicine (TRAN1-09814). This chapter, in part, is a reprint of the material as it appears in Methods 2019. The authors are Melissa J. Hernandez, Grace E. Yakutis, Emma I. Zelus, Ryan C. Hill, Monika

Dzieciatkowska, Kirk C. Hansen, and Karen L. Christman. The dissertation author was the primary investigator and author of this material.

References

1. Hussey GS, Dziki JL, Badylak SF. Extracellular matrix-based materials for regenerative medicine. *Nature Reviews Materials*, 1 (2018).

2. Spang MT, Christman KL. Extracellular matrix hydrogel therapies: In vivo applications and development. *Acta Biomater* **68**, 1-14, doi:10.1016/j.actbio.2017.12.019 (2018).

3. Brown BN, Badylak SF. Extracellular matrix as an inductive scaffold for functional tissue reconstruction. *Translational Research* **163**, 268-285, doi:10.1016/j.trsl.2013.11.003 (2014).

4. Traverse JH, Henry TD, Dib N, Patel AN, Pepine C, Schaer GL, DeQuach JA, Kinsey AM, Chamberlin P, Christman KL. First-in-Man Study of a Cardiac Extracellular Matrix Hydrogel in Early and Late Myocardial Infarction Patients. *JACC: Basic to Translational Science*, 357, doi:10.1016/j.jacbts.2019.07.012 (2019).

5. Hernandez MJ, Christman KL. Designing Acellular Injectable Biomaterial Therapeutics for Treating Myocardial Infarction and Peripheral Artery Disease. *JACC Basic Transl Sci* **2**, 212-226, doi:10.1016/j.jacbts.2016.11.008 (2017).

6. Ungerleider JL, Johnson TD, Rao N, Christman KL. Fabrication and characterization of injectable hydrogels derived from decellularized skeletal and cardiac muscle. *Methods* **84**, 53-59, doi:10.1016/j.ymeth.2015.03.024 (2015).

7. Crow S. Peracetic acid sterilization: a timely development for a busy healthcare industry. *Infect Control Hosp Epidemiol* **13**, 111-113 (1992).

8. Hodde J, Hiles M. Virus safety of a porcine-derived medical device: evaluation of a viral inactivation method. *Biotechnol Bioeng* **79**, 211-216, doi:10.1002/bit.10281 (2002).

9. Hodde J, Janis A, Ernst D, Zopf D, Sherman D, Johnson C. Effects of sterilization on an extracellular matrix scaffold: part I. Composition and matrix architecture. *J Mater Sci Mater Med* **18**, 537-543, doi:10.1007/s10856-007-2300-x (2007).

10. Hodde J, Janis A, Hiles M. Effects of sterilization on an extracellular matrix scaffold: part II. Bioactivity and matrix interaction. *J Mater Sci Mater Med* **18**, 545-550, doi:10.1007/s10856-007-2301-9 (2007).

11. Crapo PM, Gilbert TW, Badylak SF. An overview of tissue and whole organ decellularization processes. *Biomaterials* **32**, 3233-3243, doi:10.1016/j.biomaterials.2011.01.057 (2011).

12. Johnson TD, Dequach JA, Gaetani R, Ungerleider J, Elhag D, Nigam V, Behfar A, Christman KL. Human versus porcine tissue sourcing for an injectable myocardial matrix hydrogel. *Biomater Sci* **2014**, 60283D, doi:10.1039/C3BM60283D (2014).

13. Johnson TD, Hill RC, Dzieciatkowska M, Nigam V, Behfar A, Christman KL, Hansen KC. Quantification of decellularized human myocardial matrix: A comparison of six patients. *Proteomics Clin Appl* **10**, 75-83, doi:10.1002/prca.201500048 (2016).

14. Hill RC, Calle EA, Dzieciatkowska M, Niklason LE, Hansen KC. Quantification of extracellular matrix proteins from a rat lung scaffold to provide a molecular readout for tissue engineering. *Mol Cell Proteomics* **14**, 961-973, doi:10.1074/mcp.M114.045260 (2015).

15. MacLean B, Tomazela DM, Shulman N, Chambers M, Finney GL, Frewen B, Kern R, Tabb DL, Liebler DC, MacCoss MJ. Skyline: an open source document editor for creating and analyzing targeted proteomics experiments. *Bioinformatics* **26**, 966-968, doi:10.1093/bioinformatics/btq054 (2010).

16. Gilpin A, Yang Y. Decellularization Strategies for Regenerative Medicine: From Processing Techniques to Applications. *Biomed Res Int* **2017**, 9831534, doi:10.1155/2017/9831534 (2017).

17. Ryan MC, Christiano AM, Engvall E, Wewer UM, Miner JH, Sanes JR, Burgeson RE. The functions of laminins: lessons from in vivo studies. *Matrix Biol* **15**, 369-381 (1996).

18. Gullberg D, Tiger CF, Velling T. Laminins during muscle development and in muscular dystrophies. *Cell Mol Life Sci* **56**, 442-460 (1999).

19. Thomas K, Engler AJ, Meyer GA. Extracellular matrix regulation in the muscle satellite cell niche. *Connect Tissue Res* **56**, 1-8, doi:10.3109/03008207.2014.947369 (2015).

20. Xu Z, Ichikawa N, Kosaki K, Yamada Y, Sasaki T, Sakai LY, Kurosawa H, Hattori N, Arikawa-Hirasawa E. Perlecan deficiency causes muscle hypertrophy, a decrease in

myostatin expression, and changes in muscle fiber composition. *Matrix Biol* **29**, 461-470, doi:10.1016/j.matbio.2010.06.001 (2010).

21. Sanes JR. The basement membrane/basal lamina of skeletal muscle. *J Biol Chem* **278**, 12601-12604, doi:10.1074/jbc.R200027200 (2003).

22. Keane TJ, Londono R, Turner NJ, Badylak SF. Consequences of ineffective decellularization of biologic scaffolds on the host response. *Biomaterials* **33**, 1771-1781, doi:10.1016/j.biomaterials.2011.10.054 (2012).

23. Seif-Naraghi SB, Horn D, Schup-Magoffin PJ, Christman KL. Injectable extracellular matrix derived hydrogel provides a platform for enhanced retention and delivery of a heparin-binding growth factor. *Acta Biomater* **8**, 3695-3703, doi:10.1016/j.actbio.2012.06.030 (2012).

24. Badylak SF, Freytes DO, Gilbert TW. Extracellular matrix as a biological scaffold material: Structure and function. *Acta Biomater* **5**, 1-13, doi:10.1016/j.actbio.2008.09.013 (2009).

Chapter 7. Conclusions and Future Directions

Summary and Significance

Skeletal muscle is one of the few organs to naturally regenerate, but increasing age and other co-morbidities interfere with these inherent remodeling responses. PAD and RCTs represent two conditions which lead to skeletal muscle injury, and therapeutics are still greatly needed to treat these patient populations. My doctoral work focused on the steps required for the translation of a decellularized skeletal muscle ECM hydrogel for these two skeletal muscle applications. Although the efficacy of a therapy is ultimately paramount, other important considerations can hinder and even prevent translation to the clinic. Beginning with thorough literature reviews and expanding to important manufacturing considerations, I extensively evaluated this skeletal muscle ECM hydrogel as a therapeutic option for PAD and RCTs. The results from my doctoral research demonstrate the promise of our decellularized skeletal muscle ECM hydrogel for skeletal muscle applications involving ischemia and chronic unloading, and these findings will contribute to the clinical translation of this biomaterial.

In Chapter 1, background for skeletal muscle regeneration was briefly discussed. Several types of skeletal muscle injuries exist, and the skeletal muscle regenerates and/or remodels in response to the specific injury. Prior to optimizing and evaluating a therapeutic for skeletal muscle injuries, it was important to understand the pathophysiology of various diseases and what pathways should be targeted to promote skeletal muscle regeneration. This chapter served to contrast the challenges associated with utilizing the skeletal muscle ECM hydrogel for PAD and RCTs.

In Chapter 2, acellular injectable biomaterials for PAD were discussed with regards to various design criteria. Material properties, such as material selection, physical properties, degradation properties, manufacturing, etc., are important to consider when designing new biomaterials, and this review highlighted important biomaterial characteristics for PAD. Current

biomaterial therapies for PAD have failed to address these important design parameters, which led to unsuccessful results in clinical trials. The downfalls of these clinical trials were analyzed and alternative approaches, namely incorporating additional biologics, were reviewed as a solution to increase the efficacy of biomaterial-alone therapies. This chapter emphasizes the importance of certain design criteria for biomaterials to achieve success in *in vivo* studies and potentially clinical trials for PAD and could also serve as a checklist for designing new biomaterial products.

In Chapter 3, the skeletal muscle ECM hydrogel was assessed in rodent models of PAD. Previous studies were conducted with the skeletal muscle ECM hydrogel and demonstrated efficacy, but an optimal concentration was not identified prior to that study. Three concentrations of the skeletal muscle ECM hydrogel were evaluated in a young rat hindlimb ischemia model, and the results confirmed utilizing the 6 mg/mL ECM hydrogel as the optimal concentration. Young rat hindlimb ischemia models are commonly used for depicting the pathophysiology of PAD patients, but young rats do not accurately represent the PAD patient population. Many PAD patients are older and suffer from additional co-morbidities, which interfere with healing responses in the body. As a result, the 6 mg/mL ECM hydrogel was validated in an aged mouse hindlimb ischemia model, and significant improvements in blood perfusion were detected. This chapter emphasized the importance of optimizing biomaterial therapies and further evaluating them in more relevant animal models during pre-clinical studies.

In Chapter 4, the efficacy of the skeletal muscle ECM hydrogel was investigated in a more severe skeletal muscle injury – chronic RCT. Many therapies are often administered at the time of tendon repair, but the skeletal muscle regeneration process is sensitive to timing. Consequently, the ECM hydrogel was injected both at the time of tendon repair and at a later time point. The immediate injection caused an even larger inflammatory response than the repair alone, and the inflammation was persistent throughout the study. When a delayed injection approach was utilized, the inflammatory response was less severe than the immediate

injection, muscle transcription factors were upregulated, and the muscle more closely resembled healthy muscle. However, the skeletal muscle ECM hydrogel was not more effective than the saline control at the late time points, and sequential injections of the ECM hydrogel may therefore be necessary to induce extensive regeneration. These results revealed how the timing of administering a biomaterial can impact *in vivo* efficacy, and it is crucial to consider how efficacy may be altered in a more diseased environment.

In Chapter 5, the skeletal muscle ECM hydrogels were evaluated as a delivery platform for microRNA and exosome therapeutics. Biomaterial-alone approaches, such as the skeletal muscle ECM hydrogel, have yielded success in pre-clinical studies, but depending on the bioactivity of the chosen biomaterial, the efficacy may be limited; therefore, incorporating additional biologics may contribute to greater therapeutic efficacy. Many biologics, including cells and growth factors, have been loaded into biomaterials, but cells and growth factors greatly increase the costs of manufacturing, and limited success has been observed in clinical trials. A newer class of biologics, microRNAs and exosomes, were investigated in this chapter, and the skeletal muscle ECM hydrogel successfully served as a delivery platform by prolonging release and maintaining the bioactivity of the therapeutics. These results served as a proof-of-concept for utilizing ECM hydrogels as a delivery vehicle, but a cost-benefit analysis should be performed when considering a combination of therapies.

In Chapter 6, the manufacturing of the skeletal muscle ECM hydrogels was explored. Modifications, additional therapeutics, etc. may contribute to the enhanced efficacy of biomaterials, but difficult manufacturing may hinder the success of the product. Important manufacturing considerations, including animal-to-animal variability, bioburden reduction, and harvesting conditions, were examined for the skeletal muscle ECM hydrogel. The effects of animal-to-animal variability and including a bioburden reducing step did not affect the final ECM hydrogel product, but altering the harvesting conditions impacted the ECM protein composition of the hydrogels. This study indicates the extensive changes that may be required for

biomaterial products during the scale-up process and consequently necessitates the extensive evaluation of manufacturing batches prior to clinical trials.

All in all, these chapters presented the optimization and evaluation of a decellularized skeletal muscle ECM hydrogel for PAD and RCT patients. From designing a biomaterial to confirming efficacy to optimizing manufacturing in preparation for clinical trials, each phase of pre-clinical studies is essential to be successful once clinical trials are reached. Many researchers often neglect portions of the clinical translation process, and mistakes such as poor biomaterial design or utilizing an insufficient animal model could lead to a failed clinical trial. These unsuccessful trials not only eliminate that single biomaterial product from potential translation but similar products are also severely impacted as a result. By understanding why certain therapeutics have been unsuccessful in clinical trials, newer biomaterial approaches can correct those errors and then succeed in reaching the clinic.

Future Directions

A decellularized ECM hydrogel derived from porcine myocardium recently reached Phase I clinical trials (clinicaltrials.gov identifier NCT02305602), and preliminary results from the trial indicated improvements in more chronic myocardial infarction patients.[1] With safety and initial efficacy demonstrated in this ischemic model, this gives precedence to utilizing the skeletal muscle ECM hydrogel in PAD patients. However, it must be determined whether the results presented in this dissertation are sufficient for proceeding with clinical trials.

Several studies have validated the skeletal muscle ECM hydrogel in hindlimb ischemia models of PAD, but overall, this model inadequately captures the pathophysiology of PAD. As seen with the chronic rabbit RCT model, the ECM hydrogel did not yield improvements over the saline control, which could be attributed to the chronic environment of the RCT model compared to the acute environment of a hindlimb ischemia model. PAD is not an acute injury but rather a

chronic condition, and that is not reflected in a hindlimb ischemia model. No animal models are currently available in which animals develop substantial atherosclerosis with resulting ischemia in the skeletal muscle, but the PAD patient population can still be more accurately modeled. The skeletal muscle ECM hydrogels were assessed in aged mice, but older animals or other co-morbidities could also be investigated. The aged mice used in the study were comparable to 45 human years, but PAD is more prevalent in older populations. Similarly, individuals with diabetes and hypercholesterolemia are more likely to develop PAD. As a result, it would be beneficial to evaluate the skeletal muscle ECM hydrogel in these other animal models that impair normal healing responses and establish or identify boundary conditions for the efficacy of the skeletal muscle ECM hydrogel.

In addition to utilizing an improved animal model, the skeletal muscle ECM hydrogel may not produce enough therapeutic benefits with a single dose. All studies to date have administered the ECM hydrogel at one time point, but large skeletal muscles and chronic diseases may require several injections of the material. Studies have been conducted for the repeated administration of decellularized ECM products, and no adverse effects or developed sensitivities to porcine products have been identified.[2-4] The skeletal muscle ECM hydrogels degrade after 3-4 weeks, and performing sequential intramuscular injections would be feasible. In turn, multiple injections of the skeletal muscle ECM hydrogel over time should be tested, especially in large muscles and chronic animal models, to determine whether the skeletal muscle ECM hydrogel will remain efficacious in PAD patients.

Prior to initiating a clinical trial with the decellularized skeletal muscle ECM hydrogel, the studies mentioned above should be completed. The experiments performed for the chronic rabbit RCT model indicated a possible limit to the efficacy of the skeletal muscle ECM hydrogel, which requires further probing. The lack of therapeutic benefits may result from the inability of the ECM hydrogel to reverse the fibrosis, muscle atrophy, fatty infiltration, and muscle degeneration in the chronic RCT model. It may also be due to insufficient scaling from rats to

rabbits and therefore utilizing too little material throughout the targeted muscle. Administering the ECM hydrogel multiple times over the course of a study would provide verification for whether the ECM hydrogel can be effective in a chronic condition like PAD. These additional studies will prolong the timing for initiating clinical trials, but the corresponding results could be crucial to the success of a clinical trial and subsequently providing a treatment for skeletal muscle injuries.

References

1. Traverse JH, Henry TD, Dib N, Patel AN, Pepine C, Schaer GL, DeQuach JA, Kinsey AM, Chamberlin P, Christman KL. First-in-Man Study of a Cardiac Extracellular Matrix Hydrogel in Early and Late Myocardial Infarction Patients. *JACC: Basic to Translational Science*, 357, doi:10.1016/j.jacbts.2019.07.012 (2019).

2. Allman AJ, McPherson TB, Badylak SF, Merrill LC, Kallakury B, Sheehan C, Raeder RH, Metzger DW. Xenogeneic extracellular matrix grafts elicit a TH2-restricted immune response. *Transplantation* **71**, 1631-1640 (2001).

3. Daly KA, Stewart-Akers AM, Hara H, Ezzelarab M, Long C, Cordero K, Johnson SA, Ayares D, Cooper DK, Badylak SF. Effect of the alphaGal epitope on the response to small intestinal submucosa extracellular matrix in a nonhuman primate model. *Tissue Eng Part A* **15**, 3877-3888, doi:10.1089/ten.TEA.2009.0089 (2009).

4. Raeder RH, Badylak SF, Sheehan C, Kallakury B, Metzger DW. Natural anti-galactose alpha1,3 galactose antibodies delay, but do not prevent the acceptance of extracellular matrix xenografts. *Transpl Immunol* **10**, 15-24 (2002).